UNIVERSITY OF CALIFORNIA SAN DIEGO

Design and Synthesis of Ligands Targeting a Structured Viral RNA

A dissertation submitted in partial satisfaction of the requirements for the degree
Doctor of Philosophy

in

Chemistry

by

Walter W. Frauman V

Committee in charge:

Professor Thomas Hermann, Chair
Professor Michael Gilson
Professor Tadeusz Molinski
Professor Navtej Toor
Professor Jerry Yang

2022

The Dissertation of Walter W. Frauman V is approved, and it is acceptable in quality and form for publication on microfilm and electronically.

University of California San Diego

2022

EPIGRAPH

Every day you may make progress. Every step may be fruitful. Yet there will stretch out before you an ever-lengthening, ever-ascending, ever-improving path. You know you will never get to the end of the journey. But this, so far from discouraging, only adds to the joy and glory of the climb.

Winston Churchill

TABLE OF CONTENTS

LIST OF ABBREVIATIONS

ACN	Acetonitrile
AcOH	Acetic Acid
$AlCl_3$	Aluminum Trichloride
BBr_3	Boron Tribromide
Boc	*tert*-butyloxycarbonyl
^{13}C NMR	Carbon Nuclear Magnetic Resonance
CMC	1-cyclohexyl-(2-morpholinoethyl)-carbodiimide metho-p-toluene sulfonate
DCM	Dichloromethane
DIBAL	Diisobutylaluminum Hydride
DIC	*N*,*N'*-Diisopropylcarbodiimide
DIPEA	Diisopropylethylamine
DMA	Dimethylacetamide
DMF	Dimethylformamide
DMSO	Dimethylsulfoxide
EC_{50}	Half maximal effective concentration
EDC	1-Ethyl-3-(3-dimethylaminopropyl) carbodiimide
EtOAc	Ethyl Acetate
EtOH	Ethanol
FRET	Förster Resonance Energy Transfer
HCl	Hydrochloric Acid

HI	Hydroiodic Acid
Hex	Hexanes
^{1}H NMR	Proton Nuclear Magnetic Resonance
HPLC	High Performance Liquid Chromatography
HRMS	High Resolution Mass Spectrometry
IC_{50}	Half Maximal Inhibitory Concentration
IPA	2-Propanol
IR	Infrared Spectroscopy
IRES	Internal Ribosome Entry Site
IVT	*In Vitro* Translation
K_2CO_3	Potassium Carbonate
LAH	Lithium Aluminum Hydride
MeOH	Methanol
NaOH	Sodium Hydroxide
NH_4OH	Ammonium Hydroxide
PBS	Phosphate Buffered Saline
RT (or r.t.)	Room Temperature
$SnCl_2$	Tin (II) Chloride
t-BuOH	*tert*-butyl alcohol
TFA	Trifluoroacetic Acid
TEA	Triethylamine
TLC	Thin Layer Chromatography

LIST OF FIGURES

LIST OF SCHEMES

ACKNOWLEDGEMENTS

First, I would like to thank my PI, Dr. Thomas Hermann for being there for me through this whole graduate school process and being a supportive and helpful boss and mentor. Without his help and his encouragement, I would not have been able to get to this point. I would like to thank my committee for all their help through this process as well. I would also like to thank Dr. Anthony Mrse for his help and support in recording NMR spectra, and Dr. Yongxuan Su and the entire molecular mass spectrometry facility for help in providing mass spectrometry characterization for my compounds. I would like to thank Dr. Jake Bailey, Dr. Milan Gembicky and the rest of the crystallography facility for their help in determining small molecule structures. My labmates in the Hermann Lab have been excellent coworkers during my graduate studies and I would like to specifically thank Dr. Mark Boerneke and Austin Yu, who ran the vast majority of the assays involved in testing the compounds for this project, as well as Brian Charrette and Kevin Walsworth who were able to help with working through and troubleshooting syntheses. I want to thank my undergraduate advisors as well, Dr. Andrew Koch and Dr. Pamela Mertz, who helped guide an underinformed, underperforming biology major into the field of chemistry, which captured my attention and imagination. I would also like to thank my committee for all their help and advice both through this process and throughout the course of my graduate studies.

I would be remiss if I did not also thank my supportive wife, Rachel, who has been a rock throughout this whole process, including doing the majority of the work putting together our wedding last October. Deanna and Joel, my mother and father, have been very supportive and helpful through the whole process, even if they do not quite understand the actual chemistry at hand. My brother Bert has been helpful in steadying me and helping me relax when things got out

of hand. My friends in San Diego, most of whom I met through my graduate studies or one step removed, have gone above and beyond in helping me edit this thesis and improve my presentation, with a special thanks to Dr. Andrew Rudd and Dr. Chris Fisher. These friends have also been a great source of fun and stress relief while in graduate school, and I will cherish my time spent in San Diego with them for the rest of my life, regardless of where any of us wind up scattered. My cat, Hercules, has also been a calm, fluffy, and steadying figure for the process of writing this thesis.

Chapters 2 and 3, in part, are currently being prepared for submission for the publication of the material. Frauman, Walter; Walsworth, Kevin; Hermann, Thomas. The dissertation author was the primary investigator and author of this material.

VITA

Education

2013	Bachelor of Arts, Chemistry, St. Mary's College of Maryland, St. Mary's City, MD
2013-2021	Graduate Researcher, University of California San Diego
2013-2015, 2018-2021	Teaching Assistant, University of California San Diego
2016	Master of Science, Chemistry, University of California San Diego
2022	Doctor of Philosophy, Chemistry, University of California San Diego

Roles

Fellowships and Awards

2020	Teaching Assistant Excellence Award (Fall)
2015/2016	GAANN Fellowship (Renewed for second year)

Presentations

2019	Oral – University of California Chemical Symposium
2017	Oral – ACS Washington DC
2017	Oral – University of California Chemical Symposium
2016	Poster - ACS San Diego
2015	Poster – ACS Western Regional Meeting

ABSTRACT OF THE DISSERTATION

Design and Synthesis of Ligands Targeting a Structured Viral RNA

by

Walter W. Frauman V

Doctor of Philosophy in Chemistry

University of California San Diego, 2022

Professor Thomas Hermann, Chair

Hepatitis C Virus (HCV) contains an Internal Ribosome Entry Site (IRES), which is a 5' region of noncoding RNA that allows for the viral genome to initiate cap independent translation, inserting itself into the 40S subunit. It then hijacks the ribosome to translate the viral genome. This process of IRES driven translation is mediated by a conformational switch, known as an RNA switch, which allows the IRES to attach itself to the 40S subunit, but also to detach once the process of translation has been initiated by the viral genome. Both conformations are necessary for the IRES driven translation initiation. This RNA switch region is highly conserved, and therefore was an interesting target for research. The RNA switch is mediated by a ligand binding mechanism,

where a native ligand binds into a pocket in the RNA and locks it into the configuration that allows for the release of the IRES. In this work, we have used structure-guided synthesis to analyze the binding pocket and attempt to explore binding interactions of portions of the pocket that have not been previously well understood. We have synthesized a variety of compounds with different functional groups and functionality that provide us with a better understanding of this binding pocket and will allow for further study of RNA switch binding pockets as potential small molecule drug targets.

CHAPTER 1

Chapter 1: Introduction

1.1 Small Molecules for Targeting RNA Viruses

With the important role that it plays in the central dogma of molecular biology, RNA has always been a macromolecule of great interest in biological studies. Though often considered only for its role as messenger RNA (mRNA) in the process of transcription and translation, RNA is now known to have a multitude of diverse biological functions. One such function is that of noncoding RNA (ncRNA), structural RNA that can fold into stable three-dimensional structures that can interact with other macromolecules and metabolites, examples of which include the role of transfer RNA (tRNA) or ribosomal RNA (rRNA) in the process of translation. The involvement of ncRNA in a variety of interactions within cells not directly related to protein translation has opened a unique area of research looking into finding the actions of these ncRNAs[1].

The unique three-dimensional structure of ncRNAs presents the possibility of specifically targeting these regions with small molecules to bind and inhibit their mechanism of action. This is already well known in the study of antibiotics binding to the ribosome, though advances in structural and binding studies with known and newer antibiotics show that these compounds predominately bind with the rRNA portion of the ribosome, with little or no interaction with the protein components[2,3]. These complexes have also been used in the improvement of antibiotic classes with the additional knowledge of the binding sites[3]. While the ribosomal complexes with rRNA are unique in their structural composition and integration with ribosomal proteins, they are also unique in that there is an enormous amount of structural data and binding information on the ribosome, compared to other RNA small molecule targets. Other RNA targets for small molecules that have been pursued are the Tat-TAR protein-RNA complex in HIV, up to 20 riboswitches,

found mainly in bacteria, and the Internal Ribosome Entry Site (IRES) of Hepatitis C Virus (HCV) which is the focus of and the target of this work[3,4]. RNA is considered a difficult target for small molecules, due to the flexibility of the target as well as the ability of RNA to mutate quickly, especially in viruses, to avoid inhibitor complexes[5]. Therefore, current approaches to RNA drug development focus on targeting highly-conserved and structured regions of the RNA. Targeting the HCV IRES ncRNA does have this advantage (similar to other targets of interest) in that the regions of interest are highly conserved and play a vital role in the life cycle of the virus, which provides a larger obstacle for the development of resistance to any small molecules[6–9].

1.2 Hepatitis C Virus (HCV)

Hepatitis C Virus is a widespread and deadly virus, with no current vaccine. Despite there being multiple direct acting antiviral (DAA) treatments that result in a >95% cure rate, there are still 59 million people worldwide infected with HCV and 1.5 million new infections yearly. Deaths estimated in the most recent year (2019) were 290,000[10]. The current DAA treatments target the NS3 and NS4A proteases, the NS5B polymerase and NS5A protein, and the combination generally depending on the genotype of HCV involved. Resistance to individual compounds has been seen, though the combinations seem effective currently in avoiding resistance[11]. This treatment, though does not appear to provide immunity to reinfection which, while not unexpected, allows for reinfection, which is frequently observed[12]. An issue that could arise with these DAAs having the same targets but not preventing reinfection is that HCV mutates at an exceptionally quick rate, about 1 nucleotide per replication cycle, due to its polymerase not having a proofreading function. With this issue and a high turnover rate in humans many unique quasispecies of HCV are found within single individuals[13,14]. This provides good rationale for pursuing alternative targets for binding that interact with a highly conserved region of HCV RNA.

1.3 HCV Internal Ribosome Entry Site (IRES) and Domain IIa RNA Switch

HCV is an enveloped, positive-strand flavivirus with a single stranded RNA genome that serves directly as the viral messenger RNA. The 9.6 kilobase viral genome contains structured untranslated regions (UTR) that are highly conserved at both the 3' and 5' ends of the genome. The 5' UTR of the genome contains a highly structured IRES, which allows the virus to bypass the majority of the host cell initiation factors required in typical cap-dependent eukaryotic translation[15,16] (Figure 1.1). The IRES binds to the ribosomal 40S subunit and orients the AUG start codon at position 342 into the mRNA binding cleft of the ribosome, and assembling the functional ribosome around this orientation[15–18]. One region in the IRES is of particular interest is the Domain IIa region located directly within the curve of the IRES on the cryo-EM reconstruction in Figure 1.1.B. This Domain IIa region consists of an RNA switch mechanism, with an internal loop that is flexible and undergoes a ligand dependent conformational switch between the ligand bound straight conformation and the ligand-free 90° L-shaped configuration (Figure 1.2)[15]. Without the ability to switch between the two conformations, the viral RNA cannot complete the process of IRES driven translation initiation. This region is particularly interesting due to the high rate of conservation of the RNA bases in a survey of the genomes of clinical isolates of HCV (Figure 1.3). Previous studies suggest that guanine is the most likely native ligand for the RNA switch pocket during the IRES driven translation[15]. This RNA switch mechanism has been examined, and at least 11 similar IRES structures to the domain IIa region have been discovered to this point. These regions vary in sequence and local secondary structure, they show similar levels of ligand specificity in binding and would be an interesting target for small molecules[15].

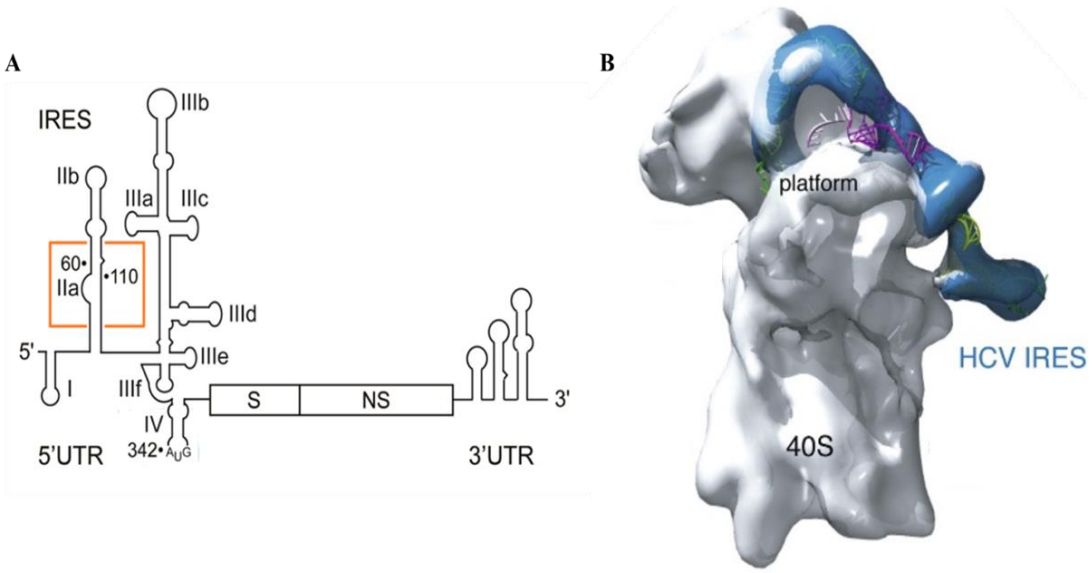

Figure 1.1 A) Hepatitis C Virus Genome, with 5' Internal Ribosome Entry Site labelled. The Domain IIa region is demarcated in orange. Figure adapted from ref[19]. B) Cryo-EM reconstruction with crystal and NMR structures of IRES modelled into cryo-EM of IRES, overlaid on Cryo-EM of the 40S subunit. Figure modified from ref[17]

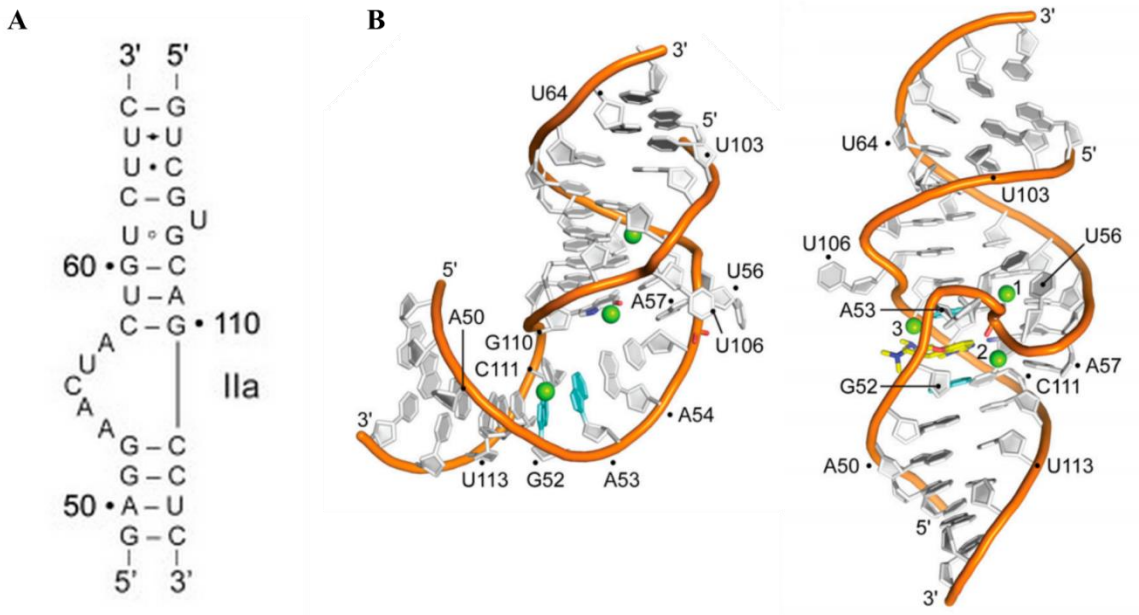

Figure 1.2 A) Secondary structure of a segment of the domain IIa internal loop and surrounding nucleotides of the HCV IRES. Figure adapted from ref[20]. B) Crystal structure of the domain IIa oligonucleotide segment in the relaxed L-shaped configuration (left) and the ligand bound straight configuration (right). Figure adapted from ref[21].

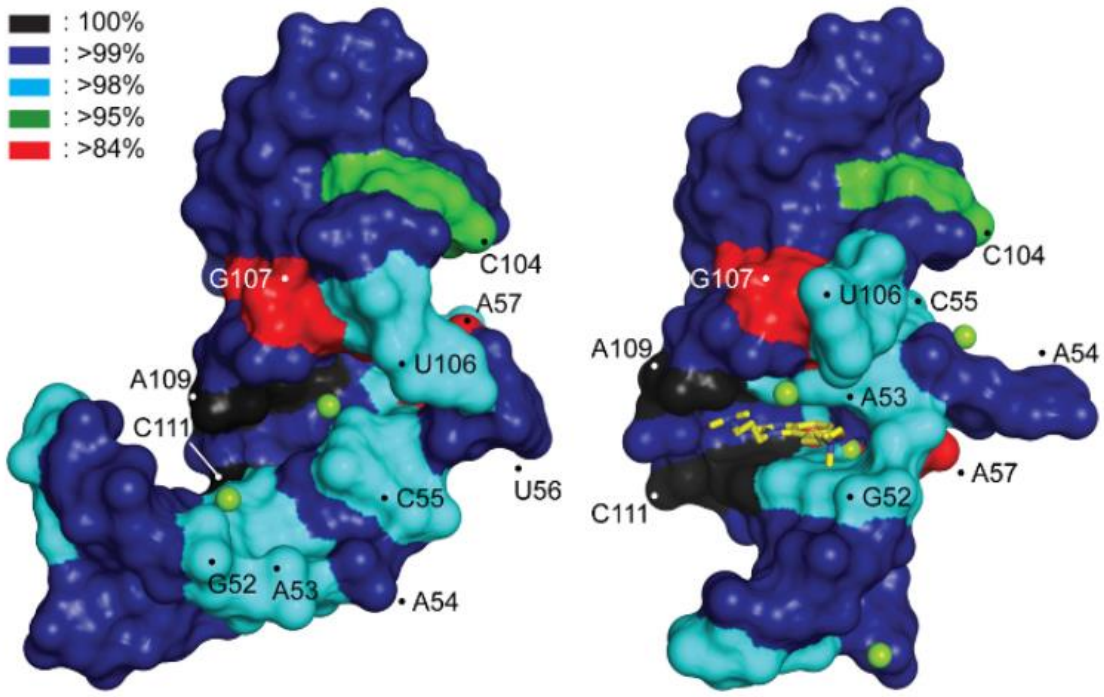

Figure 1.3 Crystal structure of the domain IIa oligonucleotide segment in the relaxed L-shaped configuration (left) and the ligand bound straight configuration (right) from Figure 1.2.B, but with the sequence conservation (from 1,601 clinical isolates) overlaid on the RNA surface. Figure adapted from ref[22,23].

1.4 RNA Switch Binding Pocket and Förster Resonance Energy Transfer (FRET) and In Vitro Translation (IVT) Binding Assays

The RNA switch binding pocket in the domain IIa region has been co-crystallized with a benzimidazole ligand that showed specificity for this pocket in an affinity screen[21,24]. The ligand bound crystal structure shows the locking in of the straight conformation of the RNA, while the non ligand bound region, when crystallized, showed a 90° L-shaped conformation. Based on this switch mechanism and the information gleaned from the crystal structure of the bound and unbound RNA, a FRET assay was designed to test compounds for binding to this RNA switch pocket[25]. Cy3 and Cy5 dyes were added on both 5' ends of the construct taken from a portion of the RNA switch corner region[26]. With the RNA in the L-shaped conformation the two dyes are within the Förster radius, and FRET transfer between the dyes is possible. With the ligand bound

straight conformation, the dyes are at a distance that is outside of the Förster radius, quenching that signal. Thus, when running this assay, the FRET signal will decrease in response to ligand binding at the RNA switch pocket (Figure 1.3).

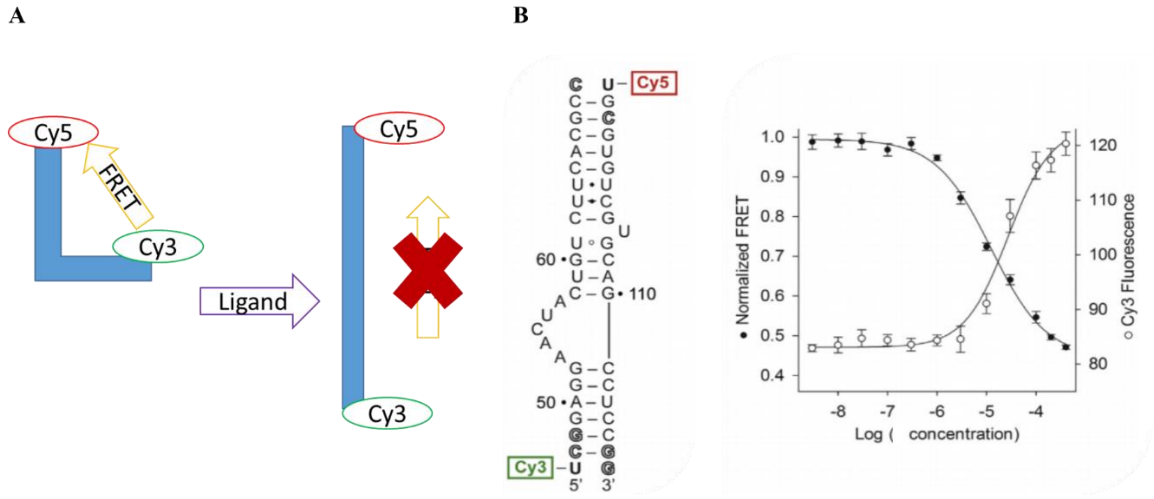

Figure 1.4 A) Cartoon representing the concept of FRET transfer in the relaxed L-shaped conformation of the FRET construct, and the quenching of FRET with the binding of ligand and conformational switch to the straight shaped conformation. B) Secondary structure of the FRET construct used in this assay, and an example graph of a compound that binds in the pocket, showing the quenching of the FRET signal at a certain concentration of compound. Figure adapted from ref[27].

The *in vitro* translation (IVT) assay uses a bicistronic complex with a cap region for cap-dependent translation initiation of a Firefly luciferase transcript, followed by the HCV IRES region for cap-independent translation of a Renilla luciferase transcript (Figure 1.4). This bicistronic construct allows for internal control of translation integrity and allow the exclusion of false-positive inhibitors which affect the ribosome independently. The Firefly luciferase acts as a control with cap driven translation initiation, while the Renilla luciferase is only translated with successful cap-independent translation initiation by the HCV IRES. Any ligand that inhibits the Renilla only inhibits the IRES driven translation initiation. Compounds tested in both the FRET and the IVT assay show that the assays both measure the inhibition of IRES driven translation initiation[26–28].

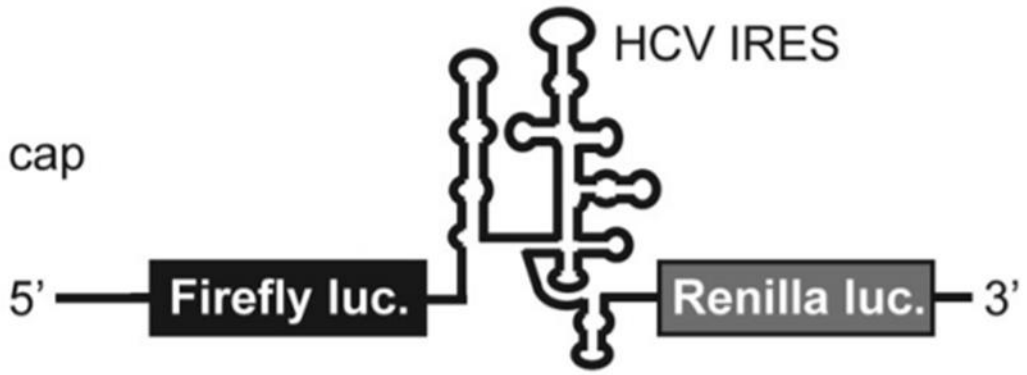

Figure 1.5 A cartoon of the bicistronic *in vitro* translation (IVT) construct, showing the 5' cap region for initiation the translation of the transcript for Firefly luciferase, followed by the IRES construct for initiation of translation of the Renilla luciferase transcript. Figure adapted from ref[27].

CHAPTER 2

Chapter 2: Compounds of Interest in Probing the RNA Switch Binding pocket

2.1 RNA Switch Binding Pocket and Previous Compounds showing Binding Affinity

While foundational work has strengthened our understanding of switch structure and function, several key questions remain about the binding pocket's unique structure and key binding interactions with small molecule substrates. This RNA switch is critical for the process of IRES driven translation, but without a fortuitous discovery of a ligand binding compound that could be cocrystallized with the RNA, the binding pocket would not have been able to be visualized. With this pocket visualized, determining binding interactions beyond and dissimilar to the initially cocrystallized compound became the next area of focus in understanding these RNA switches.

The initial benzimidazole (compound 1) that was cocrystallized with the RNA switch binding pocket was optimized from compound 2 (Figure 2.1). Compound 2 was initially identified as a compound targeting the IRES by Ionis Pharmaceuticals through a mass spectrometry based high throughput screen run against the IRES RNA[24]. Further attempts (>300) were made to improve the affinity of the original benzimidazole scaffold and produced a handful of compounds similar to 1 that bound in the low micromolar to high nanomolar range, but with low yields over many synthetic steps[6,24]. While the benzimidazole scaffold optimization did not result in a compound with strong enough affinity for Ionis to move anything further down the drug discovery pipeline, compound 2 had strong enough affinity that a cocrystal structure with the RNA ligand was feasible, resulting in further elucidation of the binding interactions of the ligands within the pocket, as well as the shape and accessibility of the pocket (Figure 2.1).

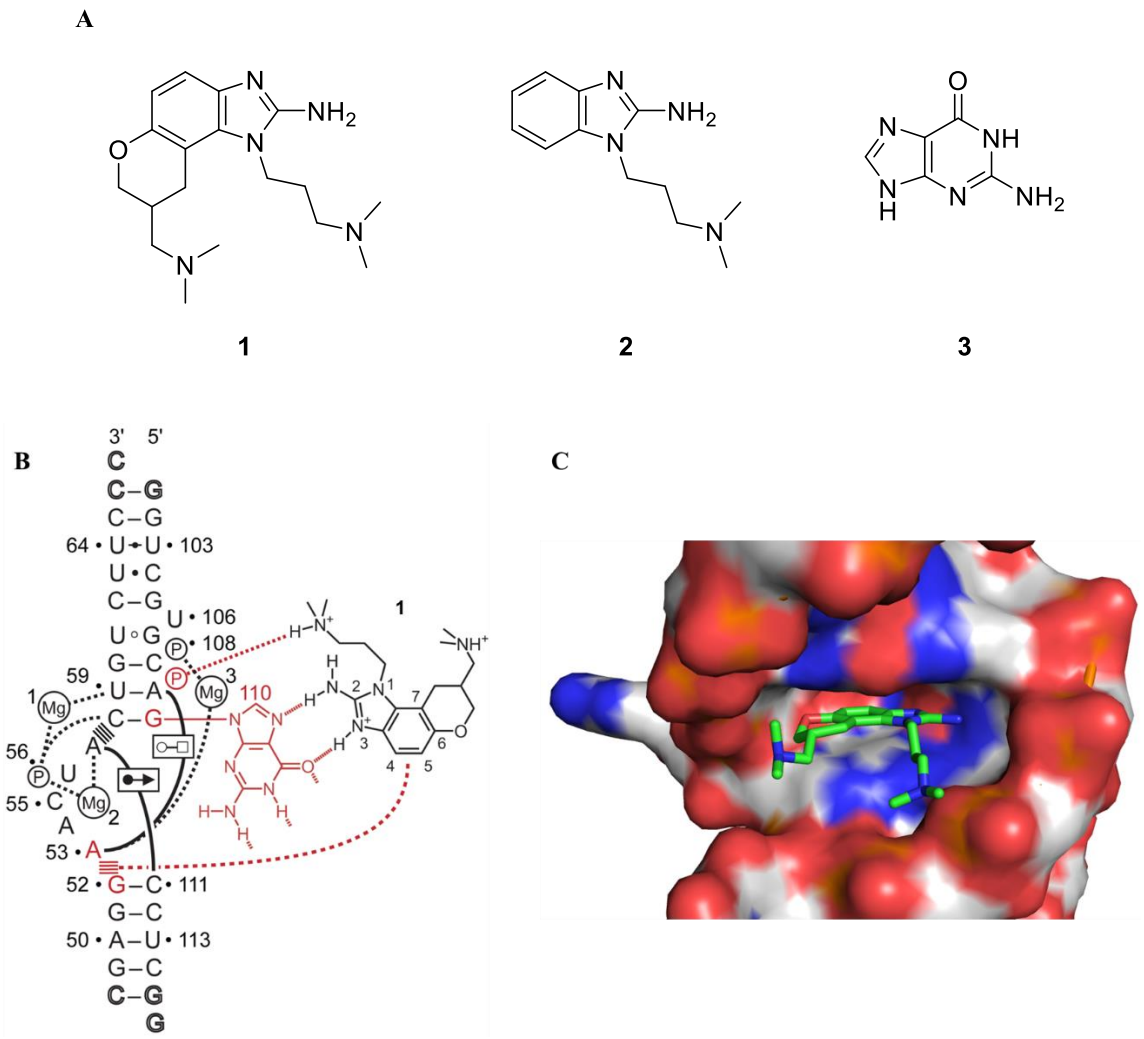

Figure 2.1 A) Early compounds determined have affinity for the domain IIa binding pocket (1: 8-((dimethylamino)methyl)-1-(3-(dimethylamino)propyl)-1,7,8,9-tetrahydrochromeno[5,6-d]imidazol-2-amine) (2: 1-(3-(dimethylamino)propyl)-1H-benzo[d]imidazol-2-amine) (3: Guanine) B) Diagram of the binding of benzimidazole compound 1 with the nucleotides of the binding pocket, showing hydrogen bonding interactions from the guanidinium segment with G110, π-stacking interactions of the phenyl group between G52 and A53, and hydrogen bonding of the dimethylaminopropyl segment with the phosphate backbone. Figure from ref[22]. C) Portion of the crystal structure with compound 1 bound, showing space filling effects and the structure of the pocket.

With the pocket able to be visualized, and the native ligand (guanine) determined, the next step was to look at the important binding motifs and the composition of the pocket. Overlaying the guanine and the benzimidazole ligand, with the guanidinium motif overlapping to align those crucial hydrogen bonding interactions (Figure 2.1, interactions of ligand with G110) provided

insight into accessible space further into the pocket that was not being filled by the benzimidazole ligand (Figure 2.2). This space in the pocket being willing to accept portions of a ligand was interesting, and encouraged us to further expand upon the interactions in that space of the binding pocket not previously explored in the benzimidazole optimizations.

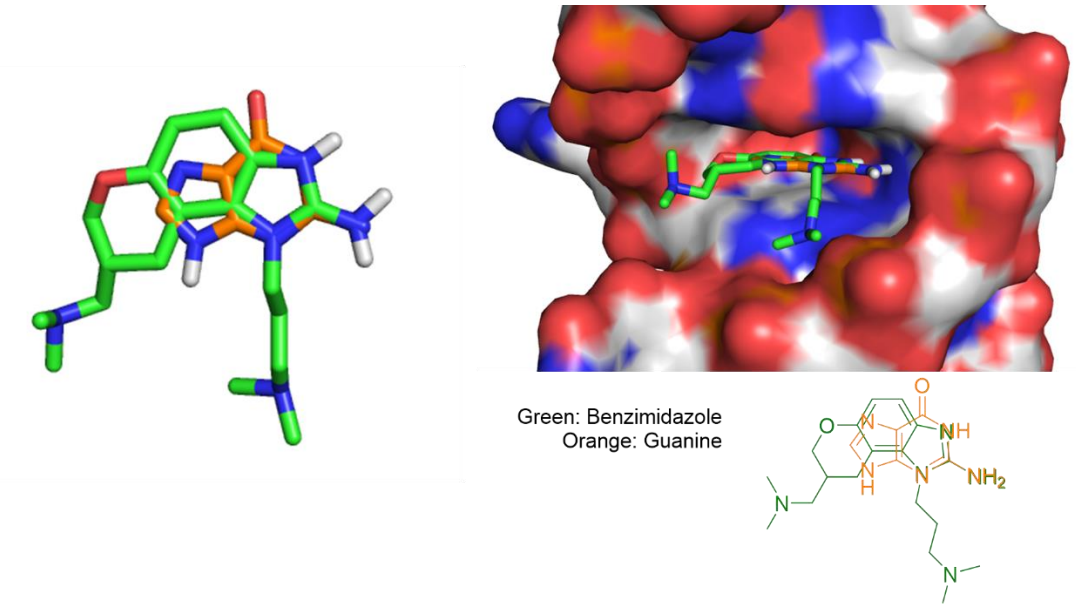

Figure 2.2 Diagram of the benzimidazole ligand (compound 1) overlapping with the native ligand (guanine) with the guanidinium motifs as the point of contact. Also shown is the crystal structure of the benzimidazole ligand bound in the RNA pocket, with a guanine manually docked in the same overlapping configuration. This shows the area of the pocket accessed by the carbonyl on guanine that is not accessed by the benzimidazole.

Through the FRET assay, the EC_{50} of guanine was determined to be approximately 1 mM, which was much weaker than the binding of the benzimidazole. A 2-amino-quinazoline compound (**3**) that has a benzene ring in place of the imidazole portion of the guanine was tested (Figure 2.3) and improved the affinity two-fold over guanine. This is likely due to the imidazole non optimally π-stacking with the G52 and A53 residues compared to the benzene ring[26,28]. Comparison of the benzimidazole, guanine and quinazoline ligands elucidates the fact that all three of the molecules are planar in the portion of the molecule binding in the pocket. Examination of the crystal structure showed a region in the back of the pocket with room to potentially accommodate a nonplanar

ligand that would provide better space filling effects with respect to binding[28]. With this knowledge, two quinazoline derivatives replacing the carbonyl with a dimethyl substituent and with a spirocyclopropyl substituent allowed for examination of what this region in the back of the pocket can accommodate (Figure 2.3). The dimethyl compound (**4**), when tested by the FRET assay, showed an EC_{50} very similar to the quinazoline compound, but the spirocyclopropyl compound (**5**), had an EC_{50} almost 5 fold lower, at 100 μM, likely due to being more compact than the dimethyl compound[28]. This space filling effect improving the binding of the ligand is slightly counterintuitive with respect to the RNA pocket being the target. RNA is a very polar macromolecule, and the spirocyclopropyl compound cannot form any hydrogen bonding interactions, but still significantly improves affinity, likely due to better filling the available space in the pocket.

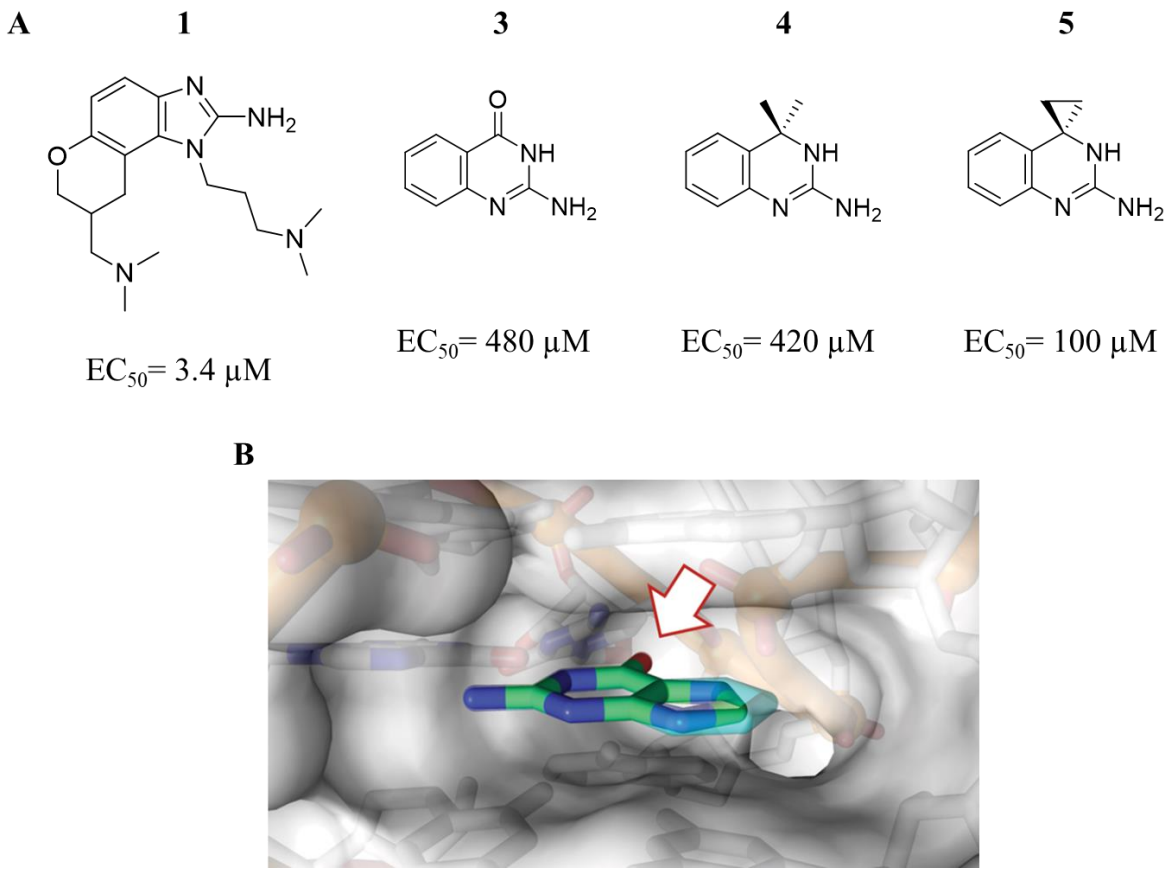

Figure 2.3 A) Compounds tested through the FRET assay and their EC_{50} values. Compounds 3-5 are designed with structural knowledge of the guanine binding ligand. Values from ref[28]. B) Visualization of available region in binding pocket. Figure adapted from ref[28].

2.2 Benzothiadiazines as a Polar Non-planar Scaffold for Filling Pocket

With the discovery of the space in the back of the pocket, as well as the improvement in binding affinity with space filling effects (despite differences in polarity), new compounds were of interest to explore the binding with this region of the pocket. For this a benzothiadiazine scaffold was proposed believing the sulfonylamide substitutent, being space filling but polar, would be able to improve the binding affinity. Benzothiadiazine scaffolds are found in numerous pharmaceuticals that have been successfully used diuretics for over half a century, as well as a scaffold of interest in HCV protease inhibition more recently[29,30]. With this, a scheme was proposed for the

development of the benzothiadiazine scaffold, as well as a substituted scaffold that incorporates the dimethylaminopropyl substituent from the benzimidazole compounds, due to the interactions shown by this group in the co-crystal structure (Scheme 2.1).

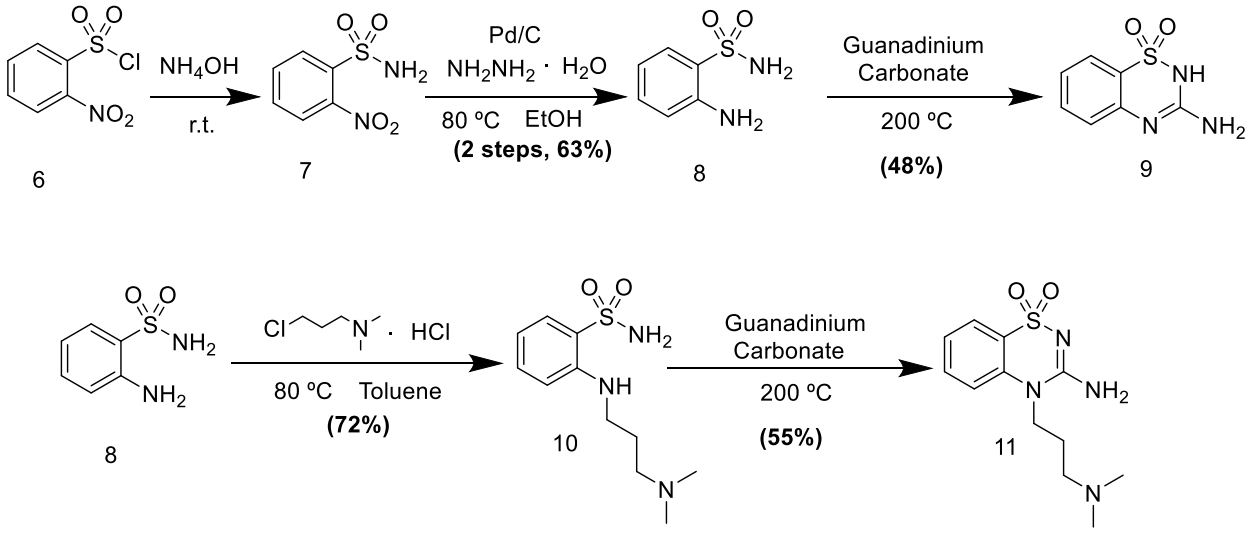

Scheme 2.1 Synthesis of benzothiadiazine scaffold (9) and the dimethylaminopropyl substituted scaffold (11). Reaction for solvent-free cyclization steps adapted from ref[31].

The benzothiadiazine scaffold that reflects the guanine/quinazoline structure was able to be synthesized on a large scale. The cyclization step is a unique, solvent-free melting reaction[31]. With compound 8 being commercially available, the basic scaffold is accessible in one step. For 11, the compound is accessible from commercially available starting materials in two steps with an initial 40% overall yield. These compounds were tested using the FRET assay discussed in the introduction. The EC_{50} of compound 9 was determined to be 47±30 μM and the EC_{50} of compound 11 was determined to be 11±7 μM (Figure 2.4). Comparing compound 11 (the substituted benzothiadiazine) and compound 2 (the initial benzimidazole hit ligand), we can see that the compounds should bind in the pocket similarly, and the benzothiadiazine has a 5 fold improvement

over the comparable benzimidazole, the initial hit in the Ionis screen. (Figure 2.5). The benzothiadiazine scaffold also has not been explored as thoroughly, as the benzimidazole compound had 300-400 analogues synthesized and tested for affinity[24]. Both compounds were tested in the beginning stages of pharmacokinetic testing, with the strategy being adapted from ref[32]. The compounds showed stability over time in solvent, and were able to be dissolved into and then extracted from mouse plasma without degradation.

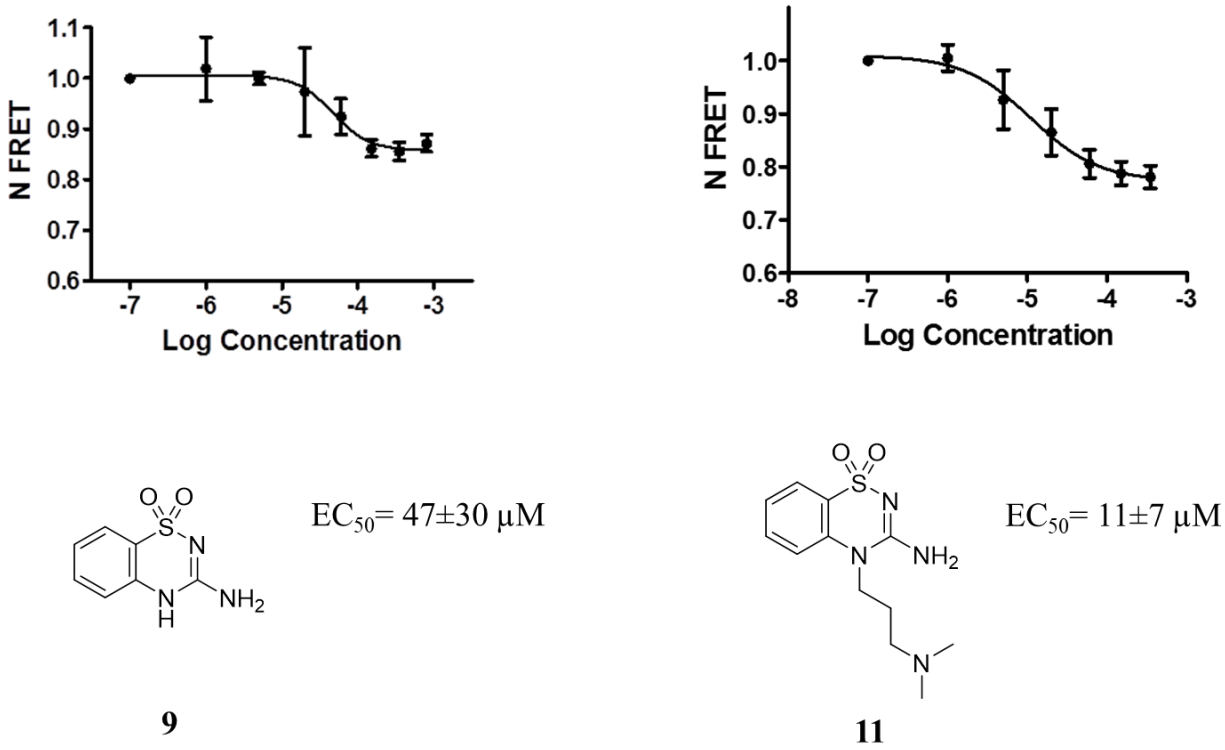

Figure 2.4 FRET binding curves and EC_{50} values of the FRET assay with the benzothiadiazine scaffold (9) and the dimethylaminopropyl substituted benzothiadiazine compound (11). Concentration measured in M.

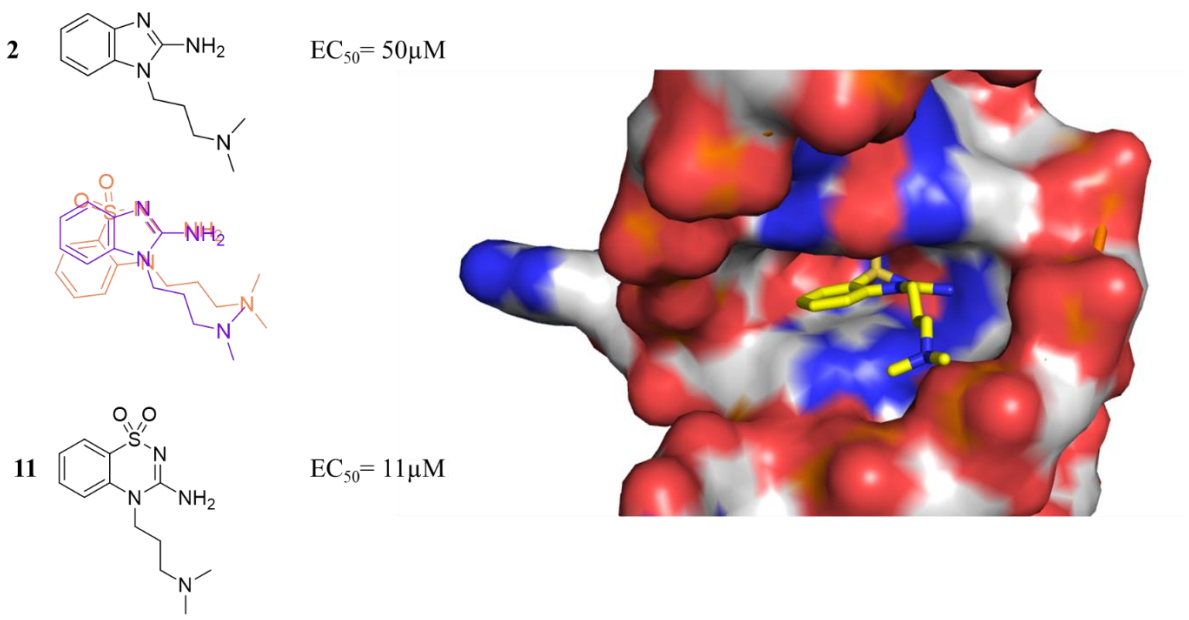

Figure 2.5 Comparison of the benzimidizole initial hit ligand with the benzothiadiazine ligand with comparable substituents. The compounds are shown overlapping at the guanidine substituent, which contains essential hydrogen bonding interactions. The structure on the right is the crystal structure of the pocket with the compound 11 manually docked with respect to those hydrogen bonding interactions.

2.3 Abolishing Hydrogen Bonding Interactions to Confirm Binding Requirements

With the benzothiadiazine compound (11) we have found a compound that accesses the open area of the binding pocket that was not accessed by the benzimidazole compounds. This structure is also one that is found in many approved drugs, as well as one that has not been explored as thoroughly. We know that this compound binds in the FRET assay, but to further confirm the benzothiadiazine interacts with the binding pocket in the same way, compounds were synthesized to abolish important hydrogen bonding interactions to confirm that these are also important to the binding of the benzothiadiazine. We were able to utilize the solvent free cyclization reaction from scheme 2.1 with urea as the cyclizing agent instead of guanidinium carbonate and replace the

exocyclic 2-amino group with a carbonyl (Scheme 2.2). Compound 12 was then recrystallized, and a crystal structure was elucidated (Figure 2.6). Neither compound 12 nor compound 13 showed any binding affinity when tested in the FRET assay, as expected. This indicates that hydrogen bonding with the exocyclic amino group is essential for binding of the ligand in the pocket.

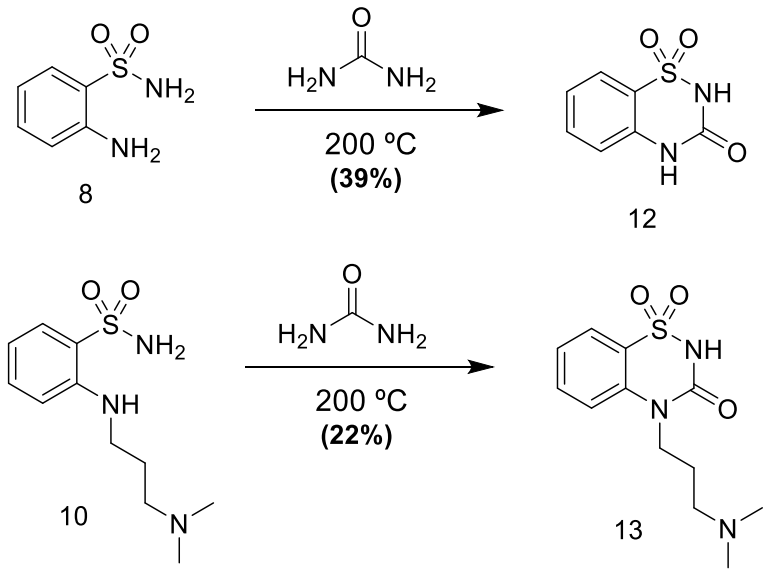

Scheme 2.2 Urea solvent-free cyclization reactions. Reaction adapted from ref[31].

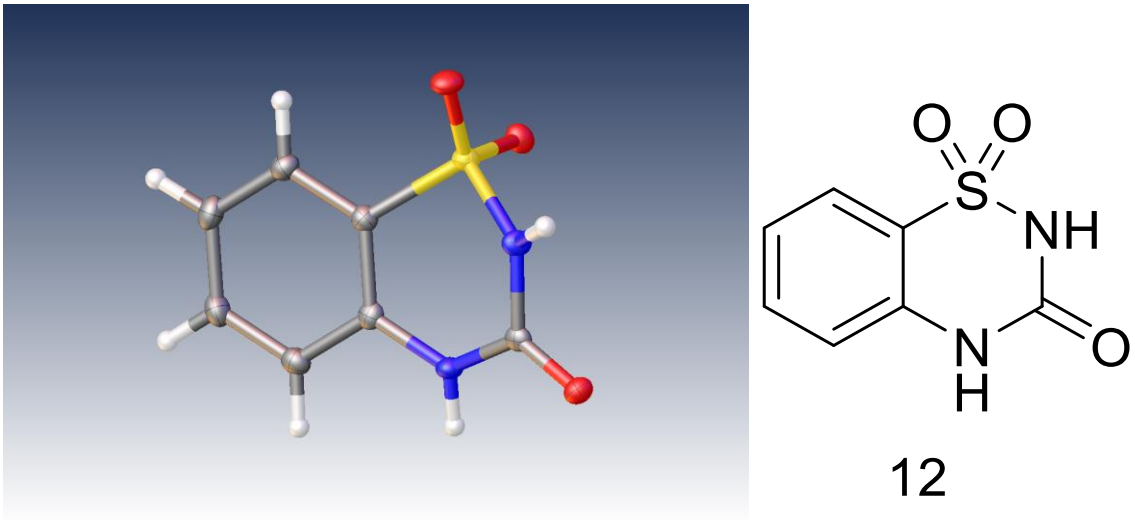

Figure 2.6 Crystal Structure of compound 12, with drawing showing tautomer.

2.4 Modification of Benzothiadiazine Fragment to Probe Binding Interactions

With the improved binding affinity of compound 11 in mind, schemes for derivatization were proposed for further elucidation of the binding interactions, as well as to attempt to improve binding affinity. With that in mind, two compounds were tested with alternative cyclization reagents through an adaption of the procedures from the solvent free cyclization that initially proved successful (Scheme 2.3)[31]. This was unsuccessful, likely due to the more harsh nature of the cyclization conditions, and with these compounds not being particularly interesting for binding further attempts to synthesize these compounds were not attempted.

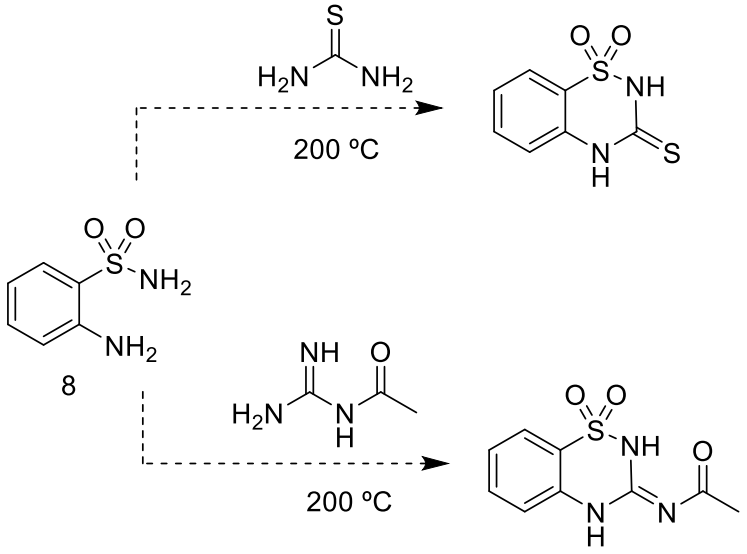

Scheme 2.3 Attempts of alternative cyclizations through solvent-free melting reaction. Reaction adapted from ref[31].

A synthetic scheme was proposed to explore the impact of replacing the dimethyl amino substituent with a methyl substituent (Scheme 2.4). The resulting compound (16) was tested in the FRET assay and found to have an EC_{50} of 68 μM, right around that of the quinazalinone species (3). This slight reduction in the binding affinity for this compound is likely due to the methyl group favoring a tautomerization of the molecule that is less favorable for the hydrogen bonding

interactions, while not having the beneficial hydrogen bonding interaction of the dimethylaminopropyl substitutent. The carbonyl cyclized compound (14) was also tested in the FRET assay, and did not show any affinity, which was expected based on the results from compounds 12 and 13.

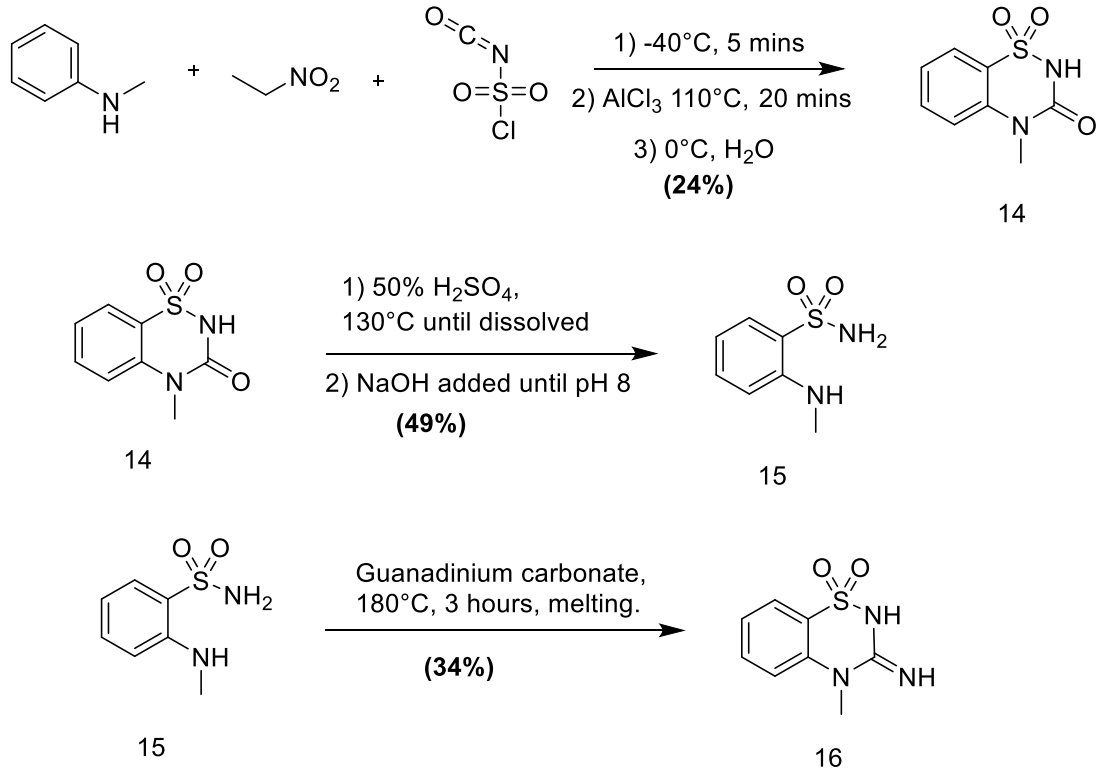

Scheme 2.4 Synthesis of methyl substituted benzothiadiazine. All steps save the cyclization are taken from ref[33]. Cyclization reaction adapted from ref[31].

Further derivatization of the benzothiadiazine was proposed through a number of different pathways. Of interest was adding groups to the far side of the benzene ring (like that of compound 1) and in positions that point out of the binding pocket (positions A and B, Figure 2.7). The first attempt at this was using *N*-bromosuccinimide (NBS) in an attempt to directly brominate compound 11[34]. After unsuccessfully attempting to adjust the procedures, this strategy was abandoned, due to the bromination product likely being favored in the C position through this

process, due to directing effects of the substitutents on the ring. Alternative ways of trying to substitute on the benzene ring were then needed.

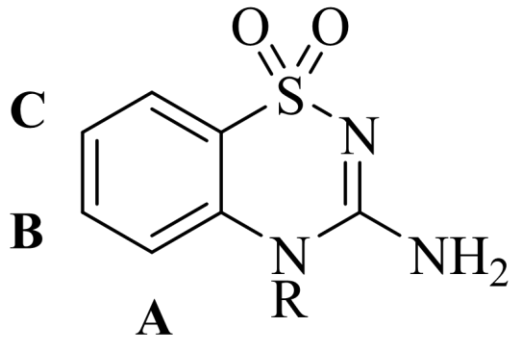

Figure 2.7 Positions of interest on the benzothiadiazine scaffold for potential addition of substituents. Positions A and B point towards the entrance of the binding pocket, while position C points into the wall of the binding pocket.

The next pathway attempted was using 2,4-dinitrobenzenesulfonyl chloride (compound 17, scheme 2.5) as a commercially available starting material, substituting to the sulfonylamide (compound 18), and then reducing the nitro groups (either mono- or di- reduction, both products were of interest) to provide a starting material that is a derivative of compound 8 with an aromatic amino group in the B position (with respect to orientation in Figure 2.7). Multiple solvent conditions and reduction reagents were used to try to accomplish this reduction, but the majority of the reactions either did not do any reduction, or led to the major production of the 2,4-dinitroaniline (compound 19). This was curious, but through research and examination of the compound, it was determined that an intramolecular Meisenheimer complex was forming and kicking out SO_2 to form the aniline compound 19 (Figure 2.8). With this as a roadblock, alternative methods were needed.

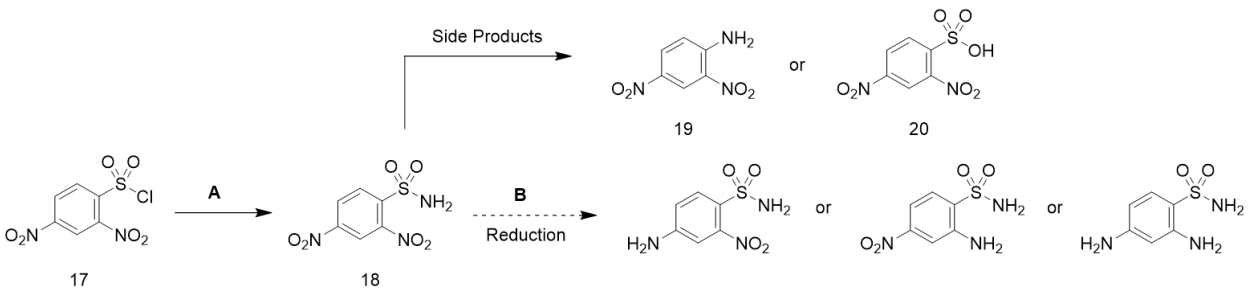

Rxn	Reagent Reaction A	Temp. Reaction A (°C)	Reaction Time (A) (hrs)	Reagent B (Reduction)	Solvent B (Reduction)	Temp. Reaction B (Reduction) (°C)	Reaction Time (B) (Reduction) (hrs)	Resulting compound
1	NH_4OH	0	16	N/a	N/a	N/a	N/a	18/ 19
2	NH_4OH	0	16	N/a	N/a	N/a	N/a	18
3	$(NH_4)_2CO_3$/ AcOH	0	3	N/a	N/a	N/a	N/a	Unknown
4	NH_4OH/ MeOH	0	1.5	Fe	Glacial AcOH / EtOH / H_2O	30	3	18
5	NH_4OH/ EtOH	0	1.5	Fe	IPA/EtOH/H_2O/ NH_4OH	80	3	Unknown
6	IPA / NH_4OH	0	1.5	10% Pd/C and H_2	MeOH	RT	2	18/19
7	NH_4OH / Acetone	RT	0.5	Fe	IPA / Glacial AcOH	100	4.5	Unknown
8	NH_4OH / Acetone	0	5	Fe	EtOH/ conc. HCl	80	16	Unknown
9	0.5 M NH_3 in dioxane / Dioxane	RT	1.5	Zinc	H_2O	60	16	20

Scheme 2.5 Scheme showing attempts at functionalizing benzene through substitution of the sulfonyl chloride of compound 17 to the sufonylamide of compound 18, followed by reduction of the nitro groups (without definite control of mono or di-reduction). Scheme shows the products that were desired, as well as the side products that were produced through these reaction conditions (Resulting Compound column).

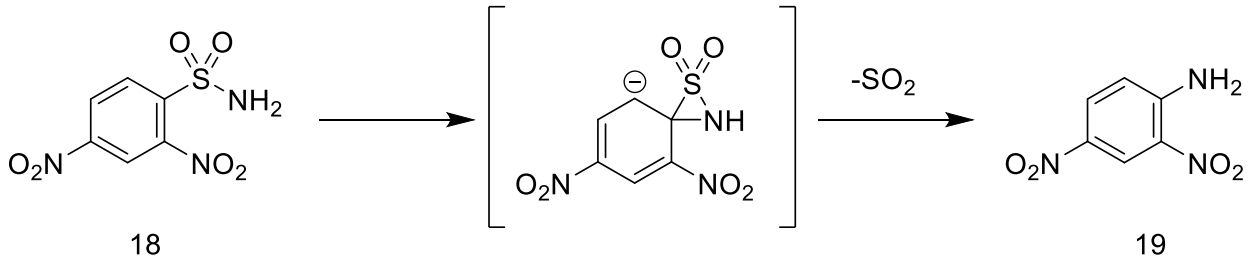

Figure 2.8 Purported mechanistic reasoning for the failure of the reduction of compound 18, where instead under reaction conditions the compound forms a Meisenheimer complex and desulfonylation occurs. This is more favorable than expected, due to the strong electron withdrawing effects of the two nitro groups. Figure process derived from ideas contained within ref[35].

Following a similar vein from the 2,4-dinitrobenzenesulfonylamide pathway, the next pathway was proposed starting with a 4-chloro-2-nitro compound (21) that does not have the same electron withdrawing effects as the dinitro compound (18), and as a result potentially would be able to avoid the desulfonylation seen previously (Figure 2.8) The scheme was essentially equivalent to the scheme for forming compound 11 (Scheme 2.1), and was designed to form the dimethylaminopropyl substituted product (26). Three alternative reduction reactions were attempted to perform the transformation from compound 23 to compound 24, to avoid the possibility of hydrodehalogenation, which is frequently accomplished with the Pd/C catalyst used in the reduction of compound 7 to compound 8 (Scheme 2.1)[36,37]. The first attempt was a reduction with iron powder and glacial acetic acid, adapted from two references with aryl nitro reduction[38,39]. This route was not optimal, due to the effort required to purify the reaction and remove the iron hydroxides produced in the reaction, as well as the yield being only 20%. The next attempt was using 57% hydroiodic acid, adapted from ref[40] but the product was not able to be purified even with many workup steps. Finally, a tin (II) chloride reduction was used for this reduction (procedure adapted from ref[38]) and the compound was easy to isolate in a 78.5% yield, and was thus used to create compound 23 moving forward. The initial conditions for running of the solvent-free cyclization reaction (last step scheme 2.6, cyclization of compound 25) were done at 220 °C instead of 180-200 °C, which lead to a mixture of compounds 26 and compound 27, due to difficulties with isolation of the correct starting material in the previous step. Compound 27 was able to be isolated from this reaction, and therefore direct cyclization was not attempted with compound 23. The reaction was re-run under slightly milder conditions (175 °C) and with the correct starting material solely, and then purified by HPLC to isolate compound 26. Both compounds were tested in the FRET assay. Compound 26 was not soluble in the assay and

precipitated out of solution, so no EC_{50} could be determined. Compound 27 did not saturate the FRET signal at the concentrations we measured, so we determined that the EC_{50} was >1 mM. With both of these compounds being difficult to isolate and having issues with solubility, as well as showing reduced binding made this pathway seem less promising.

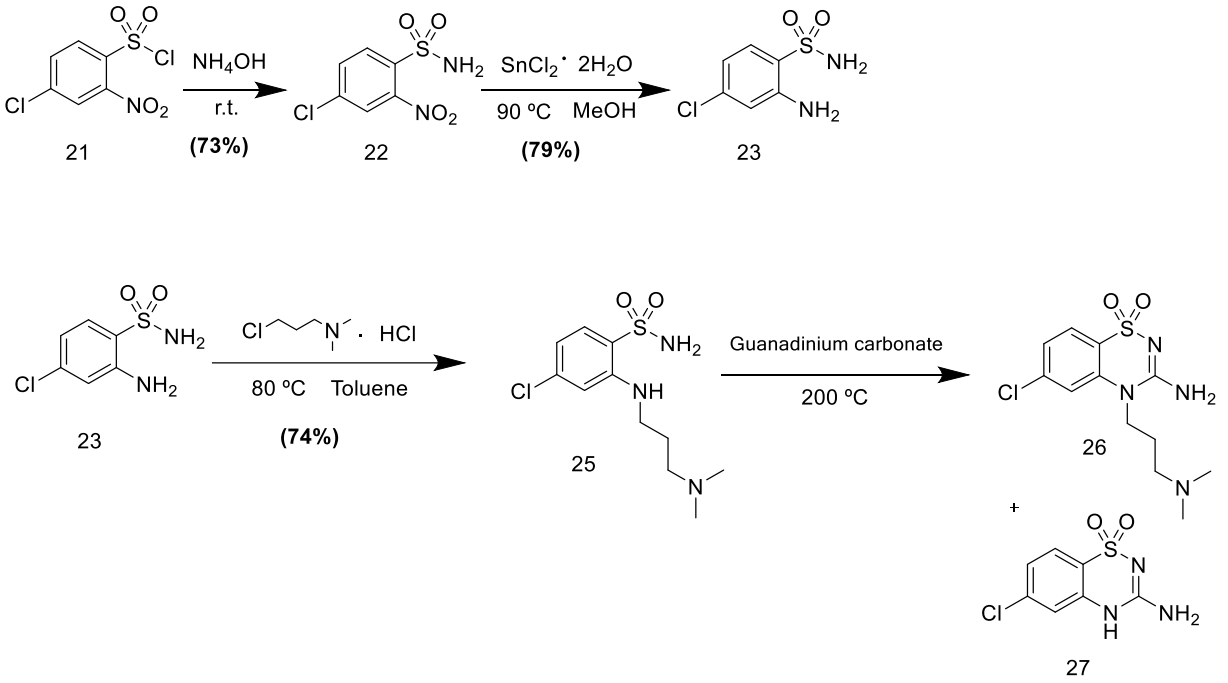

Scheme 2.6 Synthesis of 3-amino-6-chloro-4-(3-(dimethylamino)propyl)-4H-benzo[e][1,2,4]thiadiazine 1,1-dioxide (compound 26) and 3-amino-6-chloro-4H-benzo[e][1,2,4]thiadiazine 1,1-dioxide. All steps are adapted from Scheme 2.1. Cyclization reaction adapted from ref[31].

2.6 Conclusion

In summary, we have demonstrated that there is value in attempting to derivatize around the native guanine ligand and its interactions in the HCV IRES domain IIa RNA switch binding pocket. The benzothiadiazine ligands are straightforward to synthesize and compounds with comparable binding interactions to the benzimidazole initial hit ligand show a better affinity for

the pocket, likely due to the space filling interaction that is absent in the benzimidazole binding interaction. Derivatives of these compounds have been made to eliminate important hydrogen bonding interactions, giving us further evidence that these compounds do bind in the same way to the pocket as the benzimidazoles. Various derivatives of the benzothiadiazines have been synthesized and tested in the FRET assay, and routes that are ineffective have been observed and attempted to be bypassed. The derivatives that have been made have been tested, but the compounds synthesized did not appear to increase the binding affinity, and many had solubility issues that either precluded testing in the FRET assay and/or made purification very difficult. With this, exploring other fragments to explore the impact of different scaffolds on binding became the focus of this research.

Chapter 2, in part, is currently being prepared for submission for the publication of the material. Frauman, Walter; Walsworth, Kevin; Hermann, Thomas. The dissertation author was the primary investigator and author of this material.

CHAPTER 3

Chapter 3: Alternative Ligand Scaffolds

3.1 Benzothiadiazines as a Ligand for Targeting the HCV IRES Domain IIa RNA Switch

When thinking about shifting the scaffold for testing other fragments for binding to the RNA switch, benzothiadiazapines and benzodithiadiazapines were an interesting modification from the benzothiadiazines discusses previously. Benzothiadiazapines, while more recently explored than the related benzodiazapines, are a common and useful scaffold in medicinal chemistry, and are found in a number of approved drugs and bioactive molecules[41]. For our purposes, the most interesting of these benzothiadiazines are those incorporating sulfonylamide groups, like our benzothiadiazines. The 7 membered rings also have the added benefit of potentially breaking planarity at more than just the sulfonylamide substituent. Compounds in the literature include pyrrolobenzothiazepine compounds that incorporate sulfonamide fragments have been shown to be inhibitors of the HIV-1 reverse transcriptase, while Ziresovir, another benzothiadiazapine with a sufonylamide fragment, has shown good antiviral activity against respiratory syncytial virus (RSV), and is currently in clinical trials[42–44]. With these examples and our benzothiadiazine compound as inspiration, schemes were devised to access fragments of interest.

3.2 Synthetic Attempts for Synthesis of Benzothiadiazapines and Benzodithiadiazapines

The two basic scaffolds of interest are seen in Figure 3.1. They are designed around the similar structures of the previously synthesized benzothiadiazines. The disulfonamide scaffold is particularly interesting due to the fact that a non-substituted derivative could potentially bind the same in the pocket with either sulfonamide accessing the back portion of the pocket. A scheme was devised (Scheme 3.1) for the synthesis of the disulfonamide scaffold (29) through direct cyclization with guanidine and guandine derivatives. With this step, there is a likelihood of synthesizing the 5 membered substituent instead, so also proposed was the synthesis through substitution to the disulfonylamide compound (31) with an ammonia reagent. The compound (31) is then proposed to be cyclized through either the guanidinium carbonate melting reaction discussed previously or cyanogen bromide cyclization to get the non-substituted compound.

Multiple attempts were made at direct cyclization with guanidine and guanidine derivatives, with a variety of reaction conditions (scheme 3.2) but these reactions did not produce the desired compounds (29). With these results, as well as with the likelihood that any cyclization would probably prefer the 5-membered ring, a different scheme for synthesis of these 7-membered rings was needed. The next method attempted was to convert the disulfonyl chloride compound (30) directly to the disulfonylamide (31), similarly to how this was accomplished with the benzothiadiazines (scheme 3.1). Unfortunately, this reaction instead produced a cyclization to compound 33, the 5-membered ring (scheme 3.3). With these direct methods being unable to produce the benzodithiadiazapine, another method needed to be found. Reviewing the literature, we found an alternative set of reactions to undergo the substitution from compound 30 (the disulfonyl chloride) to compound 31 (the disulfonamide). The scheme (Scheme 3.3) involves first reacting with the sulfonyl chlorides with tert-butylamine, which likely provides enough steric

hindrance to prevent the intramolecular cyclization and produces the ditert-butylamine (34) in good yield. The alkyl group is then cleaved using boron tribromide, resulting in the production of compound 31 in 70% yield over two steps, with a facile workup. Cyclization was then attempted multiple times with this compound (Scheme 3.5), but was unsuccessful thus far in producing the compound of interest (compound 32).

For the monosulfonamide scaffold (compound 28), direct cyclization from the sufonyl chloride was not possible from commercially available compounds. We needed to be able to install a benzylic functional group (preferably an amine) at the ortho position to the sulfonyl chloride, similar to the benzothiadiazine pathway. With the benzylic functional group, cyclization and deriviatization could produce the monosulfonamide 7-membered ring compounds. The first attempt at this was through O-methyl compounds, which were treated with NBS in a variety of conditions (Scheme 3.6) to try to add a benzylic bromine to the methyl group. A variety of starting reagents were tried, and a number of different NBS conditions were attempted, but no products appeared to form through this method. From there, another method for functionalizing the benzyl position was needed, and we attempted this through the reduction of a cyano substitutent at the 2 position. Based on review of the literature, a borane-tetrahydrofuran complex ($BH_3 \cdot THF$) was adapted from ref[45], but did not show conversion to the product of interest, or anything besides the starting material (Scheme 3.7).

An alternative Pd/C reduction was attempted, adapting procedures from refs[46,47]. This reaction initially produced little expected product, and had a side reaction where the benzylamine cyclized after being formed, turning into compound 36. This compound was purified, and a crystal structure was solved for it (Figure 3.2). Compound 36 was then tested in our FRET assay, and as expected did not show affinity for the target, due to a lack of guanidinium fragment. The Pd/C

reaction was optimized (Scheme 3.7) but was not able to produce high yields, even with high catalyst loading. Therefore, we explored alternative reduction methods in an attempt to synthesize the benzylamine.

The next attempt at reduction of compound 34 was using a lithium aluminum hydride (LAH) solution in THF (Scheme 3.8). This procedure was loosely adapted from ref[48]. This reaction was able to produce high yields and purity of the product (compound 35). Cyclization reactions were then attempted with compound 25 (from the LAH reduction as well as small quantities isolated from the Pd/C reduction) using the methods described in scheme 3.5. These reactions did not produce the desired cyclized product (compound 28, R=H).

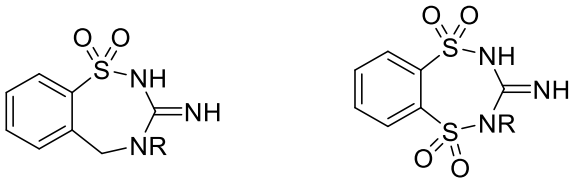

28 29

Figure 3.1 Benzothiadiazine (28) and benzodithiadiazine (29) scaffolds of interest for synthesizing and derivatizing.

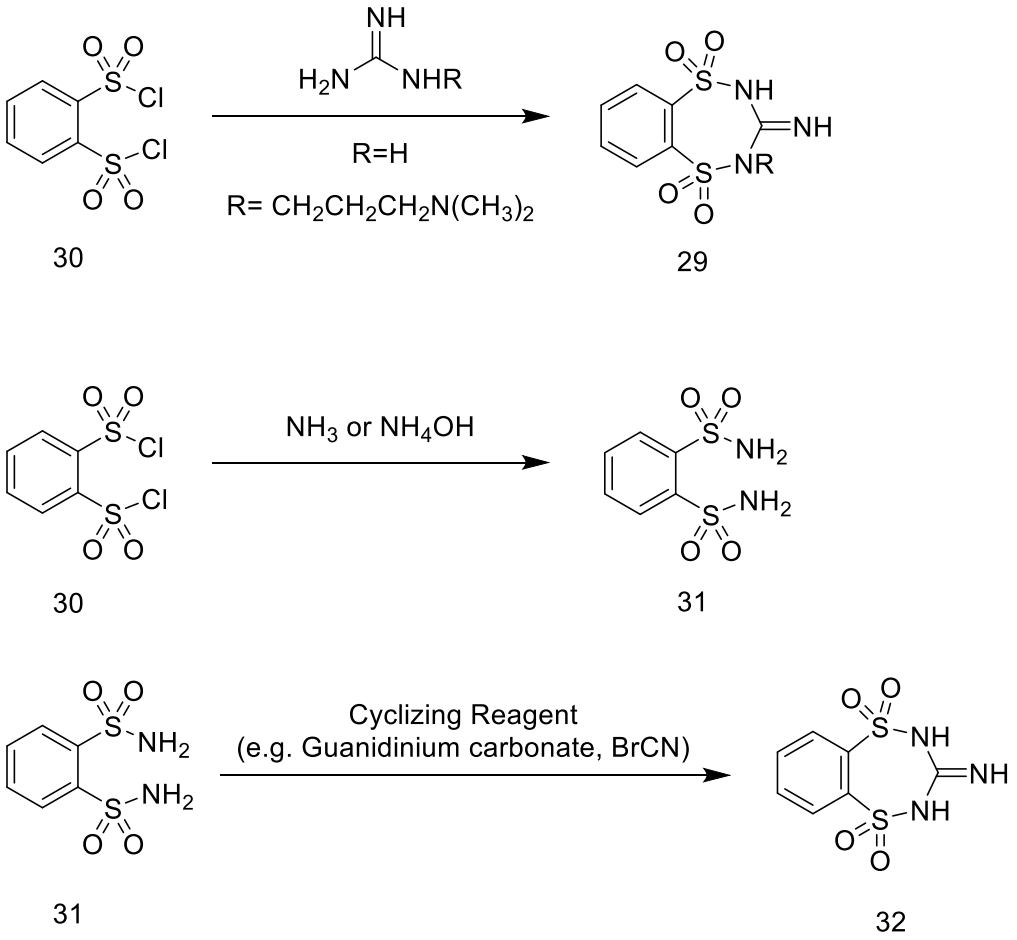

Scheme 3.1 Proposed scheme for synthesis of the dimethylaminopropyl scaffold (29), using either direct cyclization with the disulfonyl chloride or producing the disulfonylamide and cyclizing in the next step.

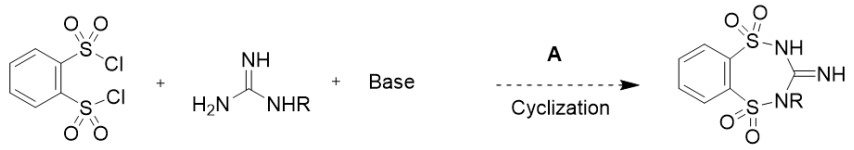

30 29

Rxn	R	Base (in excess)	Solvent	Temp. Reaction A (°C)	Reaction Time (A) (hrs)	Major Resulting compound
1	R=H (HCl Salt)	K_2CO_3	THF	0 to RT	16	Addition of guanidine to both sulfonyls
2	R=H (HCl Salt)	TEA	THF	0 to RT	16	Disulfonic Acid
3	R=H (HCl Salt)	K_2CO_3	Toluene	0 to RT	16	Unknown compound
4	R=H (HCl Salt)	TEA	DMF	RT	60	O-Benzenedisulfonimide and Disulfonic acid
5	$R=CH_2CH_2CH_2N(CH_3)_2$	K_2CO_3	THF	0 to RT	16	Unknown compounds
6	$R=CH_2CH_2CH_2N(CH_3)_2$	K_2CO_3	DMF	0 to RT	16	Disulfonic acid and it's Na/K salts
7	$R=CH_2CH_2CH_2N(CH_3)_2$	K_2CO_3	DMF	0 to RT	16	Unknown Compounds
8	$R=CH_2CH_2CH_2N(CH_3)_2$	TEA	DMF	0 to RT	48	Disulfonic acid
9	$R=C(=O)CH_3$	TEA	THF	RT	48	Solid and filtrate show product

Scheme 3.2 Attempted cyclization reactions of disulfonyl chloride (30) to the benzodithiadiazapine compound of interest (29).

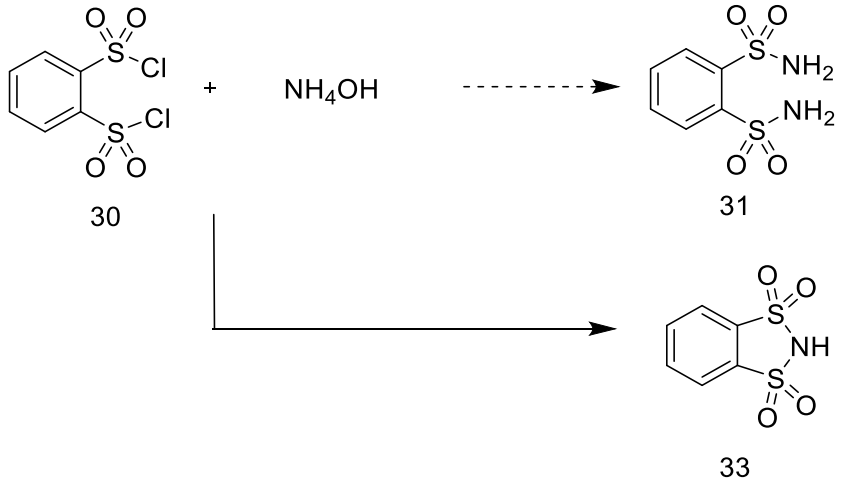

30 31 33

Scheme 3.3 Attempted transformation of the disulfonyl chloride (30) to the disulfonamide (31). The reaction did not go as planned, and compound 33 was the resulting product instead.

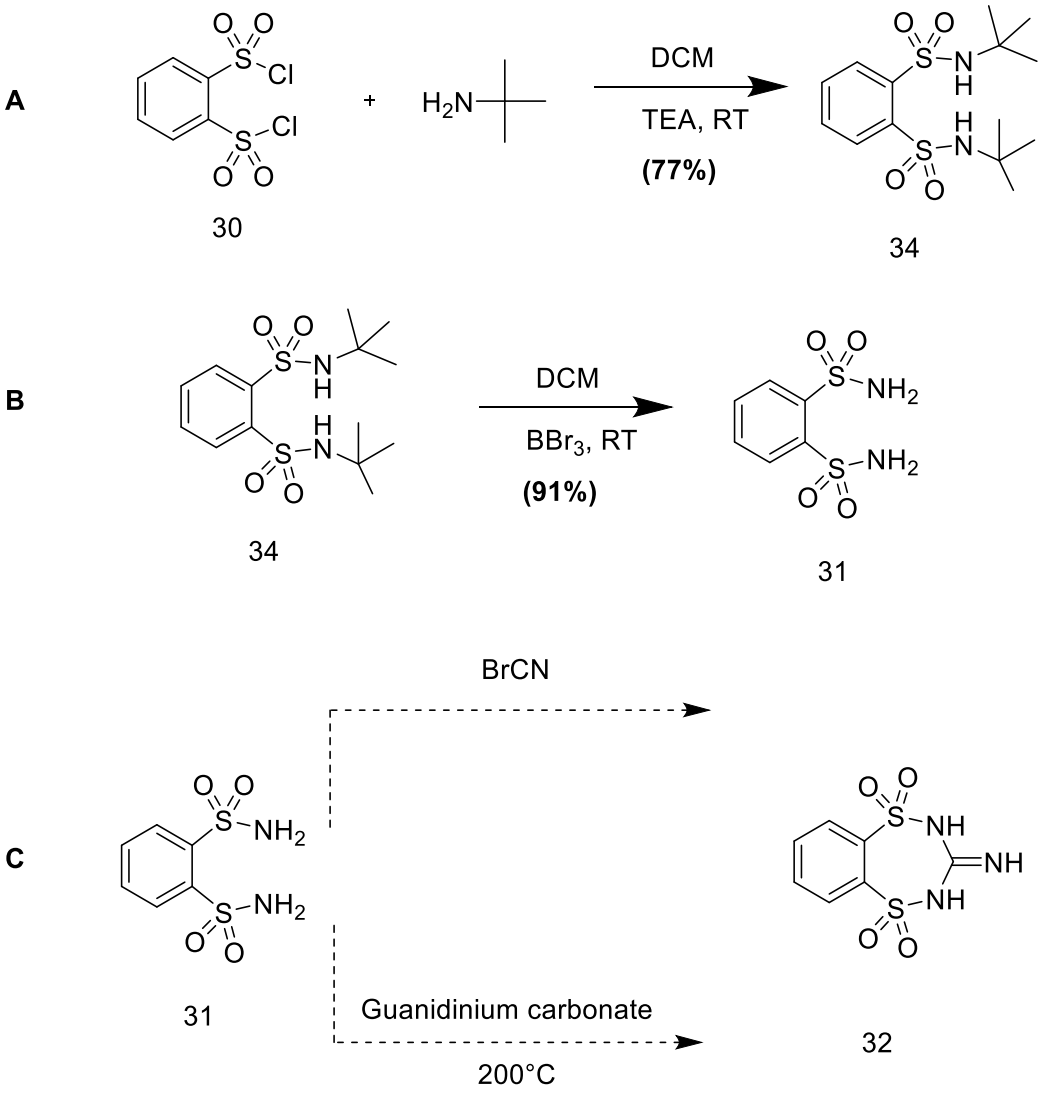

Scheme 3.4 Alternative synthetic scheme to access compound 31. A) Substitution of the sulfonyl chlorides to tert-butyl sulfonylamides. B) Boron tribromide dealkylation of tert-butyl group. C) Attempted cyclization reactions (not full extent of conditions attempted). Reaction conditions for steps 1 and 2 taken from ref[46].

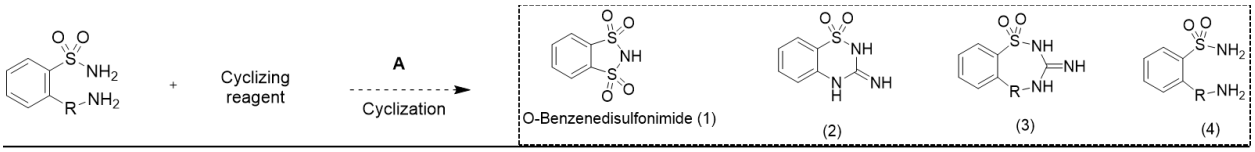

Rxn	R	Cyclizing reagent	Base (A)	Solvent (A)	Temp. Reaction A (°C)	Reaction Time (A) (hrs)	Major Resulting compound (determined by mass spectrometry)
1	$R=S(=O)_2$	Guanadinium Carbonate	N/a	N/a	200	3	Mixture of 1, 2, and 3 plus other compounds
2	$R=S(=O)_2$	Guanadinium Carbonate	N/a	N/a	210	3	Compounds 1 and 4
3	$R=S(=O)_2$	BrCN	TEA	THF/ACN	0 to RT	16	Mixture of 3, 4, and 1
4	$R=S(=O)_2$	1H-pyrazole-1-carboximidamide	TEA	THF	75	22	Only SM (4)
5	$R=S(=O)_2$	1H-pyrazole-1-carboximidamide Hydrochloride	TEA	MeOH	0 to RT	16	Mostly SM (4) and other compounds
6	$R=S(=O)_2$	Guanadinium Carbonate	N/a	N/a	210	7	Unknowns
7	$R=S(=O)_2$	BrCN	N/a	THF	0 to RT	330	SM (4)
8	$R=CH_2$	BrCN	N/a	ACN	0 to RT	24	SM (4)
9	$R=CH_2$	BrCN	N/a	ACN	0 to RT	48	SM (4)
10	$R=CH_2$	BrCN	TEA	MeOH/ACN	0 to RT	72	Potentially MeOH adduct of (3), mostly unknown
11	$R=CH_2$	BrCN	TEA (Before BrCN)	THF	0 to RT	72	Possible (3), mostly diaddition of CN and SM (4) and unknown
12	$R=CH_2$	BrCN	TEA (After BrCN, followed by more BrCN)	THF	0 to RT	12	Some slight conversion (3) but mostly unknowns
13	$R=CH_2$	BrCN	$NaHCO_3$	THF	0 to RT	16	Unknown higher mass compound
14	$R=CH_2$	BrCN	$NaHCO_3$	THF	0 to RT	48	Unknown compounds
15	$R=CH_2$	BrCN	N/a	THF/MeOH	RT	48	Unknown compounds
16	$R=CH_2$	1H-pyrazole-1-carboximidamide Hydrochloride	TEA	MeOH	65	48	Unknown compounds
17	$R=CH_2$ (crude)	Guanadinium Carbonate	N/a	N/a	180	2	Largely unreacted benzylcyanide compound, some conversion to (3)
18	$R=CH_2$	Guanadinium Carbonate	N/a	N/a	200	3	Mostly SM (4), possible hydrate of product (3)

Scheme 3.5 Attempted cyclization reactions of mono and disulfonylamide starting materials to attempt to form the 7 membered ring. Reactions 1 through 7 are the disulfonylamide attempts (using compound 31) and reactions 8 through 18 are the cyclization reactions of the monosulfonamide and 2-benzylamine (compound 35 from scheme 3.7).

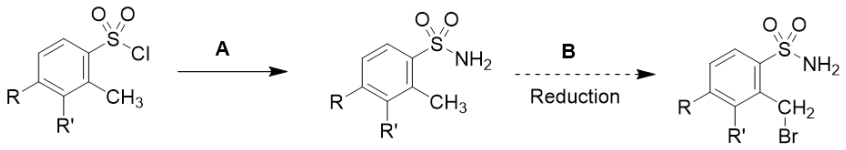

Rxn	R/R'	Reagent Reaction A	Temp. Reaction A (°C)	Reaction Time (A) (hrs)	Reagent(s) Reaction B	Solvent (B)	Temp. (B) (°C)	Reaction Time (B) (hrs)	Resulting compound
1	R=H, R'=H	(starting with sulfonamide)	N/a	N/a	NBS/AIBN	ACN	80	5	SM
2	R=H, R'=H	(starting with sulfonamide)	N/a	N/a	NBS/AIBN	Toluene	90	2	SM/Unknown
3	R=Br, R'=H	NH_4OH	0	16	NBS/AIBN	ACN	60	3	SM
4	R=Br, R'=H	NH_4OH	0	16	NBS/AIBN	ACN	60	120	Unknown Br addition
5	R=Br, R'=H	NH_4OH	0	16	NBS/AIBN/ $AlCl_3$	Toluene	90	12	Unknown
6	R=Br, R'=H	NBS/AIBN/ACN	80	72	NH_4OH	ACN	0	12	Unknown Br addition
7	R=H, R'=Cl	NH_4OH	0	16	NBS/AIBN	ACN	80	150	Unknown

Scheme 3.6 Attempted benzyl bromination of a variety of toluene 2-sulfonyl compounds. Reaction 1 and 2 were run with 2-methyl benzenesulfonamide, Reactions 3 to 6 were run with 4-bromo-2-methylbenzenesulfonyl chloride. Reaction 7 was run with 3-chloro-2-methylbenzenesulfonyl chloride. None produced the product of interest, resulting compounds labelled "SM" returned the starting sulfonylamide compound for that step.

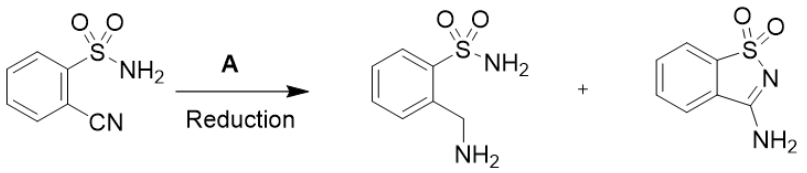

34 35 36

Rxn	Reduction Reagent	Solvent	Additional Reagents/ Conditions	Temp. Reaction A (°C)	Reaction Time (A) (hrs)	Resulting compound
1	BH_3·THF	DMF	N/a	RT	4	34
2	BH_3·THF	DMF	Sealed tube	RT	4	34
3	BH_3·THF	DMF	Sealed tube	55	48	34
4	10% Pd/C, H_2	MeOH	4M HCl	RT	12	Mostly 36, Some oxidized 36, Some 34, Slight amount product
5	10% Pd/C, H_2	MeOH	4M HCl	RT	4	34
6	10% Pd/C, H_2	MeOH	4M HCl	RT	19	Mostly 34, Some 35
7	10% Pd/C, H_2	MeOH	4M HCl, more H_2 balloons	RT	27	Still contains 34, 35 isolated (53% yield)
8	10% Pd/C, H_2	MeOH	4M HCl, H_2 balloons bubbling into solution	RT	16	Mostly 34, 35 extracted and isolated (33 % yield)
9	10% Pd/C, H_2	MeOH	4M HCl,	RT	60	Mostly 34, 35 isolated (27% yield)
10	10% Pd/C, H_2	MeOH	4M HCl Balloons replaced and left overnight	RT	36	Mostly 34, 35 isolated (13% yield)

Scheme 3.7 Attempted reductions of 2-cyanobenzenesulfonamide (34) with a variety of reducing agents. Reactions 1-3 were run in conditions adapted from ref[45]. Reactions 4-10 were adapted from refs[47,49].

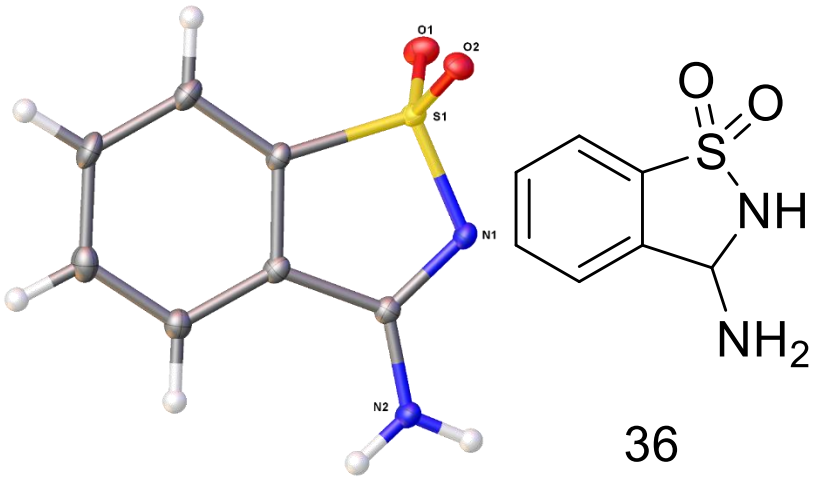

Figure 3.2 Crystal structure of compound 36. With structure.

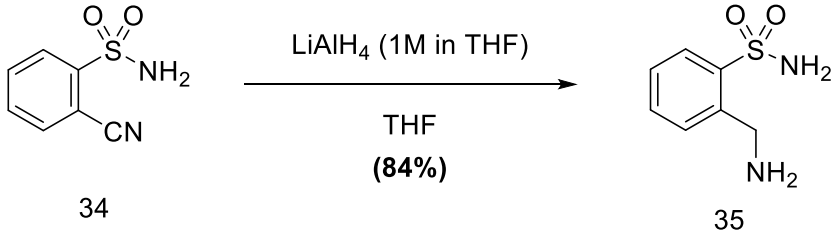

Scheme 3.8 Successful and high yielding reduction of 2-cyanobenzenesulfonamide (34) with Lithium Aluminum hydride (LAH) in THF. Reactions was run in conditions adapted from ref[48].

3.3 A Unique, Facile Saccharin Insertion Ring Opening Reaction for Accessing Certain Benzothiadiazapines and Benzodithiadiazapines

While attempting the cyclization of the benzothiadiazapines and benzodithiadiazapines from section 3.2, we discovered a novel pathway for accessing benzothiadiazapines with a guanidine substituent through a saccharin ring opening reaction[50]. This reaction, a reflux of

saccharin and a carbodiimide species is a one-step ring opening reaction that transforms the 5-membered ring of saccharin into a 7-membered benzo[1,2,4]thiadiazapine compound (Scheme 3.9). This reaction is high yielding, and works for a broad variety of carbodiimide species, with the only cyclization issues coming from more sterically hindered carbodiimides, such as di-tertbutylcarbodiimide (DTBC). The previous work in the literature had explored this reaction with a small selection of carbodiimides, but there were many that were of interest to this work that had not yet been tested and synthesized.

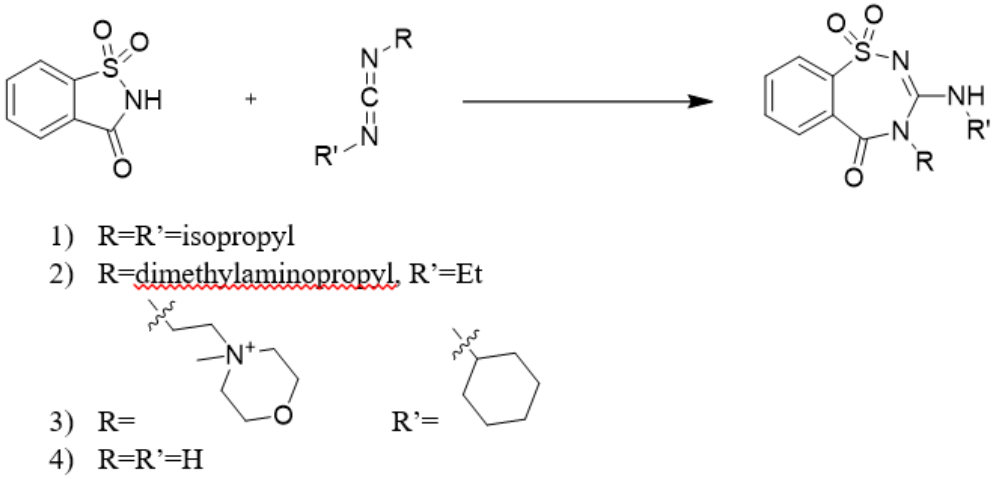

Scheme 3.9 Saccharin ring opening reaction of run with a variety of carbodiimide compounds. Reaction 1 was conducted in ref[50] and resynthesized here through overnight acetone reflux. Reaction 2 was conducted using commercially available 1-Ethyl-3-(3-dimethylaminopropyl)carbodiimide (EDC) through overnight acetone reflux. Reaction 3 was conducted using commercially available 1-cyclohexyl-(2-morpholinoethyl)carbodiimide metho-p-toluene sulfonate (CMC) through overnight acetone reflux. Reaction 4 was run with cyanamide, as it is a tautomer of methanediimine, originally with an overnight acetone reflux, and then at harsher conditions to encourage tautomerization. All reactions were run in conditions adapted from ref[50].

We were interested in testing the usefulness of this reaction with carbodiimides that could potentially produce products that were similar to the goal benzothiadiazapine scaffold or for precursors that could be modified in a way that approaches that benzothiadiazapine scaffold. We

ran this reaction successfully with *N*,*N'*-diisopropylcarbodiimide (DIC), as they had in the paper, and successfully synthesized the diisopropyl product (Reaction 1, Scheme 3.9). This compound (37) was tested in the FRET assay and showed an EC_{50} of 100 μM, similar to that of the spirocyclopropyl compound (5). This reaction was also run with 1-(3-Dimethylaminopropyl)-3-ethylcarbodiimide (EDC), to determine how an asymmetric carbodiimide would behave in this reaction. The product of this reaction was purified by column chromatography and the structure solved by x-ray crystallography. We found that a single structural isomer formed with the ethyl group substituted on the exocyclic nitrogen (Figure 3.4). This compound (38) was tested in the FRET assay and showed an EC_{50} of 160 μM, slightly worse than compound 37, surprisingly. The assumption when synthesizing this compound was that the dimethylaminopropyl substituent could potentially bind similarly to the interactions seen previously in the benzimidazole ligand (1). Compound 39 was also produced, through reaction with 1-cyclohexyl-(2-morpholinoethyl)carbodiimide metho-p-toluene sulfonate (CMC), but the compound precipitated when tested in the FRET assay and an EC_{50} was not able to be determined. Further attempts were made to synthesize a non-substituted version, by attempting to react with the minor tautomer of cyanamide in solution, and work on this method is ongoing, with initial crude mass spectra having peaks that would correspond with the product peak.

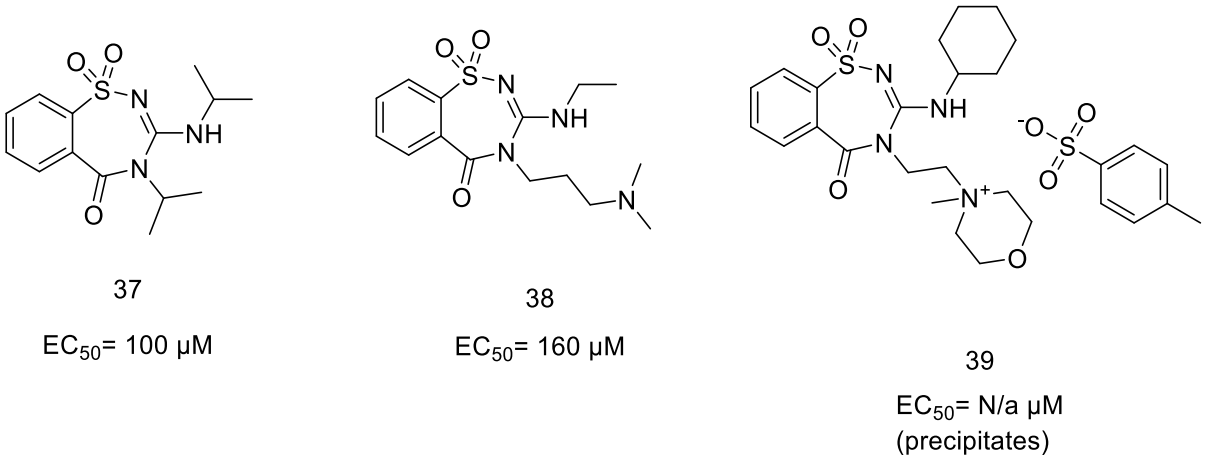

Figure 3.3 Benzothiadiazapines synthesized through the saccharin and carbodiimide ring expansion reaction that were tested by FRET assay. EC_{50} of the compounds is included, when it could be determined.

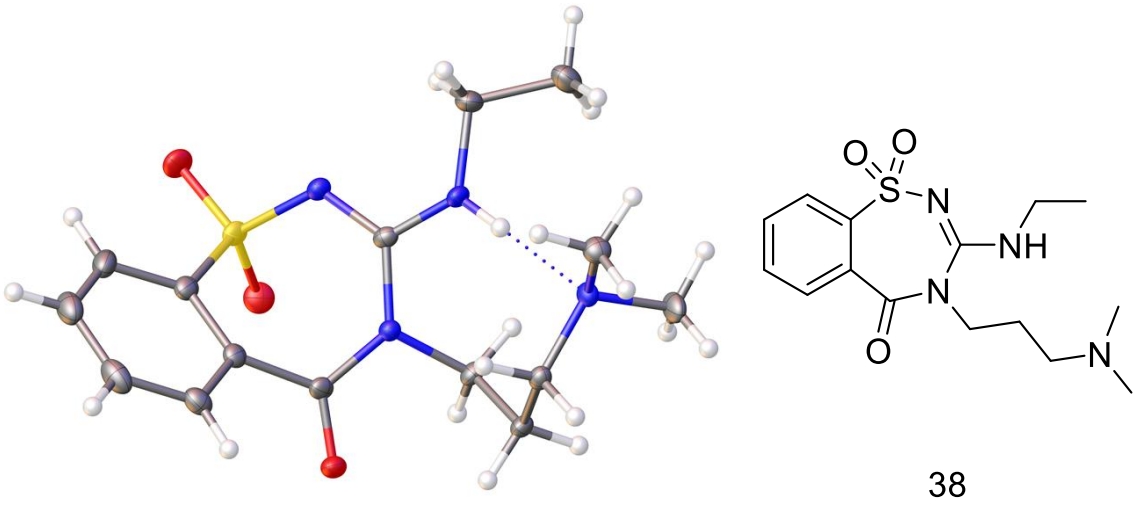

Figure 3.4 Crystal structure of compound 38, the product of scheme 3.9 reaction 2. The crystal structure shows that the ethyl group is located on the exocyclic nitrogen as seen in the drawing of the compound.

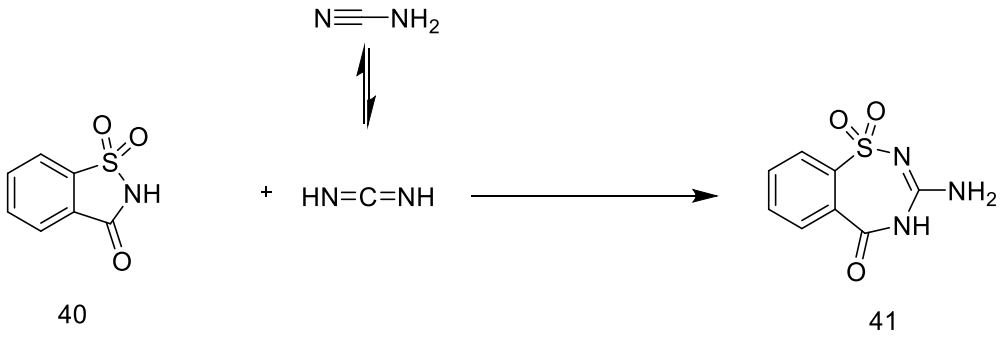

Scheme 3.10 Proposed mechanism for saccharin ring opening reaction with *in situ* tautomerization of cyanamide to methyldiimine. Idea was derived from refs[51,52].

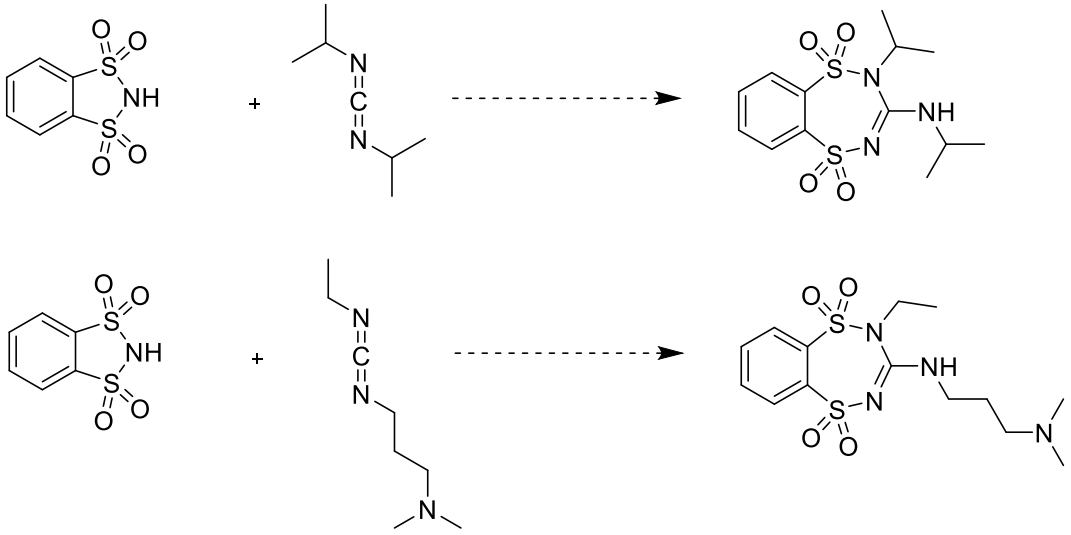

Scheme 3.10 Attempts at modifying this reaction using o-benzenedisulfonimide as the initial 5 membered ring. Run under the same conditions as 37-39 (acetone reflux overnight). Did not prove successful, giving insight that the carbonyl is vital to the reaction to proceed.

3.4 Synthesis of 1,2-dihydro- I-hydroxy-2,4,1-benzodiazaborine

Having testing several potential HCV IRES domain IIa RNA switch ligands, we discovered two distinct types of functional groups that access a previously unknown portion of the ligand binding pocket. The first group is the nonpolar spirocyclopropyl group, which showed improved affinity through space filling interactions. The remainder of the compounds tested have carbonyl or sulfonyl groups arranged so as to interact in that region. The carbonyl and sulfonyl groups being

hydrogen bond acceptors, we were curious about the impact of a hydrogen bond donor in this pocket instead. Therefore, we attempted the synthesis of compound 43, but all attempts at direct cyclization with the starting 2-(aminophenyl)boronic acid proved to be unsuccessful, so another path for synthesis was required (Scheme 3.11).

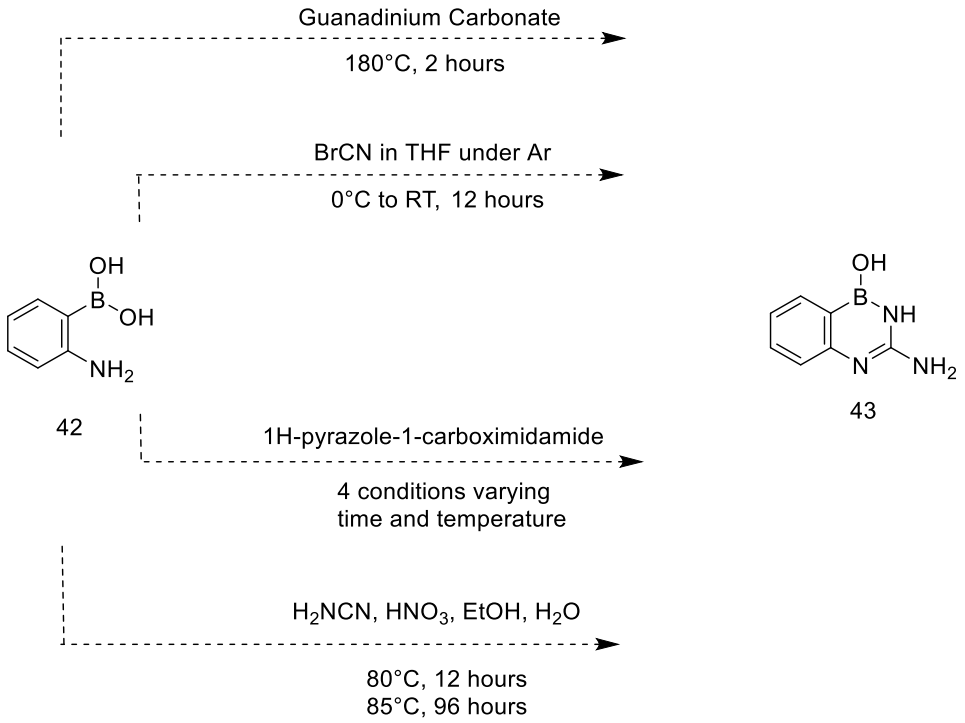

Scheme 3.11 Attempts at direct cyclization of (2-aminophenyl)boronic acid (compound 42) to the desired 3-aminobenzo[c][1,5,2]diazaborinin-1(2H)-ol product (43). These conditions were not successful, requiring an alternative pathway.

In the literature, we found a route to compound 43 (Scheme 3.12) and carried out the synthetic route[53,54]. Using this route, we were able to synthesize compound 46 in high yields and purity through the three previous steps. The reference mentioned that the last catalytic hydrogenation step produced the compound we wanted (43) only as a side product, but we were hopeful that it would be able to be isolated and tested. Unfortunately, the only compound that

could be isolated and purified from the final step, despite many attempts, was compound 47. Alternative routes to create 43 are still in progress in our lab.

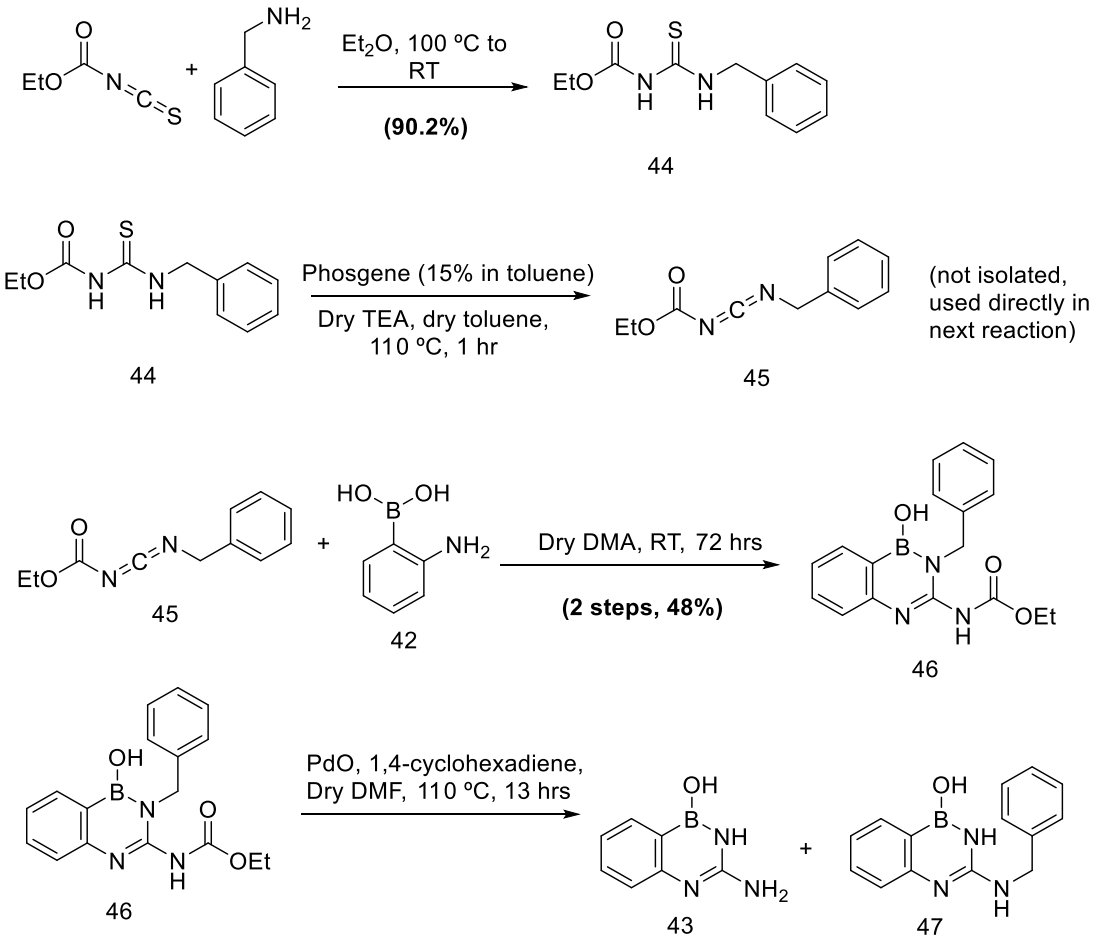

Scheme 3.12 Alternative route to transform (2-aminophenyl)boronic acid (compound 42) to the desired 3-aminobenzo[c][1,5,2]diazaborinin-1(2H)-ol product (43). The final step lead to a mixture of the compounds, and only compound 47 was able to be successfully isolated. This pathway was adapted from refs[53,54].

3.5 Synthesis of 3-Amino-1,2,4-benzotriazine 1-oxide

Another interesting substitution we wanted to pursue was adding a more polar group in the binding pocket. To do this we, adapted a previously published route to 3-amino-1,2,4-benzotriazine-1-oxide. This compound (49) has an oxide pointing into the pocket, introducing negative charge to see how that impacts binding. The reaction is a one pot, multi-step synthesis

and the compound was recrystallized afterwards from isopropanol. One attempt at this reaction erroneously ran long, resulting in the diaddition of the cyanamide and another fortuitous compound of interest (50). Both compounds were tested in the FRET assay, but neither showed affinity to the target and we were not able to determine an EC_{50} for either of them, likely showing that the oxide is likely not a beneficial substituent, and could potentially even negatively impact binding with the RNA switch mechanism.

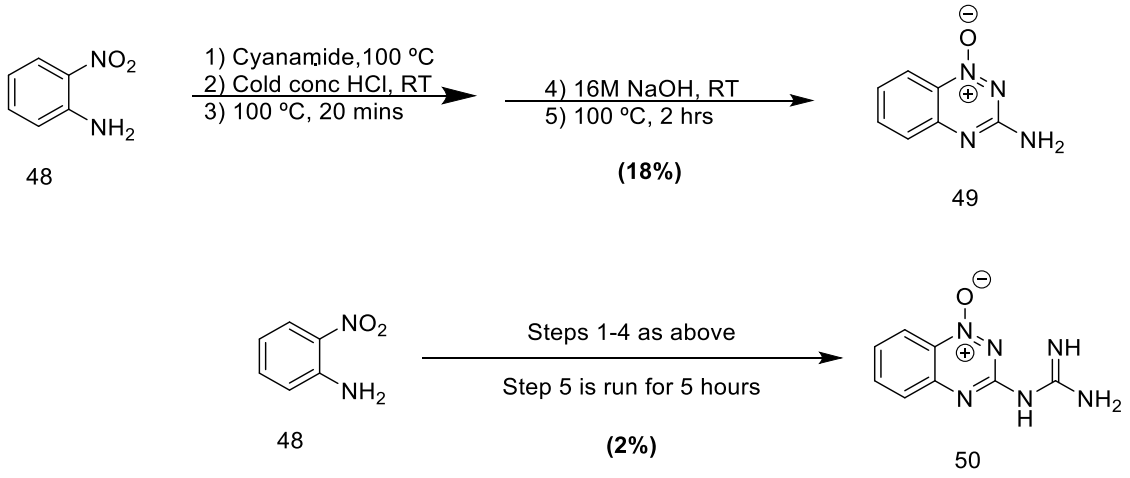

Scheme 3.13 One pot multistep synthesis of 3-amino-1,2,4-benzotriazine-1-oxide (49). This reaction was run too long erroneously in one attempt and the diaddition of the cyanamide was observed on the exocyclic nitrogen (50). Neither compound showed binding in the FRET assay. This pathway was adapted from ref[55].

3.6 Hydrazine addition to quinazoline-2,4-diamine[56] and 2,4-dichloroquinazoline[57]

A final scaffold attempt was that of a direct mono or dihydrazine addition to quinazoline derivatives. Two routes were proposed, one for monoaddition of the hydrazine to quinazoline-2,4-diamine (51) and one for diaddition to the 2,4-dichloroquinazoline (53). The routes are shown in scheme 4.4 and adapted from refs[56,57]. Compounds 52 and 54 were not able to be isolated, and with the arrangement of the double bond limiting the viability of the guanidinium binding, further attempts at synthesis were not conducted.

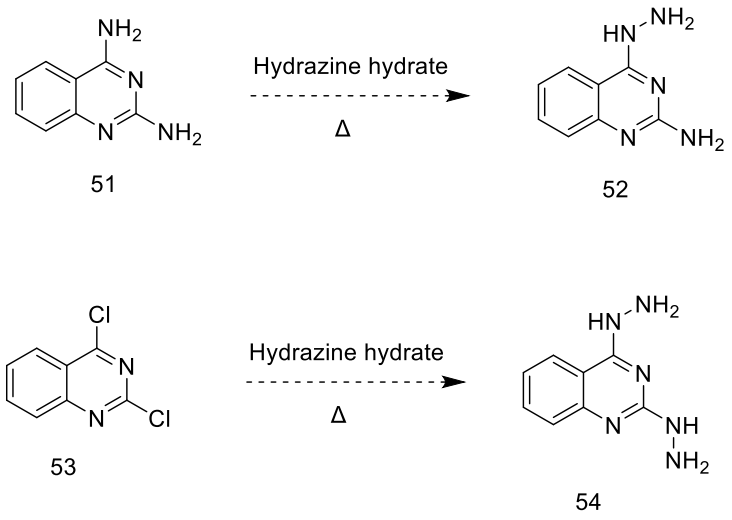

Scheme 3.14 Synthetic routes for monoaddition of hydrazine hydrate to quinazoline-2,4-diamine (51) and for diaddition of hydrazine hydrate to 2,4-dichloroquinazoline (53). Reactions were adapted from refs[56,57].

3.7 Conclusions

In conclusion, while the comparable benzothiadiazapine and benzodithiadiazapine ligands for direct comparison with the benzothiadiazine hit ligands were not successfully synthesized, many advances have been made on these pathways. We have gotten to the point where the penultimate precursors of these compounds are accessible and have improved the yields and methods to get to these precursors. Cyclization attempts did not yield the products we want, but with these advances it should allow for easier access to attempt this in future studies. Meanwhile, a route to access benzothiadiazapines through a saccharin ring opening reaction with carbodiimides has been explored and derivatives created through this process were tested and showed binding affinity to the RNA switch on our FRET assay. This pathway also appears to be a fruitful mechanism to synthesizing derivatives of these compounds.

The other compounds in this section were synthesized in an attempt to modify the substituent that replaces the carbonyl and determine what impact differently polar and differently hydrogen bonding substituents would have on the binding in the back region of the pocket. The oxide compounds (49 and 50) appeared to negatively impact the binding, the benzodiazaborine compound (43) was unable to be successfully synthesized, but the pathway was confirmed and alternative routes to the compound are in progress in the lab.

Chapter 3, in part, is currently being prepared for submission for the publication of the material. Frauman, Walter; Walsworth, Kevin; Hermann, Thomas. The dissertation author was the primary investigator and author of this material.

CHAPTER 4

Chapter 4: Conclusions

4.1 Compounds synthesized and Conclusions

In this thesis, compounds have been synthesized and tested to explore small molecule interaction at a ligand binding pocket of the HCV IRES domain IIa RNA switch. The RNA switch is a highly conserved region of the viral genome, and provides a unique target for small molecules within the native ligand binding pocket. Other RNA switches have been found in different viral IRESes, and exploring the binding pocket of this HCV RNA switch gives more insight into the RNA switch as a potential drug target. In this work, we have focused on exploring a specific region of the binding pocket that is visible in the previously determined crystal structure of an RNA-ligand complex, but not accessed by previously tested benzimidazole ligands. This was done through the combination of testing compounds that accomplish space filling effects, similar to those of the spirocyclopropyl compound, compounds that expand the possible space and potentially introduce more non-planarity through the formation of 7-membered rings, as well as compounds that have different polar functionalizations, to better understand the intricacies of this binding pocket. The compounds that show the best affinity for the binding pocket are benzothiadiazine derivatives (9 and 11) that fill this space in the binding pocket with a nonplanar, polar sulfonyl group. These compounds are straightforward to synthesize, over a minimal number of steps and with good yield, and therefore can be a potential jumping off point for further studies attempting to improve inhibition of the HCV RNA IRES driven translation. Other compounds, such as the benzotriazine oxides (49 and 50) have shown that their scaffolds are not as optimal for binding to the pocket. The benzothiadiazapene compounds (37 and 38) have shown weaker

affinity, but with the arrangement of the bulky alkyl groups on the molecule, this affinity still is interesting in the context of the binding of the 7-membered ring scaffolds. Other compounds suffered from poor solubility in the target binding assay and would need further derivatization to increase aqueous solubility and determine the impact of the groups that have been installed, in a sort of scaffold-hopping way, for the purposes of evaluating binding impact. Testing of the compounds' target binding in the FRET assay helps to determine the properties and derivatization sites available for future improvements on space filling and binding in the RNA pocket. Some of these compounds tested have also helped to eliminate potential derivatives. With this work we have also taken steps towards various pathways to modifications of some of the better binding compounds, and those steps could be expanded upon to further modify and improve the binding of those compounds. Other compounds have been optimized to the penultimate precursor, with synthetic routes improved. While the many attempts at cyclization have not to this point been successful, this will allow for future research to more easily access these precursors to find routes to derivatize and cyclize these compounds. With this work, we have provided the initial structures to potentially provide a small molecule inhibitor of the HCV IRES target with a stronger binding affinity required for lead compounds towards the development of antiviral therapeutics. We have also helped expand upon the knowledge of this RNA binding pocket found in this novel RNA switch mechanism, which is potentially applicable to the broader range of RNA switches found in other viruses.

APPENDIX

Appendix: Experimental Methods and Spectra

Experimental Methods

Pharmacokinetic Studies on Benzothiadiazine Compounds 9 and 11

1.9 mg compound 9 was dissolved in 1 mL PBS buffer, and 1.6 mg compound 11 was dissolved in 6 mL PBS buffer. The samples were left at ambient temperature in indirect sunlight and aliquots were taken at time intervals of 0 mins (T0), 80 mins (T80), 6 hours 10 minutes (T610), 24 hours (T24). The samples were checked for degradation, which did not occur within 24 hours. 3.9 mg compound 9 was dissolved in 5 mL ACN to determine solubility. 4.8 mg compound 9 was dissolved in 9 mL PBS (0.533 mg/mL) and 3.5 mg compound 11 was dissolved in 10 mL PBS (0.35 mg/mL). Both samples were filtered through 0.2 µm Nalgene syringe filters (25 mm Nylon Membrane). 1 ng, 0.1 ng, and 0.0 ng stock solutions of both samples were created from an original 10 ng stock solution. Mouse plasma solutions, obtained from a collaborator, were then spiked with their corresponding sample of 9, followed by 11. Samples were then vortexed for 90 seconds, followed by centrifuging for 5 minutes at 13.2x1000 RPM. The supernatant was removed, and 50 µL anhydrous ACN was added to the pellet and vortexed for 90 seconds. The solution was centrifuged for 5 minutes at 13.2x1000 RPM, and then the supernatants were added to the previously removed supernatant from the first vortex/centrifuge step. The final samples were spun in and dried using a speedvac system for 55 minutes on medium, then placed on dry ice. The compounds were dissolved in mouse plasma, and were detectable by mass spectrometry after extraction from the plasma (with a mouse plasma compound running at similar and slightly faster rate, showing small peak directly before sample peak). Study procedures adapted from ref.

2-nitrobenzenesulfonamide (7)

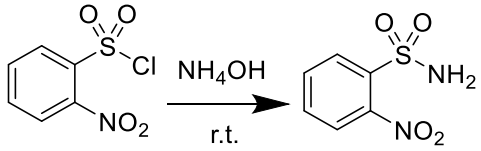

6 7

To a solution of 200mL concentrated NH_4OH, 22 g of 2-nitrobenzenesulfonyl chloride (992.7 mmol) was added and stirred overnight at room temperature. The solution was cooled to 0°C and concentrated HCl was added to lower the pH of the solution to ~2. A white precipitate formed which was filtered, washed with minimal cold H_2O, and then dried on vacuum. 25.51 g of crude product was isolated. MS (ESI-TOF) [m/z (%)]: 205 ($[M-H]^-$).

2-aminobenzenesulfonamide (8)

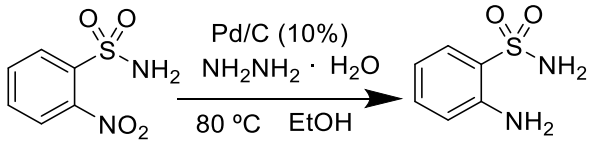

7 8

25.51g of crude 2-nitrobenzenesulfonamide (126.2 mmol) was dissolved in 200mL EtOH. 17 mL Hydrazine hydrate (350.4 mmol) was added to the flask, and 127 mg 10% Pd/C (1.2 mmol) was added slowly as a powder, and the solution was refluxed at 80°C overnight. The reaction was checked by TLC, revealing significant remaining starting material. Another 480mg of 10% Pd/C (4.5 mmol) was added, and the solution was refluxed for 2 more hours. Then, 256 mg more 10% Pd/C (2.4 mmol, total added was 8.1 mmol) was added and refluxed at 80°C overnight. Afterwards, H^1 NMR of the reaction solution showed significant conversion. The final product was rotovaped to a white crystalline solid. Water was added, and the solution filtered. The wet filtered precipitate was dried in the oven. Overall yield from reaction to form compound 7 and reaction to form compound 8=63%.

3-amino-4H-benzo[e][1,2,4]thiadiazine 1,1-dioxide (9)

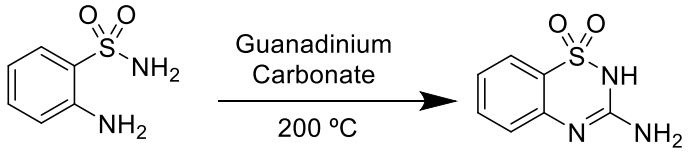

8 **(48%)** 9

These reaction conditions were adapted from a previously reported method[31]. In a thick vial 660 mg 2-aminobenzenesulfonamide (1 equivalent) and 414 mg of guanidine carbonate (1.2 equivalents) were added. The solution was heated in a solvent-free reaction at 220°C for 3 hours and then at 195°C for 3.5 more hours. Concentrated HCl was added to the white and black precipitate and left for 12 hours at room temperature. The precipitate was filtered off, and recrystallized in a 1:1:1 water:ethyl acetate:methanol mixture. A white precipitate was filtered off and dried overnight, with 106.4 mg being isolated. Yield=48%. MS (ESI-TOF) [m/z (%)]: 196 ($[M-H]^-$). ^1H NMR (400 MHz, DMSO): 10.71 (s, 1H), 7.65 (d, 1H), 7.52 (t, 1H), 7.23 (t, 1H), 7.15 (d, 1H) 6.96 (bs, 2H).

2-((3-(dimethylamino)propyl)amino)benzenesulfonamide (10)

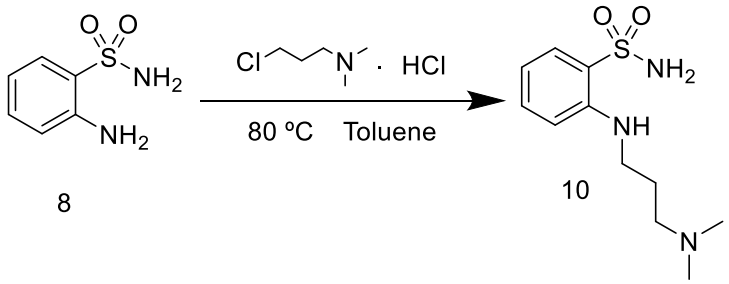

176.8 mg of 2-aminobenzensulfonamide (8) was added to a flask, along with 305 mg 3-chloro-*N*,*N*-dimethylpropan-1-amine hydrochloride. Then, 3 mL of toluene was added, and the flask was heated to reflux for an hour. TLC was used to determine the reaction progress. After the reaction was complete, the flask was left at room temperature overnight. The toluene was removed under reduced pressure and 1M NaOH was added. The compound was then extracted with EtOAc and the organic layer was dried overnight. Yield= 72%. ^{1}H NMR (400 MHz, DMSO): 7.60 (d, 1H), 7.33 (t, 1H), 7.26 (bs, 2H), 6.77 (d, 1H), 6.62 (t, 1H), 5.92 (bt, 1H), 3.17 (q, 2H), 2.28 (t, 2H), 2.11 (s, 6H), 1.70 (t, 2H).

3-amino-4-(3-(dimethylamino)propyl)-4H-benzo[e][1,2,4]thiadiazine 1,1-dioxide (11)

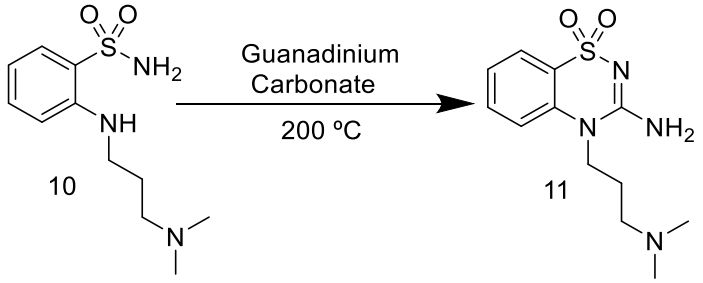

In a thick vial, 200 mg 2-((3-(dimethylamino)propyl)amino)benzenesulfonamide (0.777 mmol) and 98 mg guanidine carbonate (1.088 mmol) were combined. The mixture was stirred in a solvent free manner in a sand bath at 200°C for 48 hours. The reaction was taken off heat, water was added, and the solution was left overnight. Then, 1 mL concentrated HCl was added to the solution to allow the compound to dissolve fully. The compound was transferred to a new container and NaOH was added until the solution was basic, and then the solvent was removed under reduced pressure. The resulting product was washed and filtered with hot methanol and the solvent was removed under reduced pressure. The solid was then recrystallized from methanol, and vacuum filtered. 55.2 mg of precipitate was isolated. Total yield=55%. HRMS: (ESI-TOF) [m/z (%)]: 283.1226 ($[M+H]^{+}$) ^{1}H NMR (300 MHz, DMSO): 7.96 (s, 2H), 7.68 (dd, 1H), 7.60 (m, 1H), 7.45 (d, 1H), 7.31 (t, 1H), 3.97 (t, 2H), 2.23 (t, 2H), 2.12 (s, 6H), 1.79 (m, 2H). ^{1}C NMR (500 MHz, DMSO): 154.7, 137.7, 132.8, 126.3, 124.4, 123.3, 117.0, 55.3, 45.0, 44.3, 25.3.

2H-benzo[e][1,2,4]thiadiazin-3(4H)-one 1,1-dioxide (12)

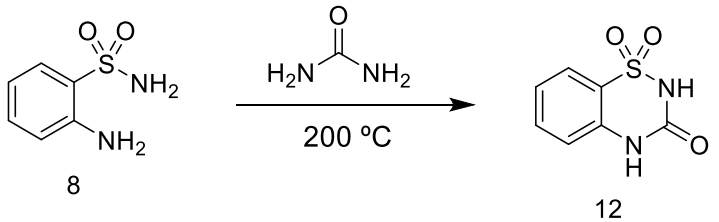

8 12

200 mg (1.16 mmol) 2-aminobenzenesulfonamide was added to a heat resistant tube, followed by 76.7 mg (1.28 mmol) of urea. The solids were reacted solvent-free by melting at 230°C for 6 hours. H_2O was added, followed by 1 mL HCl. The liquid was filtered off and 179.5 mg crude product was recovered. The crude product was recrystallized using IPA and 88.6 mg of pure compound was isolated. This was confirmed by ^{1}H NMR and mass spectrometry. The crystal structure was solved for the compound, and confirmed its identity (see figure 2.6). Yield=39%. MS (ESI-TOF) [m/z (%)]: 197 ([M-H]$^-$). ^{1}H NMR (400 MHz, DMSO): 11.18 (s, 1H), 7.76 (d, 1H), 7.62 (t, 1H), 7.24 (m, 2H).

4-(3-(dimethylamino)propyl)-2H-benzo[e][1,2,4]thiadiazin-3(4H)-one 1,1-dioxide (13)

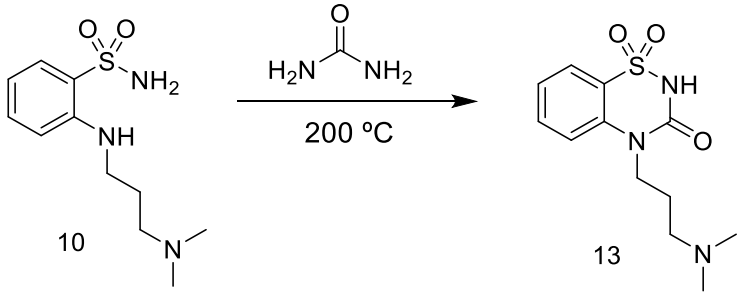

10 13

Added 499 mg (1.94 mmol) 2-((3-(dimethylamino)propyl)amino)benzenesulfonamide to heat resistant tube and heated at 170°C for 2 hours. Methanol was added to the resulting oil, and the methanol dissolved the starting material and any impurities leaving the product behind as a white crystal. The filtrate was removed and 121.0 mg of product (22% yield) was recovered. The product was confirmed by mass spectrometry. MS (ESI-TOF) [m/z (%)]: 284 ([M-H]$^-$). ^{1}H NMR (300 MHz, DMSO): 7.96 (s, 2H), 7.68 (dd, 1H), 7.60 (m, 1H), 7.45 (d, 1H), 7.31 (t, 1H), 3.97 (t, 2H), 2.23 (t, 2H), 2.12 (s, 6H), 1.79 (m, 2H). ^{1}C NMR (500 MHz, DMSO): 154.7, 137.7, 132.8, 126.3, 124.4, 123.3, 117.0, 55.3, 45.0, 44.3, 25.3. (ESI-TOF) [m/z (%)]: 283.1226 ([M+H]$^+$)

4-methyl-1,1-dioxo-1,4-dihydrobenzo[1,2,4]thiadiazin-3-one (14)

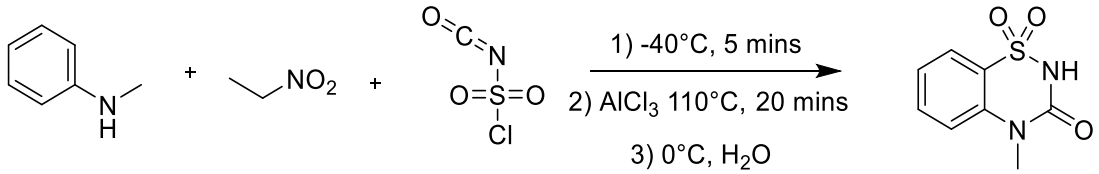

14

This compound was prepared through previously reported procedures[33]. N-Methylaniline (2.1 g, 19.7 mmol) was added to nitroethane (5 mL). The solution was then added dropwise to a solution of chlorosulfonyl isocyanate (2.1 mL, 24.2 mmol) in 25 mL of nitroethane, and stirred at -40°C. An oil bath was heated to 110°C. After 5 minutes, aluminum trichloride (3.27 g, 24.5 mmol) was added to the -40°C mixture and then that mixture was heated in the 110°C oil bath for 20 minutes and stirred at this temperature. After 20 minutes, this mixture was poured onto ice to give 4-methyl-1,1-dioxo-1,4-dihydrobenzo[1,2,4]thiadiazin-3-one. This was filtered off and rinsed with cold H_2O and MeOH. 998.6 mg of product (4.7 mmol) was isolated. Yield=23.8%. MS (ESI-TOF) [m/z (%)]: 213 ($[M+H]^+$). ^{1}H NMR (500 MHz, DMSO): 7.85 (d/m, 1H), 7.76 (t/m, 1H), 7.51 (d, 1H), 7.37 (t/m, 1H), 3.41 (s, 3H). ^{1}C NMR (500 MHz, DMSO): 150.86, 137.52, 134.72, 125.62, 123.90, 122.21, 117.31, 32.1. (ESI-TOF) [m/z (%)]: 283.1226 ($[M+H]^+$)

2-(methylamino)benzenesulfonamide (15)

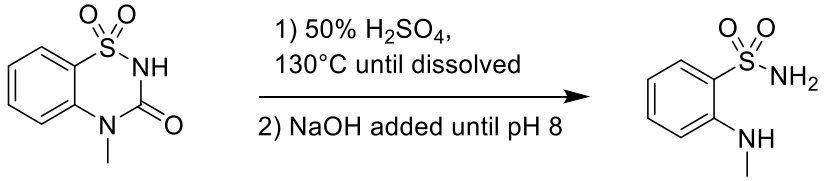

14 15

This compound was prepared through previously reported procedures[33]. The 998.6 mg of 4-methyl-1,1-dioxo-1,4-dihydrobenzo[1,2,4]thiadiazin-3-one (4.7 mmol) that was previously synthesized was added to a round bottom flask and 8 mL of 50% H_2SO_4 was added to the flask and rinsed with 2 mL H_2O. The solution was stirred and heated at 130°C in an oil bath until the compound was fully dissolved. NaOH was added until the pH was 8, and a white powder slowly precipitated (425.8 mg, 2.3 mmol). Yield=48.9%. MS (ESI-TOF) [m/z (%)]: 187 ($[M+H]^+$). ^{1}H NMR (500 MHz, DMSO): 7.60 (dd, 1H), 7.76 (t/m, 1H), 7.37 (t, 1H), 7.24 (bs, 2H), 6.73 (d, 1H), 6.65 (t, 1H), 5.85, (d, 2H), 3.41 (s, 3H). ^{1}C NMR (500 MHz, DMSO): 153.97, 136.96, 128.52, 114.88, 111.61, 30.3.

3-imino-4-methyl-3,4-dihydro-2H-benzo[e][1,2,4]thiadiazine 1,1-dioxide (16)

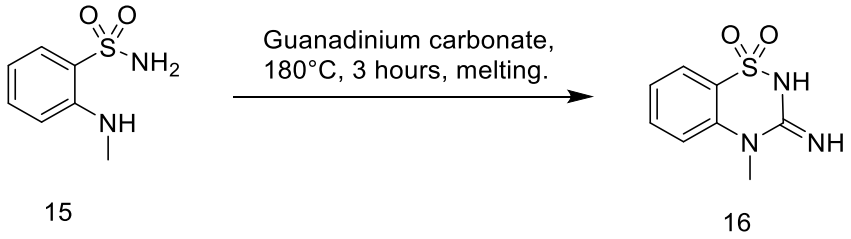

15 16

Added 187.1 mg (1 mmol) 2-(methylamino)benzenesulfonamide and powdered guanadinium carbonate (144.0 mg, 1.5 mmol) to tube, and heated to 180°C for 3 hours. After 3 hours, added 3 mL H_2O, and some dissolved. Added HCl and let cool overnight. The next day, the solution was cooled to 0°C and the solid was filtered off and rinsed with dilute HCl. 71.9 mg (0.34 mmol) of compound was recovered. Yield=34%. MS (ESI-TOF) [m/z (%)]: 212 (100) ($[M+H]^+$) 234 (10) ($[M+Na]^+$). ^{1}H NMR (500 MHz, DMSO): 7.65 (m, 3H), 7.42 (d, 1H), 7.31 (td, 1H), 3.41 (t, 3H) . ^{1}C NMR (500 MHz, DMSO): 155.38, 138.78, 132.68, 126.31, 124.44, 122.77, 116.99, 34.89.

4-chloro-2-nitrobenzenesulfonamide (22)

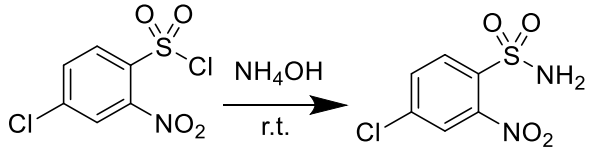

21 22

500 mg (1.95 mmol) of 4-chloro-2-nitrobenzenesulfonyl chloride was dissolved in 14 mL NH_4OH and stirred overnight at ambient temperature. After 16 hours, the solution was homogenous and pale yellow. A TLC was taken showing significant conversion of the starting material. HCl was added to the solution until a white powder precipitated out, which was then filtered out of solution. 337.8 mg (1.42 mmol) was recovered. The compound was confirmed by Hi Res mass spectrometry and ^{1}H NMR. Yield= 73.2%. HRMS (ESI-TOF) [m/z (%)]: 234.9588 ($[M-H]^-$). ^{1}H NMR (500 MHz, DMSO): 8.22 (d, 1H), 8.02 (s, 1H), 7.95 (m, 3H).

2-amino-4-chlorobenzenesulfonamide (23)

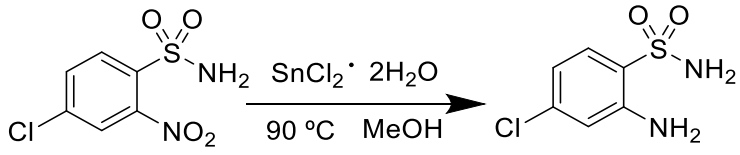

22 23

Procedures adapted from ref[38]. 200 mg of 4-chloro-2-nitrobenzenesulfonamide (0.847 mmol) was added to reaction, followed by 603 mg $SnCl_2$ dihydride (2.62 mmol, 3 equivalents). 8 mL of dry MeOH and 0.5 mL concentrated HCl were then added to the flask. The solution was stirred at 90°C overnight, and then the solvent was removed under reduced pressure, resulting in an oil. The oil was triturated with H_2O and formed a whitish-yellow solid. The solid was filtered off and 137.0 mg (78.5% yield) of product was isolated. The product was confirmed by mass spectrometry. MS (ESI-TOF) [m/z (%)]: 205 ($[M-H]^-$) ^{1}H NMR (500 MHz, MeOH): 7.51 (d, 1H), 6.84 (d, 1H), 6.64 (dd, 1H).

Alternative reactions conditions for reduction of compound 22 to compound 23:

Glacial Acetic Acid and Iron:
2-amino-4-chlorobenzenesulfonamide (23)

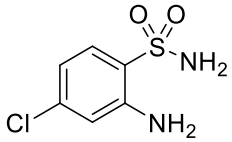

23

Procedures adapted from refs[38,39]. Added 121.6 mg of 4-chloro-2-nitrobenzenesulfonamide (0.515 mmol) to flask, then 10 mL of glacial acetic acid and 0.5 mL H_2O were then added to the flask. The solution was heated to 60°C and 231 mg of iron powder (4.122 mmol, 8 equivalents) was added and was stirred for 3 hours without conversion. The reaction was then refluxed overnight. The product was confirmed by mass spectrometry. Yield=20%. MS (ESI-TOF) [m/z (%)]: 205 ($[M-H]^-$)

HI reduction:
2-amino-4-chlorobenzenesulfonamide (23)

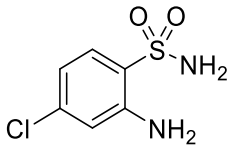

23

Procedures adapted from ref[40]. Added 237.0 mg of 4-chloro-2-nitrobenzenesulfonamide (1.0 mmol) to flask, followed by 3 mL of 57% HI. The solution was heated to 90°C for 2 hours. The reaction mixture was diluted with EtOAc and washed 2x with $Na_2S_2O_3$, 1x with $NaHCO_3$ and 1x with brine. The organic layer was dried over $MgSO_4$ and the drying agent was filtered off. The organic layer was evaporated resulting in a dry solid. The product was confirmed by mass spectrometry. MS (ESI-TOF) [m/z (%)]: 205 ($[M-H]^-$)

4-chloro-2-((3-(dimethylamino)propyl)amino)benzenesulfonamide (25)

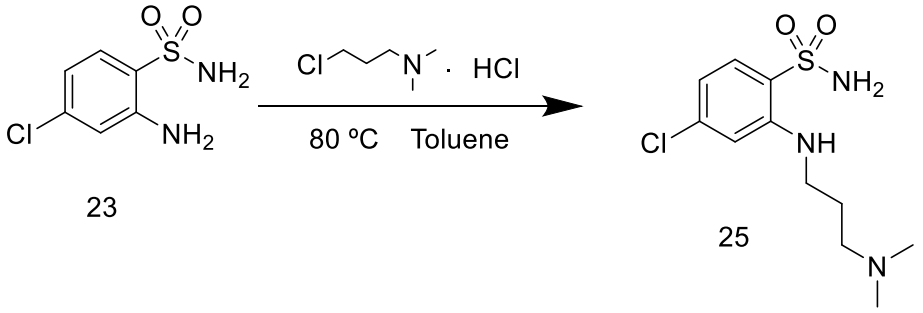

23 25

274 mg 2-amino-4-chlorobenzenesulfonamide (1.326 mmol) and 316.4 mg 3-chloro-*N*,*N*-dimethylpropan-1-amine hydrochloride (2.00 mmol, 1.5 equivalents) were added to reaction. 8 mL of toluene was added and the mixture was refluxed at 120°C for 1 hours. A grey solid

precipitated, and the solvent was removed *in vacuo* to form a brownish-orange oil. The oil was triturated with minimal H_2O and let sit overnight. A white powder formed, and then was purified by flash column chromatography. 285.3 mg of compound (0.978 mmol) was confirmed by mass spectrometry and ^1H NMR. Yield= 73.8%. MS (ESI-TOF) [m/z (%)]: 292 ($[M-H]^-$) ^1H NMR (400 MHz, MeOH): 7.68 (d, 1H), 6.81 (d, 1H), 6.67 (dd, 1H), 3.26 (t, 2H) 2.53 (t, 2H), 2.32 (s, 6H), 1.69 (s, 2H).

3-amino-6-chloro-4H-benzo[e][1,2,4]thiadiazine 1,1-dioxide (27)

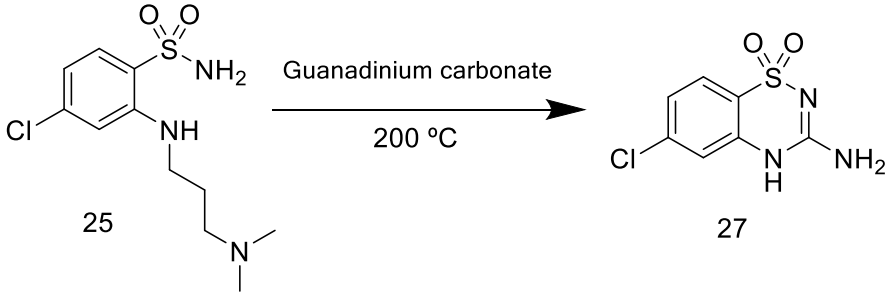

4-chloro-2-((3-(dimethylamino)propyl)amino)benzenesulfonamide 90.0 mg (0.31 mmol) and 59.5 mg (0.66 mmol, 1.5 equivalents) were added to a heat resistant tube and melted and stirred for 2 hours at 220°C. A brown oil resulted and after workup, it was determined that the dimethylaminopropyl substituent was cleaved in the course of the reaction to form the non-substituted compound. This was confirmed by mass spectrometry. 2 mg of pure compound was recovered (0.0086 mmol). Yield=1.3%. MS (ESI-TOF) [m/z (%)]: 230 ($[M-H]^-$).

3-amino-6-chloro-4-(3-(dimethylamino)propyl)-4H-benzo[e][1,2,4]thiadiazine 1,1-dioxide (26)

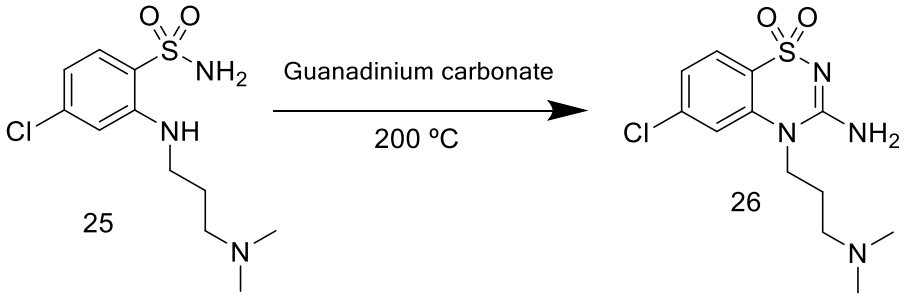

4-chloro-2-((3-(dimethylamino)propyl)amino)benzenesulfonamide 172.9 mg (0.593 mmol) and 102.0 mg (1.13 mmol, 1.9 equivalents) were added to a heat resistant tube and melted and stirred for 3 hours at 180°C. The compound was purified by dissolving in IPA and adding NH_4OH to crash the compound out of solution as a white powder. The powder was dissolved in a minimal amount H_2O with 0.25 mL of HCl. The compound was then isolated by HPLC and tested by mass spectrometry. 22.1 mg product (0.069 mmol) was recovered from the reaction. Yield= 11.6%. MS (ESI-TOF) [m/z (%)]: 315 ($[M-H]^-$)

Benzene-(1,3,2)-dithiazole (33)

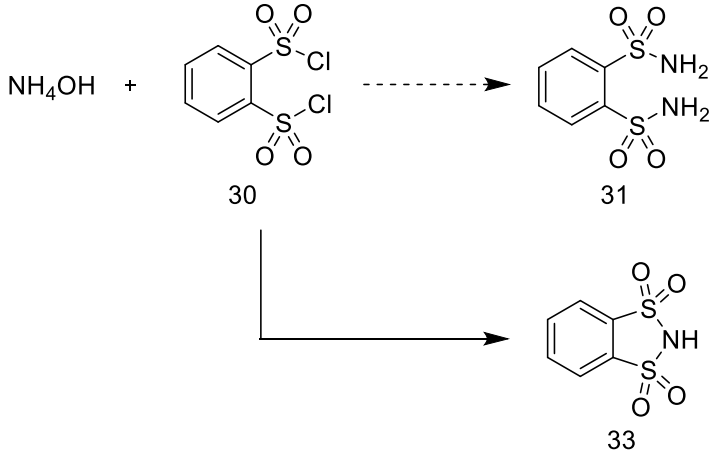

To 20 mL of NH_4OH was added 1,2-Benzenedisulfonyl dichloride (401.7 mg, 1.46 mmol) at ambient temperature. The solution was stirred over 72 hours, and conc HCl was added until solid began precipitating, and then added dropwise until no more precipitate formed. The precipitate was compounds that were unable to be clarified, but the filtrate showed full conversion to O-Benzenedisulfonimide by mass spectrometry. The filtrate was separated and the solvent removed under reduced pressure. MS (ESI-TOF) [m/z (%)]: 218 ($[M-H]^-$)

N,*N*-di-tert-butylbenzene-1,2-disulfonamide (34)

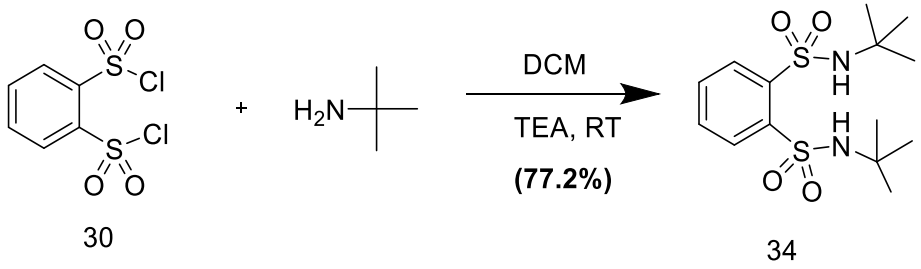

Compound was prepared through previously reported procedures[46]. A solution of benzene-1,2-disulfonyl dichloride (1.27 g, 4.62 mmol) in 15 mL dry DCM under Ar was transferred slowly to a mixture of dry *tert*-butylamine (0.76 mL, 531.7 mg, 7.27 mmol) and dry TEA (1.01 mL, 735.6 mg, 7.27 mmol) in 10 mL dry DCM under Ar. The mixture was stirred at RT for 1 hour, after which 10 mL of HCl (3% aqueous solution) was added. The aqueous and organic layers were separated and the organic layer was washed 2x with brine. The organic layer was dried over anhydrous $MgSO_4$ and the solvent was removed under reduced pressure to give 977.9 mg (77.2% yield) compound. Compound was confirmed by mass spectrometry. MS (ESI-TOF) [m/z (%)]: 371 ($[M+H]^+$)

Benzene-1,2-disulfonamide (31)

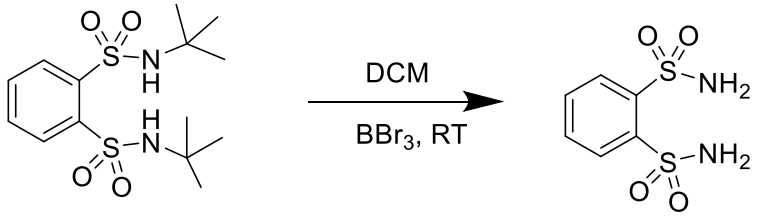

34 31

Compound was prepared through previously reported procedures[46]. *N*,*N*-di-tert-butylbenzene-1,2-disulfonamide (782 mg, 2.24 mmol) was dissolved in 16 mL dry DCM under Ar. Boron tribromide (0.10 mL, 1.12 mmol) was added dropwise to the reaction and stirred overnight, after which another aliquot (0.05 mL, 0.56 mmol) was added. A white solid precipitated out and was recovered by vacuum filtration rinsed with DCM. Yield: 483.6 mg (2.05 mmol, 91.4%). Compound was confirmed by mass spectrometry. MS (ESI-TOF) [m/z (%)]: 235 ($[M-H]^-$).

3-aminobenzoisothiazole (36)

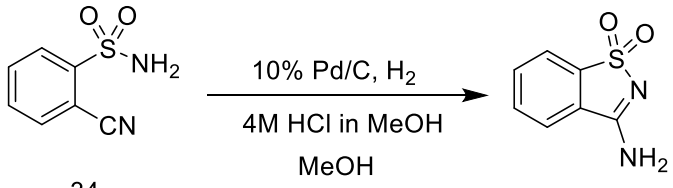

34 36

2-cyanobenzenesulfonamide (215.3 mg, 1.2 mmol, 1 equivalent) was dissolved in 5.4 mL anhydrous MeOH and stirred. 10% Pd/C (57.8 mg) was added, followed by 0.62 mL HCl (4M in dioxane, 2.4 mmol, 2 equivalents). 2 balloons of H_2 were flushed through the flask, and then a 3rd balloon was added and left overnight. 2 more balloons of H_2 were flushed through the flask, and then the insoluble solid was filtered off and rinsed with MeOH. The solution crystallized out from the MeOH in solution, and mass spectrometry and NMR analysis was done on the crystals. A crystal structure of 36 was also solved (see figure 3.2). MS (ESI-TOF) [m/z (%)]: 292 ($[M+H]^+$) ^{1}H NMR (400 MHz, MeOH): 8.93 (bd, 2H), 8.12 (d, 1H), 7.95 (d, 1H), 7.81 (d, 2H).

2-(aminomethyl)benzenesulfonamide (35)

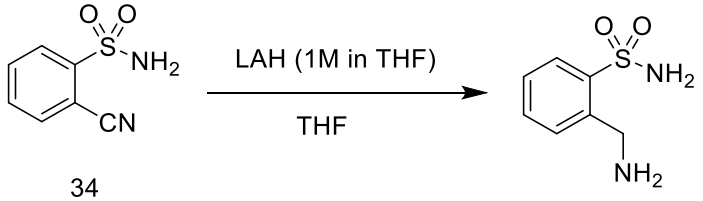

34 35

The reaction conditions were adapted from ref[48]. The general procedure for the reaction is as follows: 2-cyanobenzenesulfonamide (614 mg, 3.37 mmol, 1 equivalent) was dissolved in 35 mL THF at ambient temperature. 12.2 mL Lithium Aluminum Hydride (LAH, 1M in THF, 12.2 mmol, 4 equivalents) was added and the solution turned red. The mixture was stirred overnight and became a translucent yellow, after which 15 mL H_2O was added to quench remaining LAH.

The solution was filtered through celite and the celite was washed with additional THF. The solvent was removed under reduced pressure, and HCl (dilute aqueous solution) was added and the aqueous layer was washed 3x with EtOAc. 524.6 mg of compound was isolated, and confirmed by mass spectrometry. Yield=83.6%. MS (ESI-TOF) [m/z (%)]: 187 ($[M+H]^+$)

N,N'-diisopropyl-benzo[1,3]thiadiazepine (37)

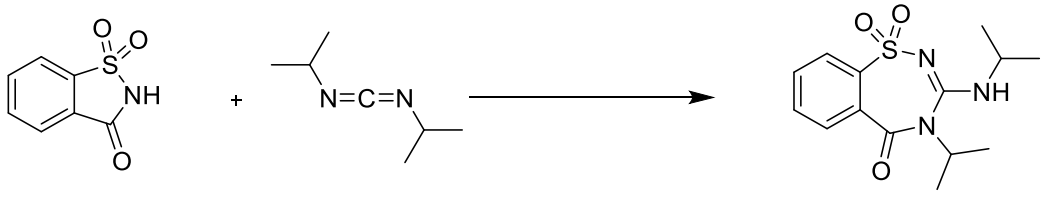

40 37

Compound was prepared through previously reported procedures[50]. Saccharin (2.74 g, 15 mmol) was dissolved in 50 mL acetone and 2.35 mL of *N,N'*-diisopropylcarbodiimide (DIC) (1.89 g, 15 mmol) was added to the mixture. The solution was stirred overnight at reflux and then insoluble products were filtered off and the filtrate was washed through a small silica plug and washed with acetone. The solvent was removed under reduced pressure to give 1.196 g product (25.7% yield). The compound was confirmed by mass spectrometry. MS (ESI-TOF) [m/z (%)]: 310 (100) ($[M+H]^+$), 332 (25) ($[M+Na]^+$).

N-ethyl-*N'*-(3-(dimethylamino)propyl)amino)-benzo[1,3]thiadiazepine (38)

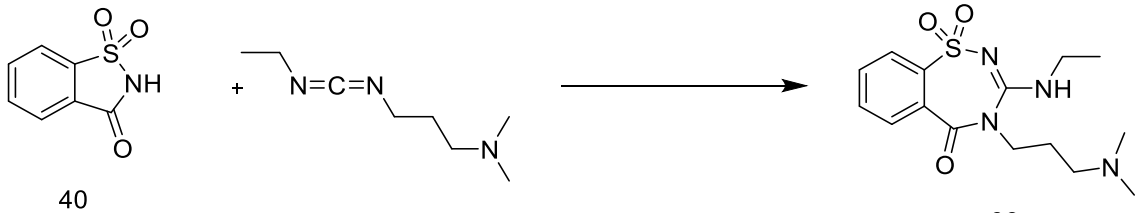

40 38

The reaction conditions were adapted from ref[50]. Saccharin (1.838 g, 10 mmol) was dissolved in 50 mL acetone, followed by the addition of 1-Ethyl-3-(3-dimethylaminopropyl)carbodiimide (EDC) (1.8 mL, 1.55 g, 10 mmol). The reaction was stirred at reflux overnight, and then allowed to cool. The solvent was removed under reduced pressure. The tautomer was unable to be determined through NMR, so a portion of the crude sample (198 mg) was purified by flash column chromatography (5:2 EtOAc:Acetone) and determined the composition of the fractions by TLC and mass spectrometry. The fasted running compound was determined to be the product, and the fractions containing it were combined and the solvent was removed under reduced pressure, affording 180 mg pure benzothiadiazepine product. This compound was transferred to a vial with minimal acetone and crystallized with the slow evaporation of solvent. The crystal structure showed the tautomer above as the sole compound (see figure 3.4). HRMS (ESI-TOF) [m/z (%)]: 339.1482 ($[M+H]^+$). ^{1}H NMR (500 MHz, DMSO): 7.71 (m, 4H), 3.95 (bs, 1H), 2.83 (bs, 7H), 2.25 (bs, 6H), 2.06 (bs, 5H), 1.13 (t, 3H). ^{1}C NMR (500 MHz, DMSO): 131.89, 131.69, 131.24, 122.72, 53.89, 49.44, 43.08, 37.66, 23.17, 13.04.

4-(2-(3-(cyclohexylamino)-1,1-dioxido-5-oxobenzo[f][1,2,4]thiadiazepin-4(5H)-yl)ethyl)-4-methylmorpholin-4-ium metho-p-toluene sulfonate (39)

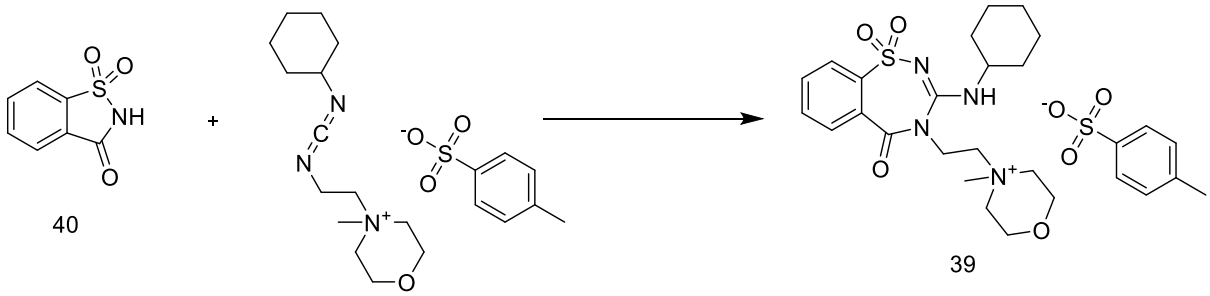

40 39

The reaction conditions were adapted from ref[50]. 1-cyclohexyl-(2-morpholinoethyl)carbodiimide metho-p-toluene sulfonate (CMC) (423 mg, 1.0 mmol) and saccharine (183 mg, 1.0 mmol) were added to 10 mL acetone. The reaction was stirred at reflux overnight and taken off heat after 16 hours. The reaction was filtered through celite and then the solvent was removed under reduced pressure. The compound was confirmed by mass spectrometry. MS (ESI-TOF) [m/z (%)]: 435 ($[M+]^+$).

1-(4,4'-Dimethoxybenzhydryl)-3-(ethoxycarbonyl)thiourea (44)

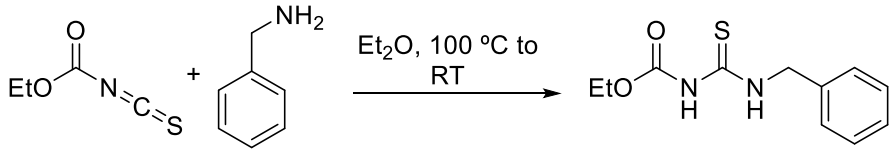

44

Compound was prepared through previously reported procedures[53,54,58]. Benzylamine (3.3 mL, 3.27 g, 30.5 mmol) was added to 40 mL dry diethyl ether under Ar and cooled to 0°C. O-ethyl carbonisothiocyanatidate (3.1 mL, 3.45 g, 28.28 mmol) was added dropwise over 5 minutes. After 20 minutes, a solid precipitated and the solution was roomed to ambient temperature. The precipitate was filtered and washed with hexanes to yield 5.650 g product (90.2% yield). Confirmed by mass spectrometry. MS (ESI-TOF) [m/z (%)]: 239 ($[M+H]^+$)

Ethyl ((benzylimino)methylene)carbamate (45)

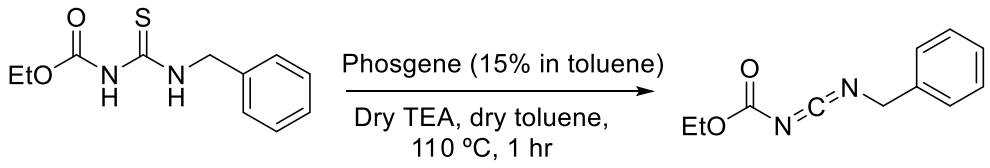

44 45

Compound was prepared through previously reported procedures[53,54,58]. 1-(4,4'-Dimethoxybenzhydryl)-3-(ethoxycarbonyl)thiourea (559.6 mg, 2.35 mmol, 1 equivalent), 10 mL dry toluene, dry TEA (0.7 mL, 499 mg, 4.94 mmol, 2.1 equivalents) were combined under Ar at ambient temperature. 15% phosgene in toluene (1.9 mL, 256 mg, 2.58 mmol, 1.1 equivalents) was added dropwise. The reaction was heated to reflux at 110°C for 1 hour, after which heat was removed and the reaction was allowed to cool to RT. The solvent was removed under reduced

pressure, and the residue was rinsed 2x with 25 mL dry diethyl ether and filtered through celite. The solvent was removed under reduced pressure and the 432 mg of sample was used immediately in the next reaction.

Ethyl-(2-benzyl-1-hydroxy-1,2-dihydrobenzo[c][1,5,2]diazaborinin-3-yl)carbamate (46)

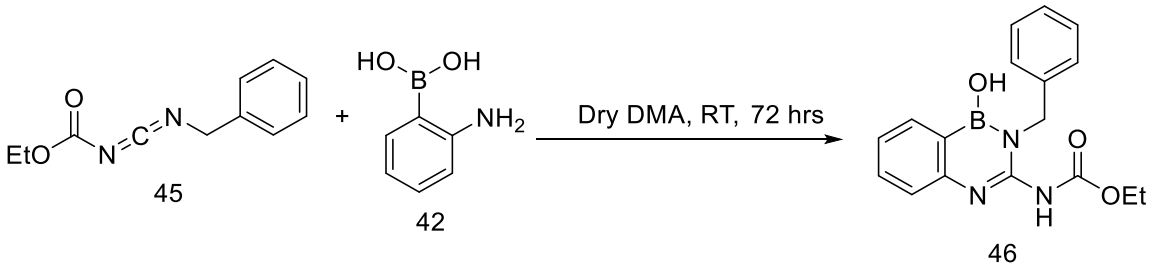

45 42 46

Compound was prepared through previously reported procedures[53,54,58]. (2-aminophenyl)boronic acid (182.6 mg, 1.33 mmol, 1 equivalent) was dissolved in 5 mL dry DMA. Ethyl ((benzylimino)methylene)carbamate (432 mg, 2.12 mmol, 1.6 equivalents) from the previous reaction (45) was added with 5 mL of dry DMA and stirred at ambient temperature overnight. The solvent was removed under reduced pressure at 50°C. The residue was triturated with MeOH and 205.6 mg (0.64 mmol) of an off-white solid was filtered off, and confirmed to be the product by mass spectrometry. Yield=48%. MS (ESI-TOF) [m/z (%)]: 324 ($[M+H]^+$)

3-(benzylamino)benzo[c][1,5,2]diazaborinin-1(2H)-ol (47)

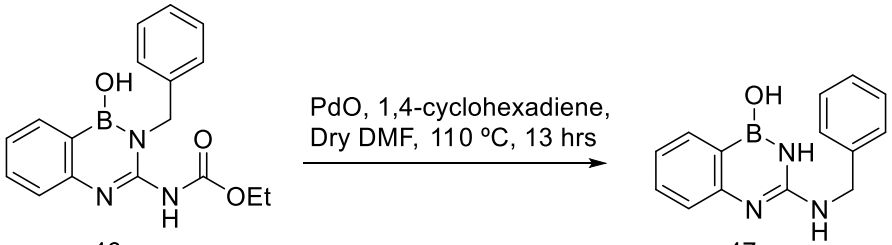

46 47

Compound was prepared through previously reported procedures[53,54,58]. PdO (215 mg, 1.76 mmol) was added to 3.5 mL dry DMF. Ethyl (2-benzyl-1-hydroxy-1,2-dihydrobenzo[c][1,5,2]diazaborinin-3-yl)carbamate (205.6 mg, 0.611 mmol) was added, and the reaction was heated to 100°C. After heating 1,4-cyclohexadiene (3 mL) was added, and the reaction was run for 13 hours. After the reaction cooled to RT, the PdO catalyst was filtered off and rinsed with MeOH. The solvent was removed under reduced pressure at 60°C. The crude residue showed mostly benzylated product with some debenzylated compound as a side product by mass spectrometry. The residue was dissolved in 20 mL of MeOH and insoluble impurities were removed by vacuum filtration. The filtrate was determined to be the product by mass spectrometry. MS (ESI-TOF) [m/z (%)]: 252 ($[M+H]^+$)

3-aminobenzo[e][1,2,4]triazine 1-oxide (49)

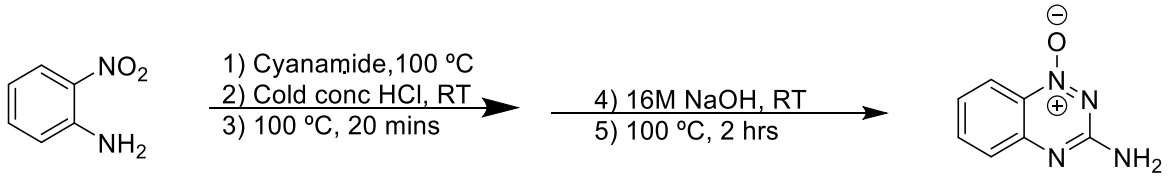

48 49

Compound was prepared through previously reported procedures[55]. 2-nitroaniline (2.482 g, 18 mmol) and cyanamide (1.515 g, 36 mmol) were combined and melted solvent-free at 100°C for 1 hour until a deep red melt formed. The solution was cooled to RT. Cold concentrated HCl (6.5 mL) was added dropwise to the solution, and then heated to 100°C for another 30 minutes, and then cooled to RT. NaOH (16M, 6.5 mL) was added in 500 µL increments over 15 minutes, and was again heated to 100°C for another 2 hours. H_2O (25 mL) was added and a yellow solid precipitated out. The solid was filtered and rinsed with H_2O and EtOAc. The compound was recrystallized twice from IPA and checked by mass spectrometry and ^{1}H NMR. MS (ESI-TOF) [m/z (%)]: 163 ([M+H]$^+$). ^{1}H NMR (500 MHz, DMSO): 8.12 (d, 1H), 7.76 (t, 1H), 7.52 (d, 1H), 7.33 (m, 3H).

Spectra

2-nitrobenzenesulfonamide (7)

WF-1-a #206-216 RT: 1.65-1.72 AV: 11 SB: 11 3.42-3.50 NL: 9.13E5
F: - c Full ms [100.00-350.00]

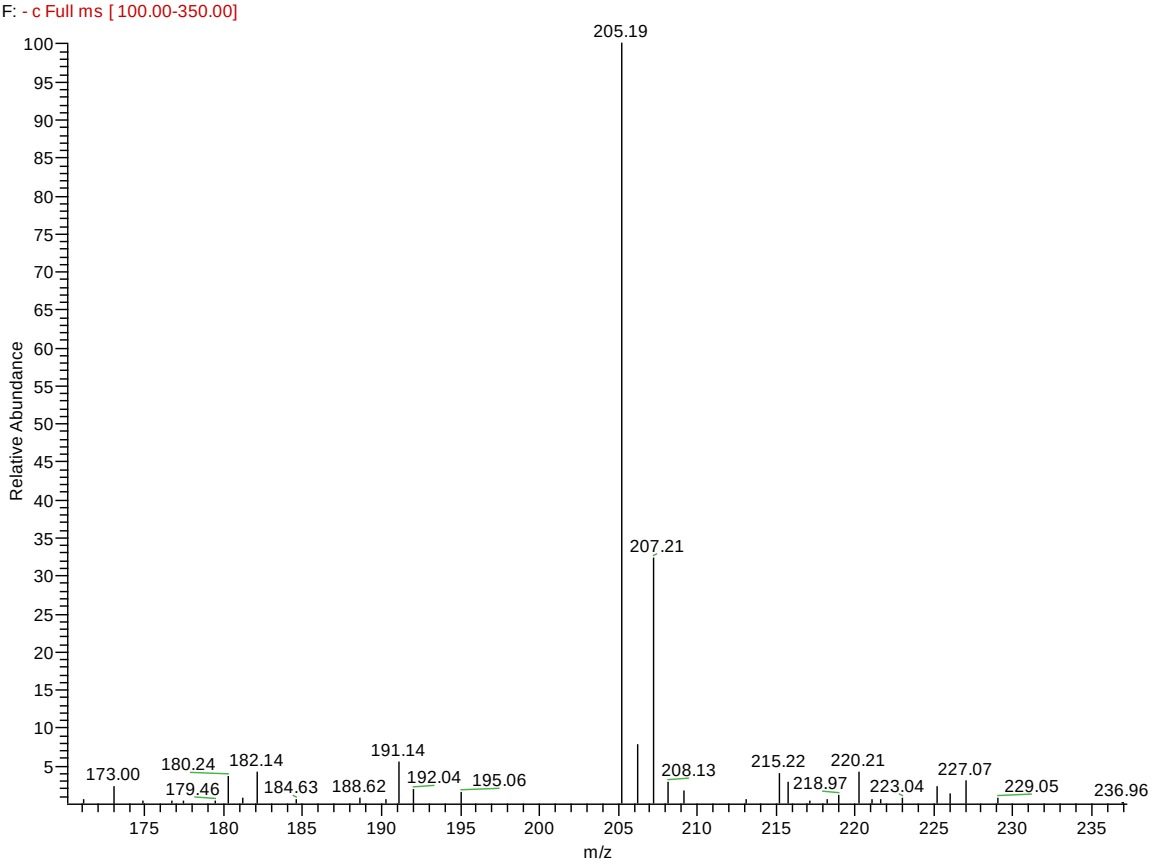

3-amino-4H-benzo[e][1,2,4]thiadiazine 1,1-dioxide (9)

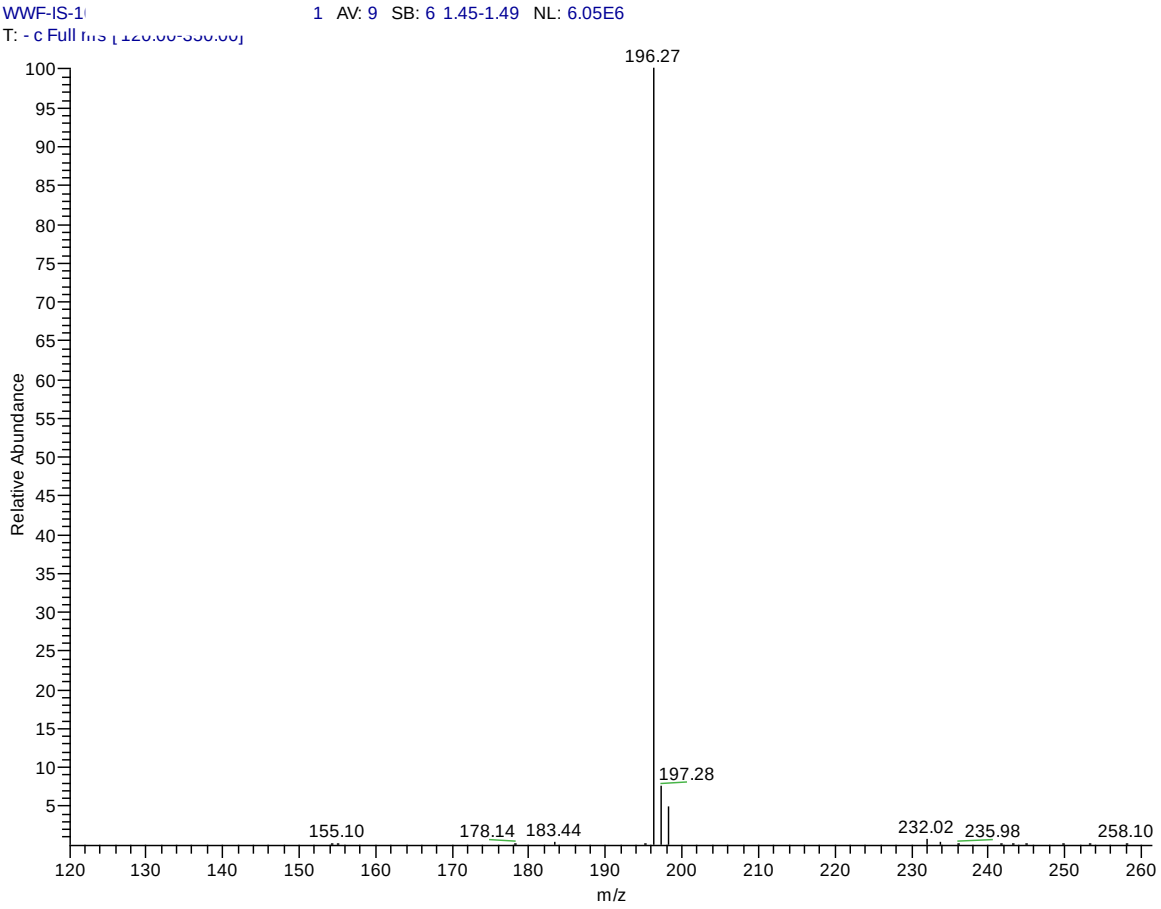

3-amino-4H-benzo[e][1,2,4]thiadiazine 1,1-dioxide (9)

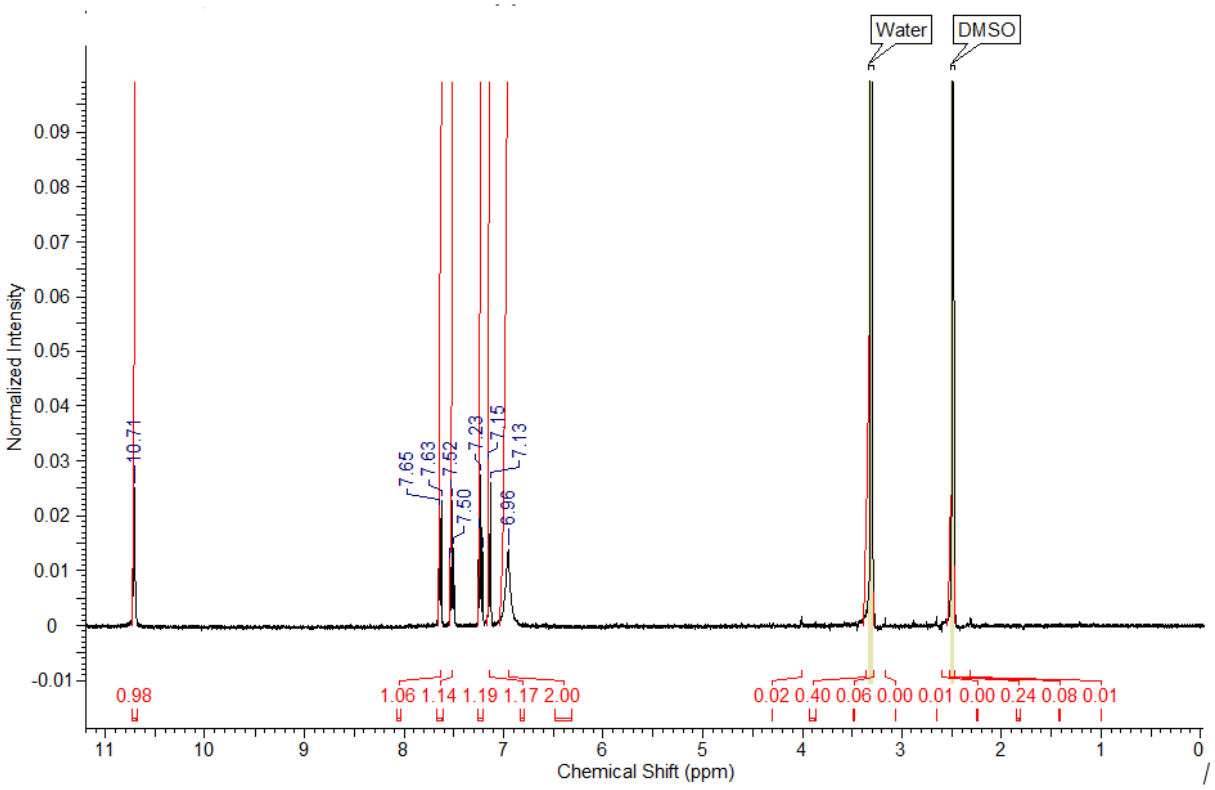

2-((3-(dimethylamino)propyl)amino)benzenesulfonamide (10)

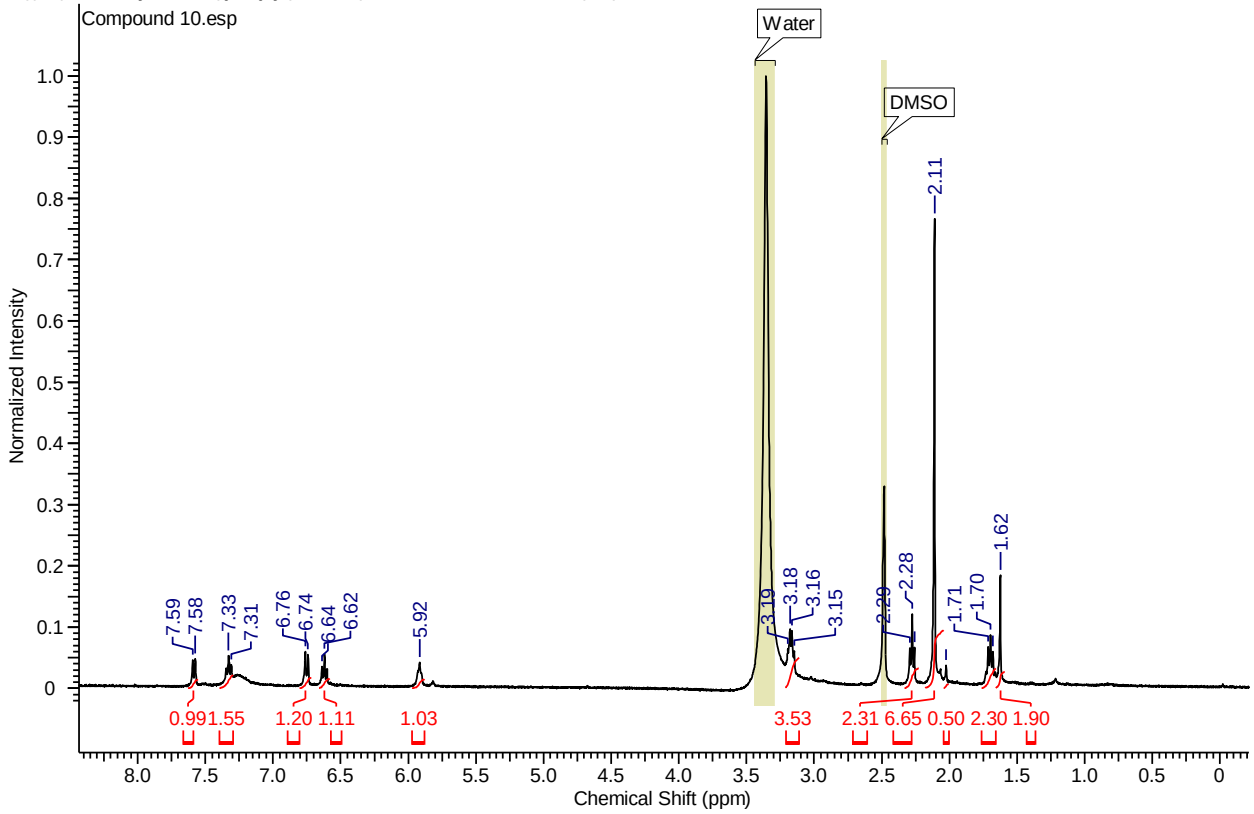

3-amino-4-(3-(dimethylamino)propyl)-4H-benzo[e][1,2,4]thiadiazine 1,1-dioxide (11)

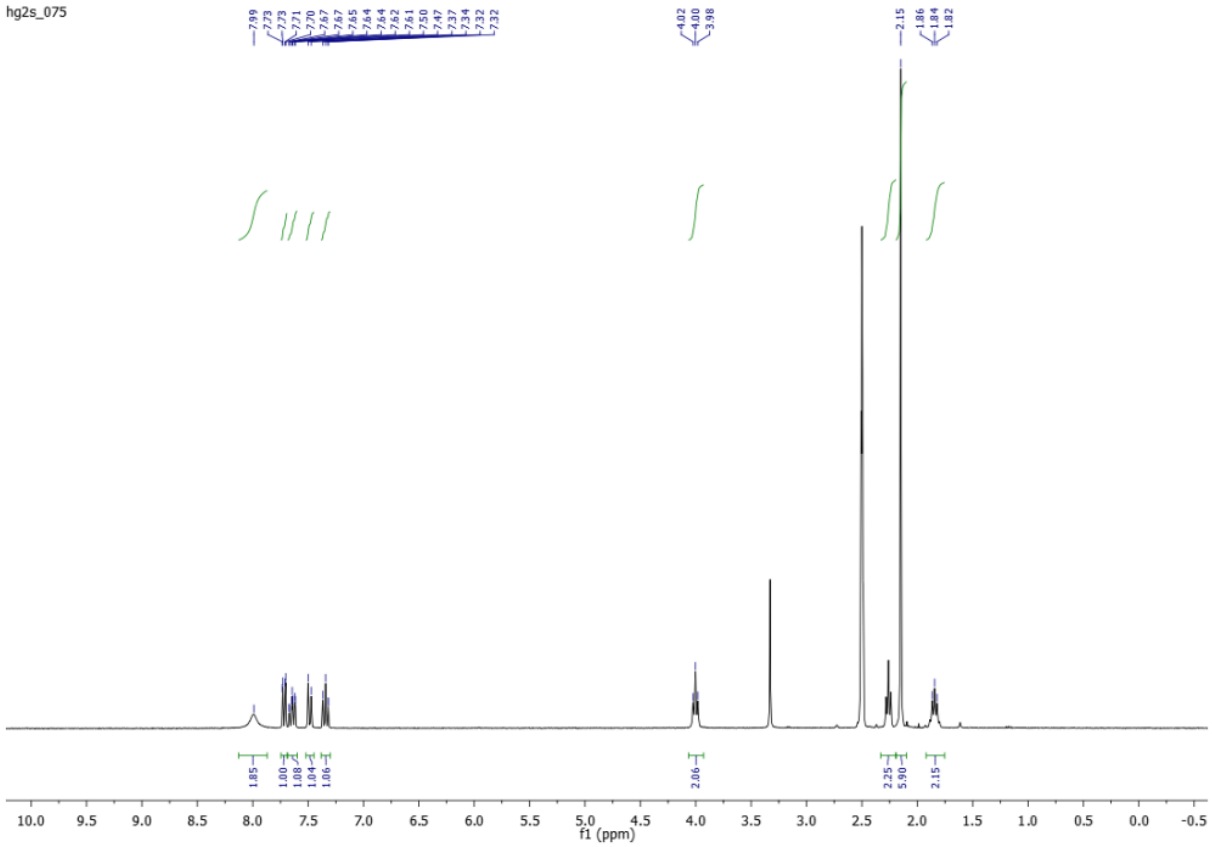

3-amino-4-(3-(dimethylamino)propyl)-4H-benzo[e][1,2,4]thiadiazine 1,1-dioxide (11)

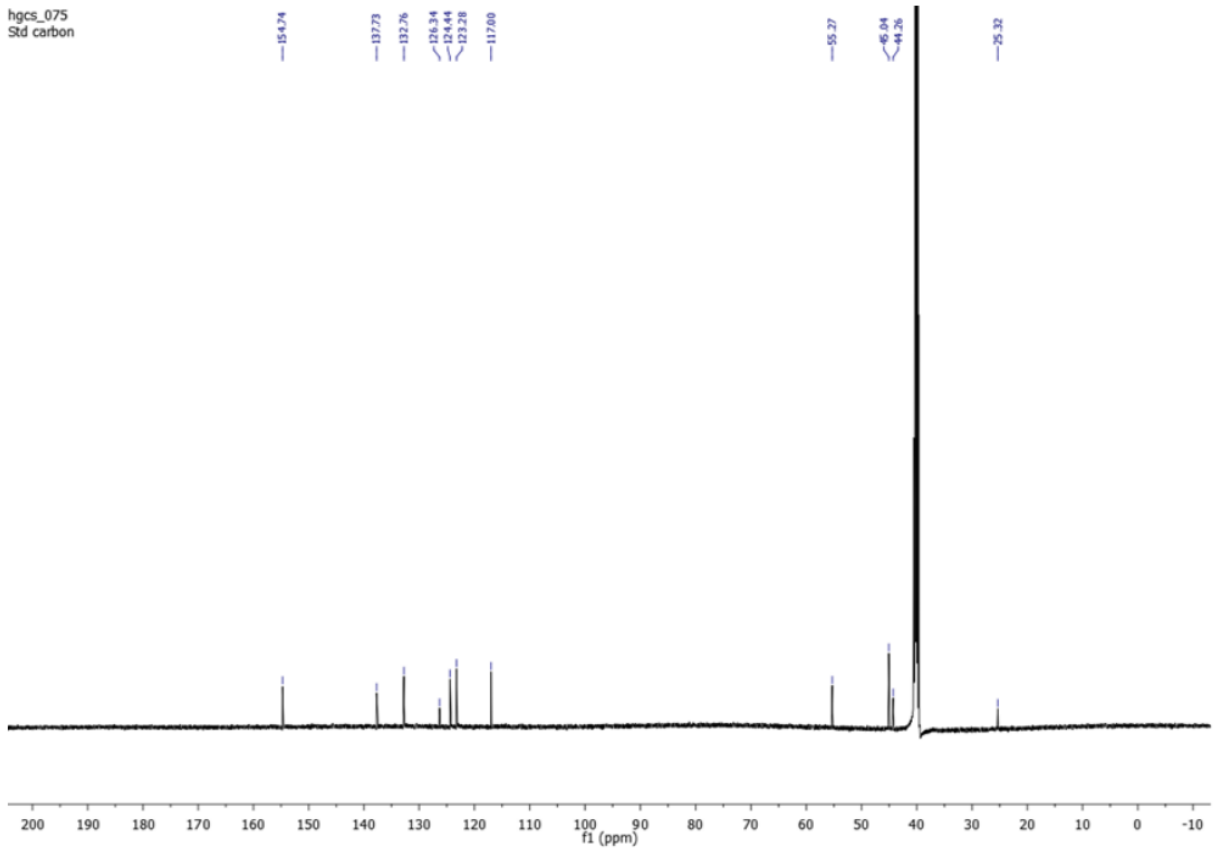

2H-benzo[e][1,2,4]thiadiazin-3(4H)-one 1,1-dioxide (12)

WF1-a #65-70 RT: 0.56-0.60 AV: 6 SB: 3 0.81-0.82 NL: 2.37E6
T: - c Full ms [120.00-350.00]

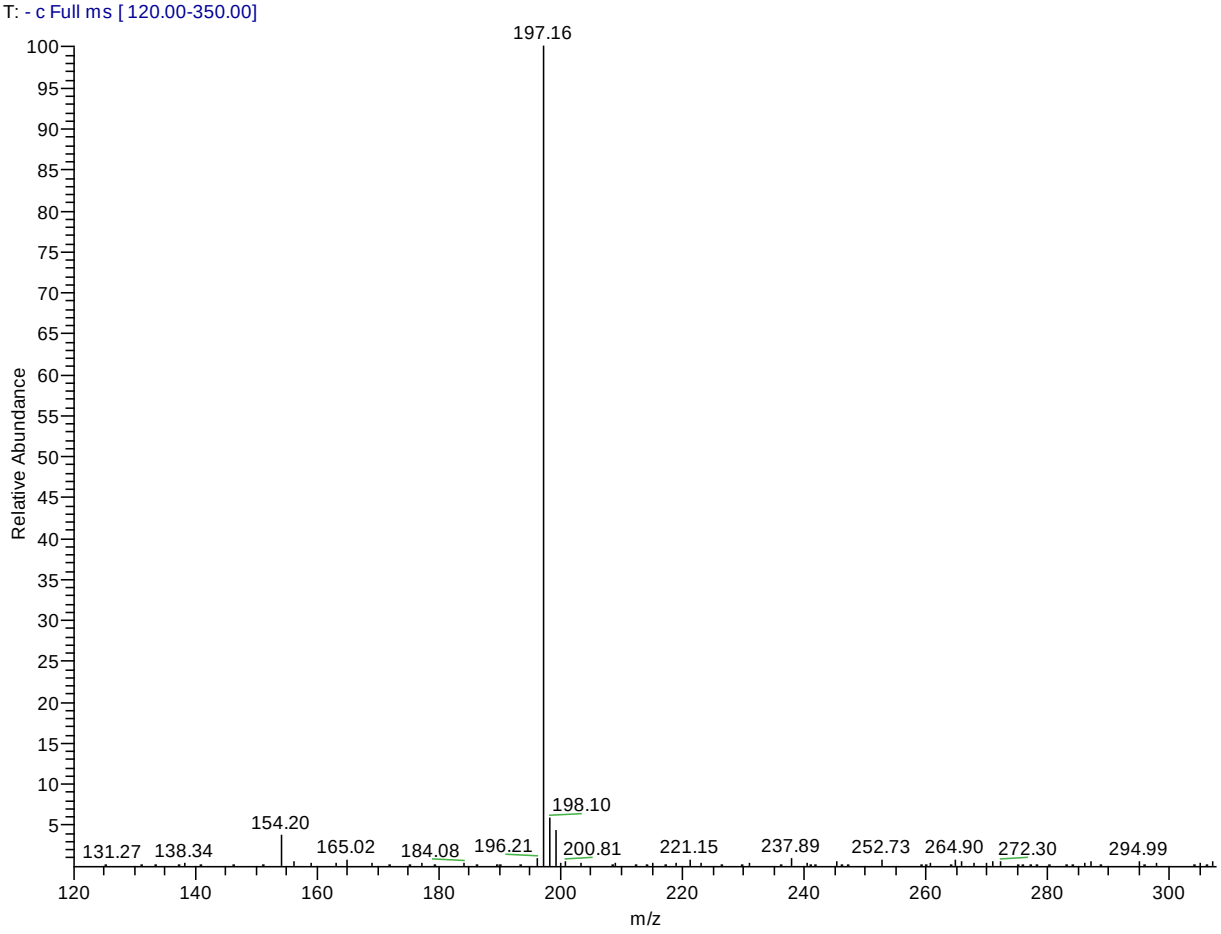

2H-benzo[e][1,2,4]thiadiazin-3(4H)-one 1,1-dioxide (12)

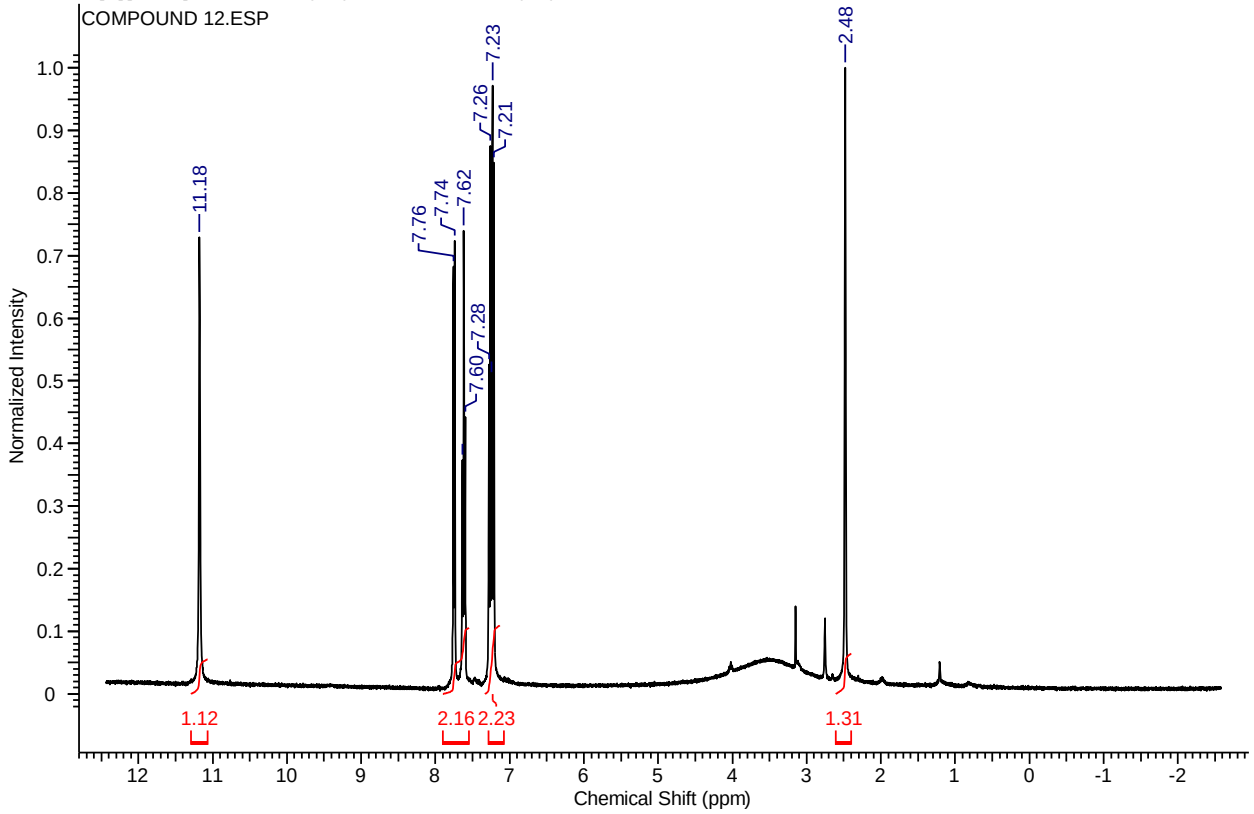

4-(3-(dimethylamino)propyl)-2H-benzo[e][1,2,4]thiadiazin-3(4H)-one 1,1-dioxide (13)

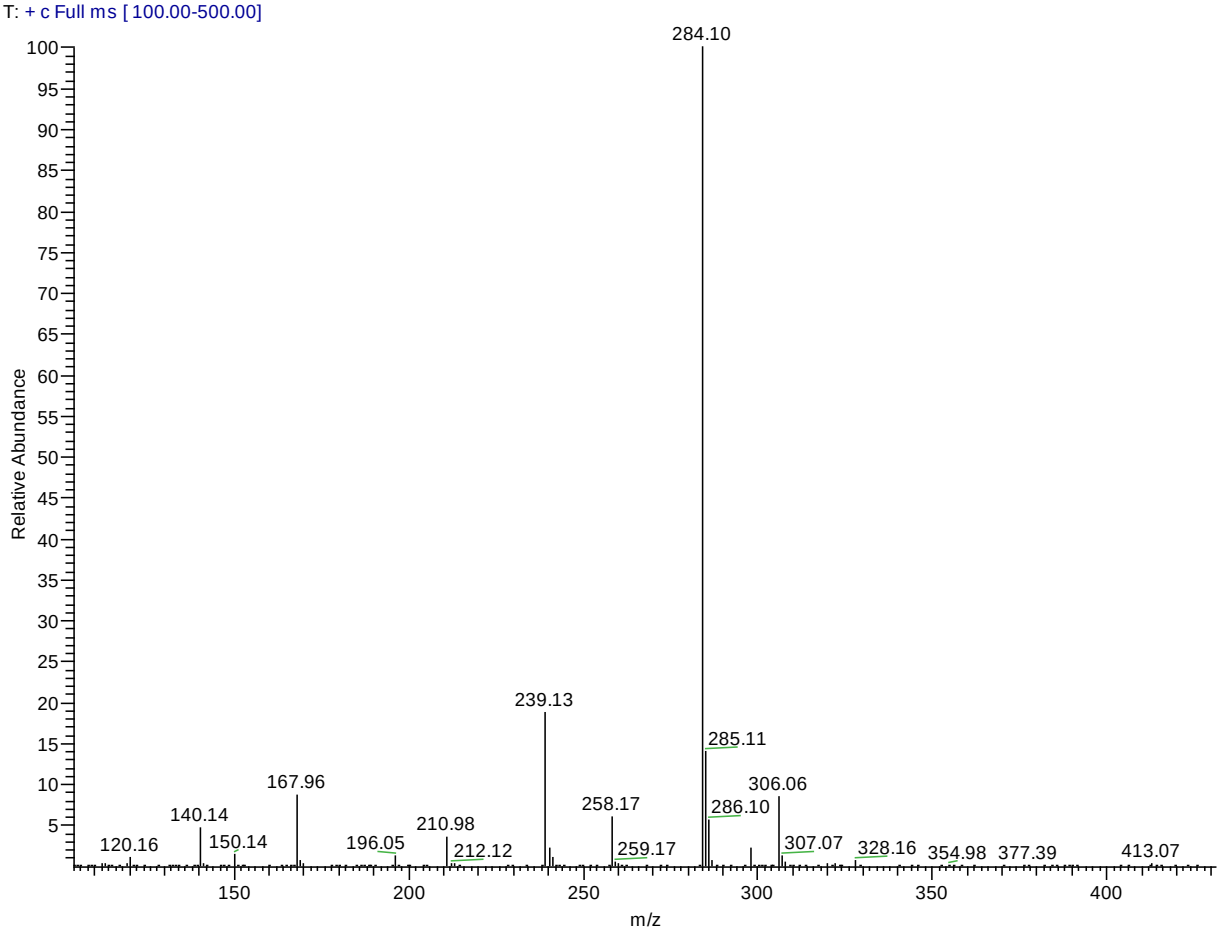

4-methyl-1,1-dioxo-1,4-dihydrobenzo[1,2,4]thiadiazin-3-one (14)

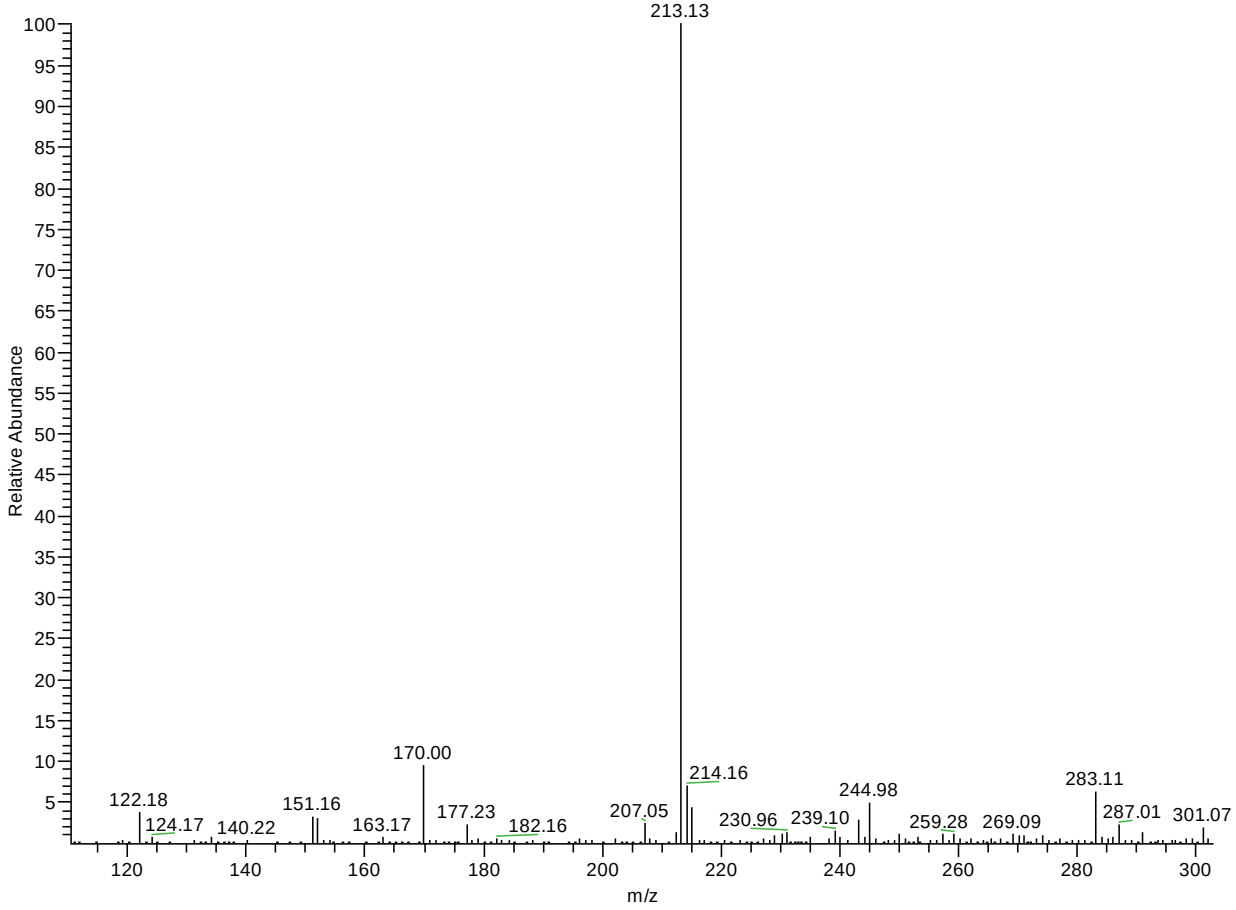

4-methyl-1,1-dioxo-1,4-dihydrobenzo[1,2,4]thiadiazin-3-one (14)

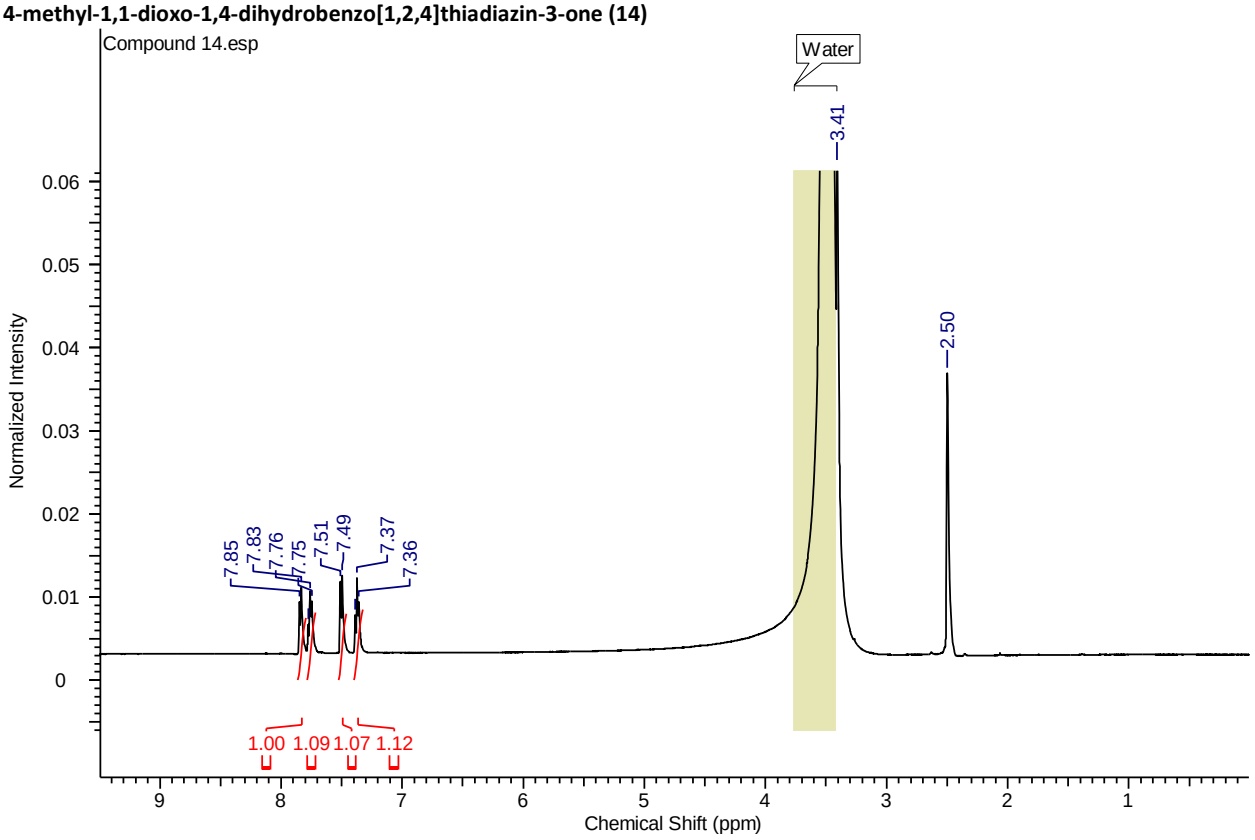

4-methyl-1,1-dioxo-1,4-dihydrobenzo[1,2,4]thiadiazin-3-one (14)

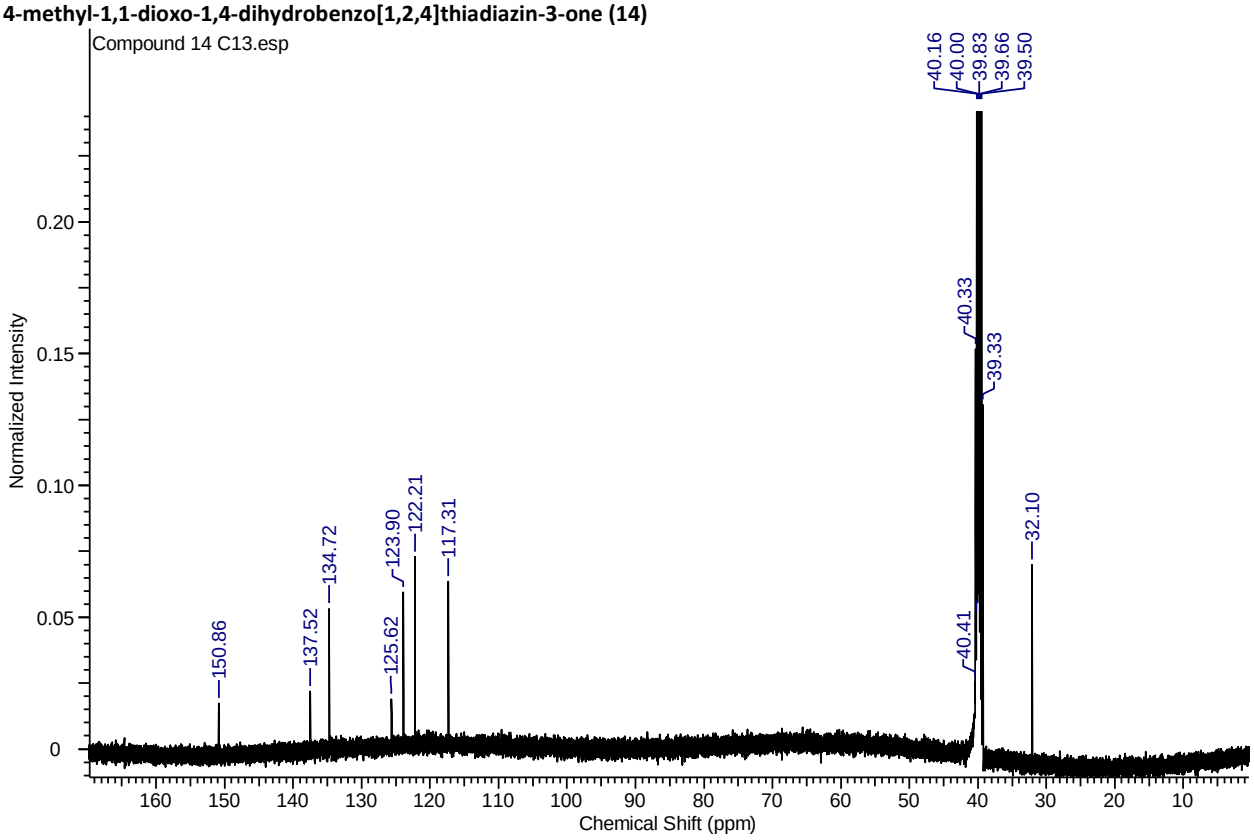

2-(methylamino)benzenesulfonamide (15)

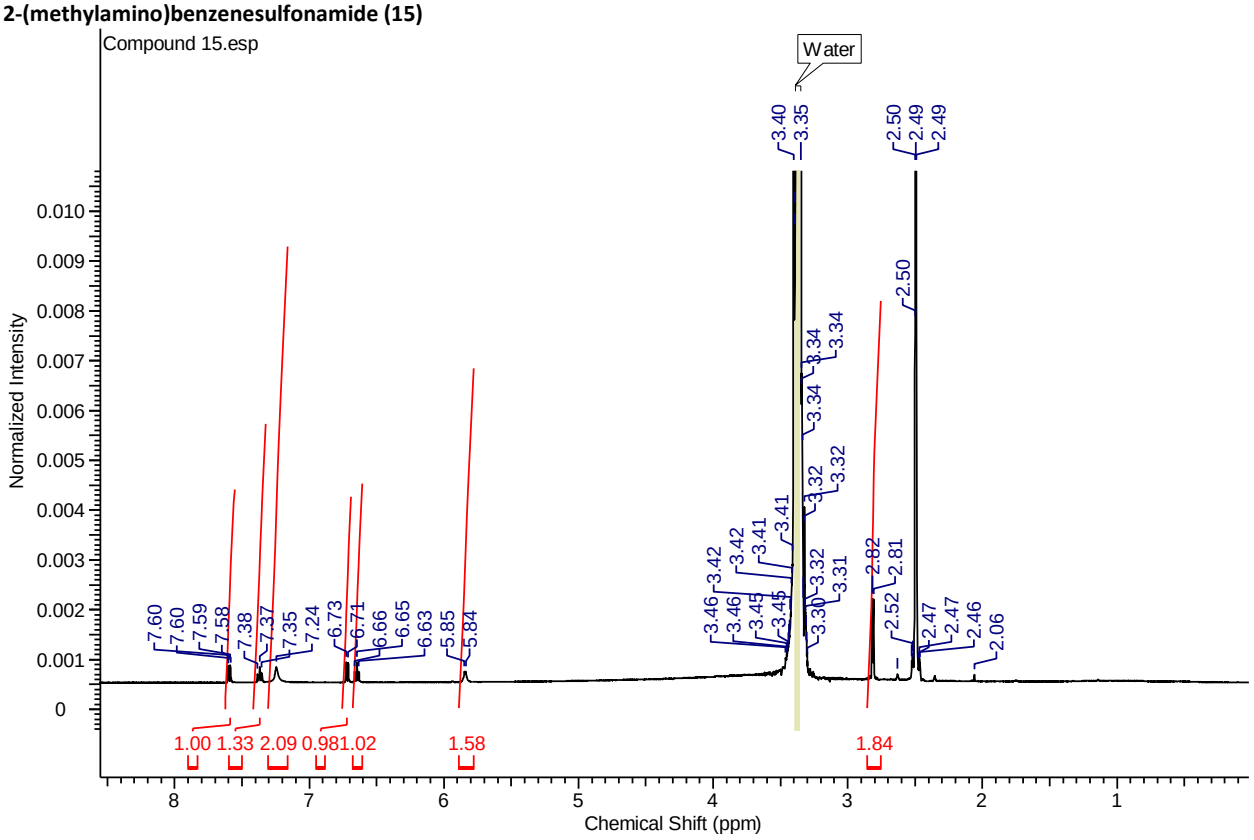

2-(methylamino)benzenesulfonamide (15)

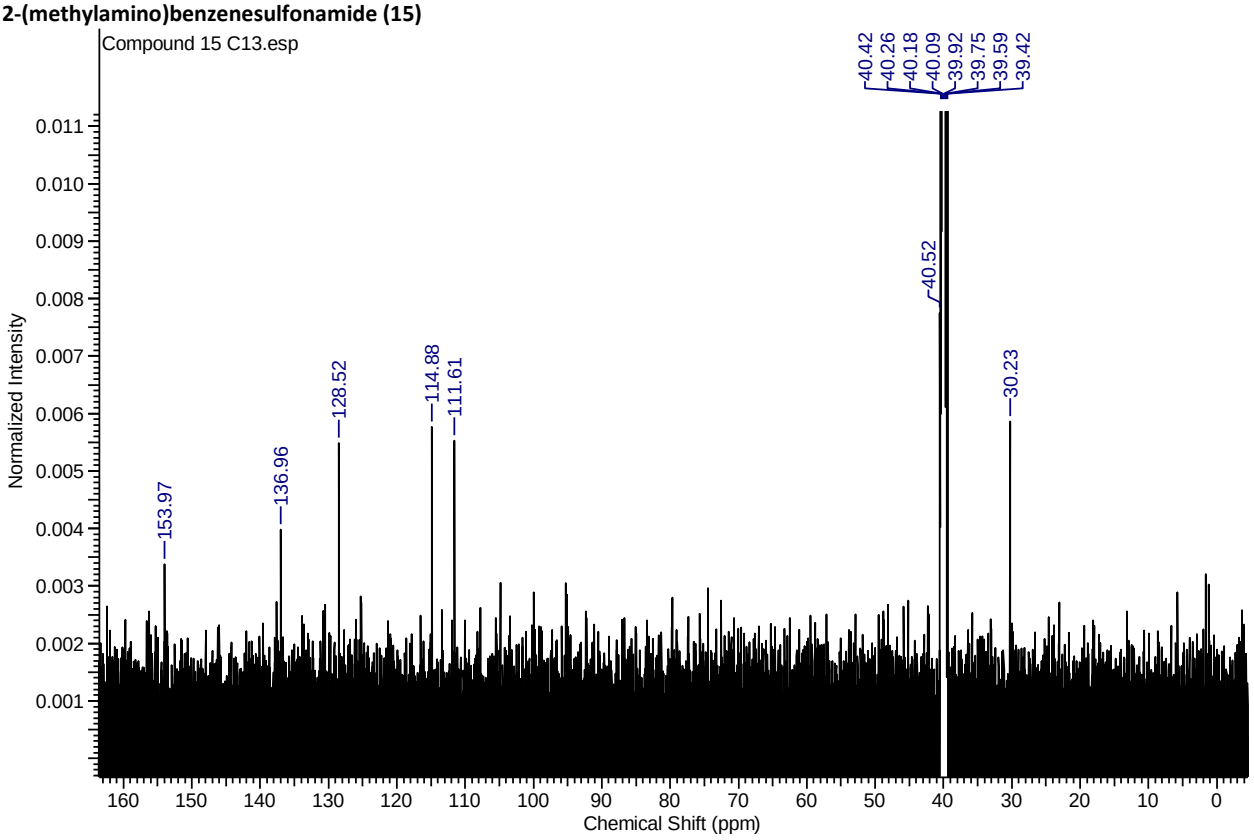

3-imino-4-methyl-3,4-dihydro-2H-benzo[e][1,2,4]thiadiazine 1,1-dioxide (16)

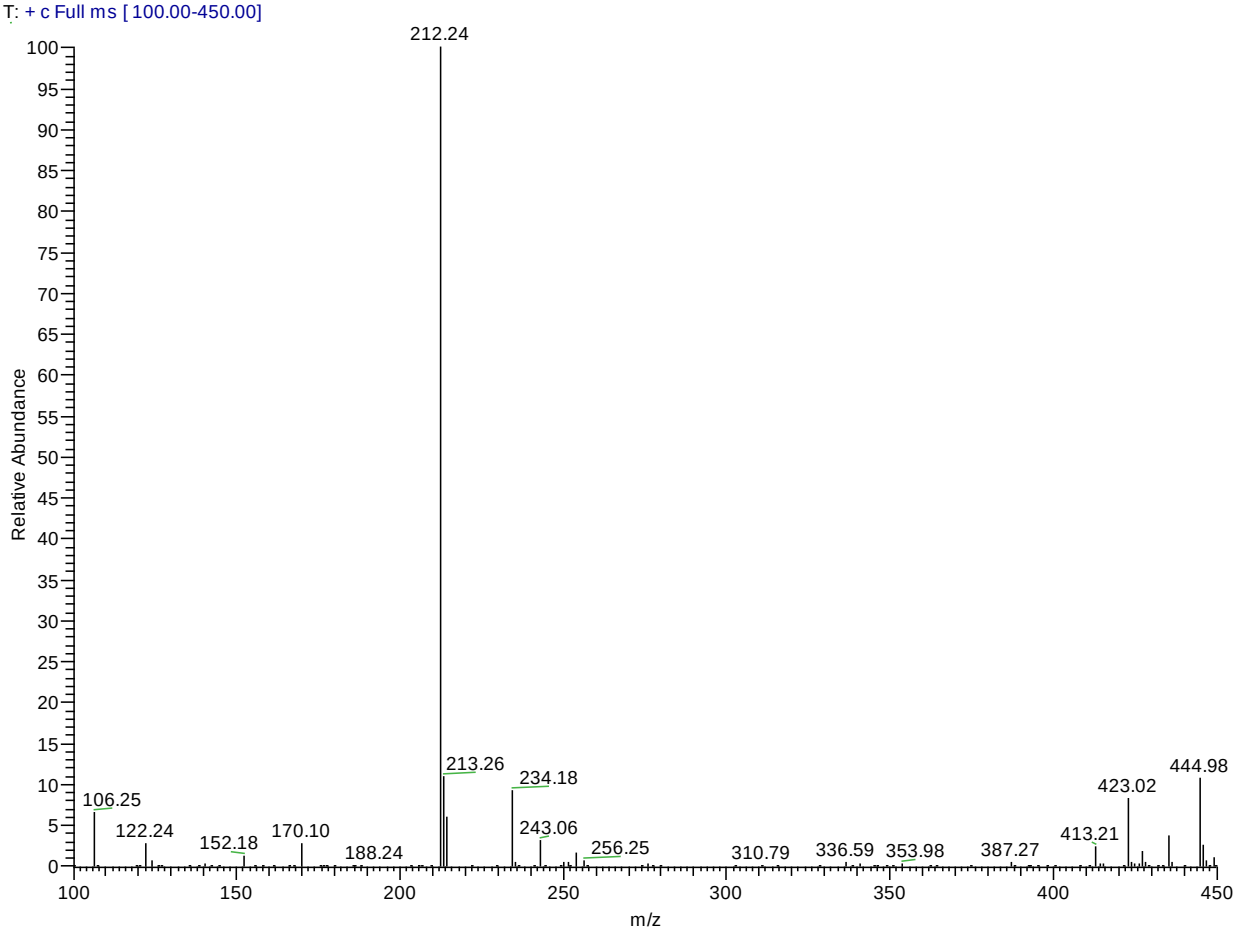

3-imino-4-methyl-3,4-dihydro-2H-benzo[e][1,2,4]thiadiazine 1,1-dioxide (16)

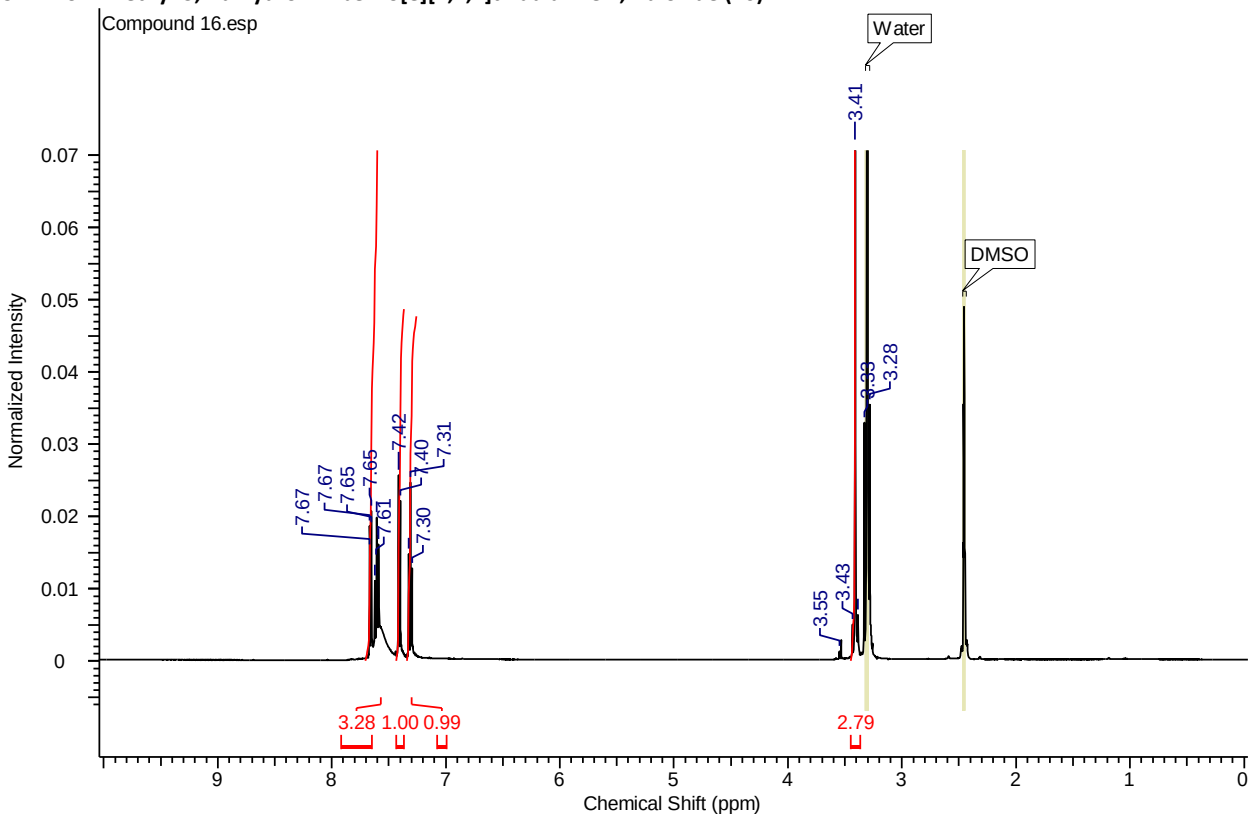

3-imino-4-methyl-3,4-dihydro-2H-benzo[e][1,2,4]thiadiazine 1,1-dioxide (16)

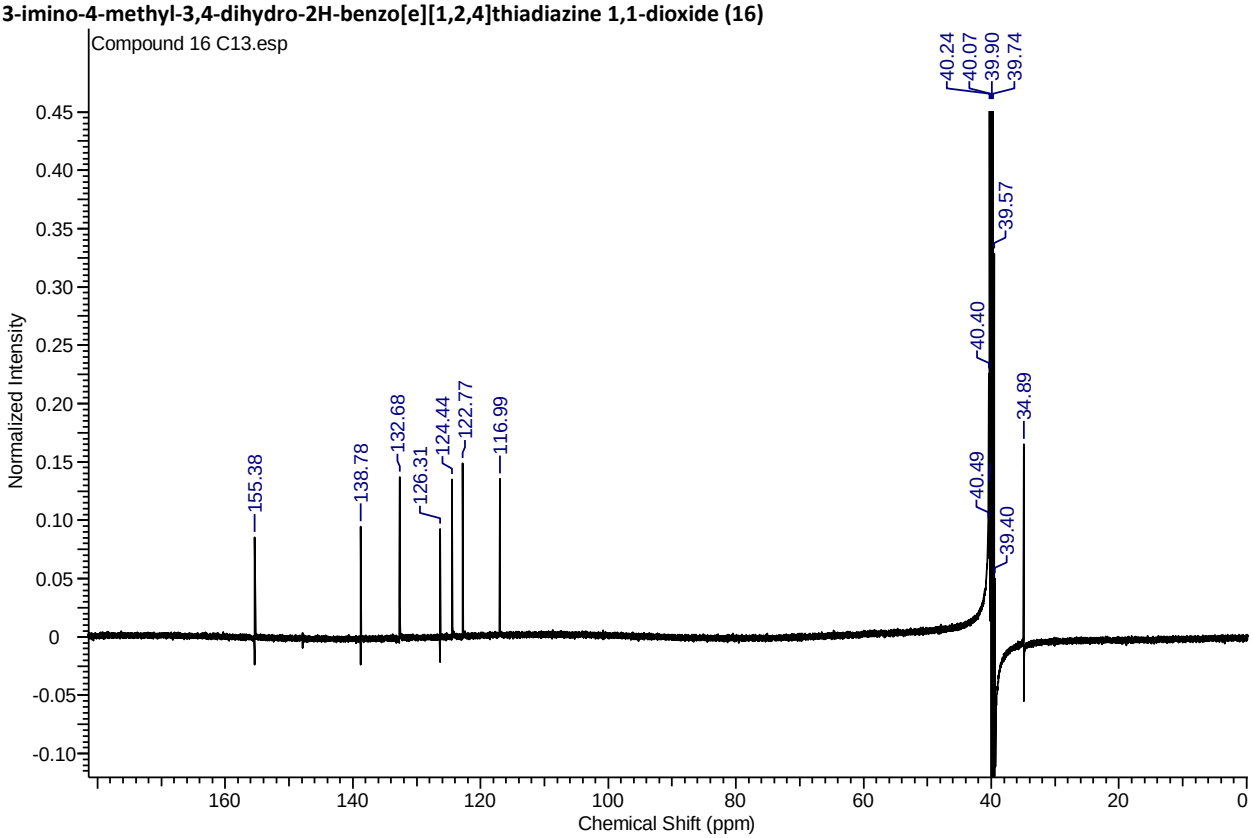

4-chloro-2-nitrobenzenesulfonamide (22)

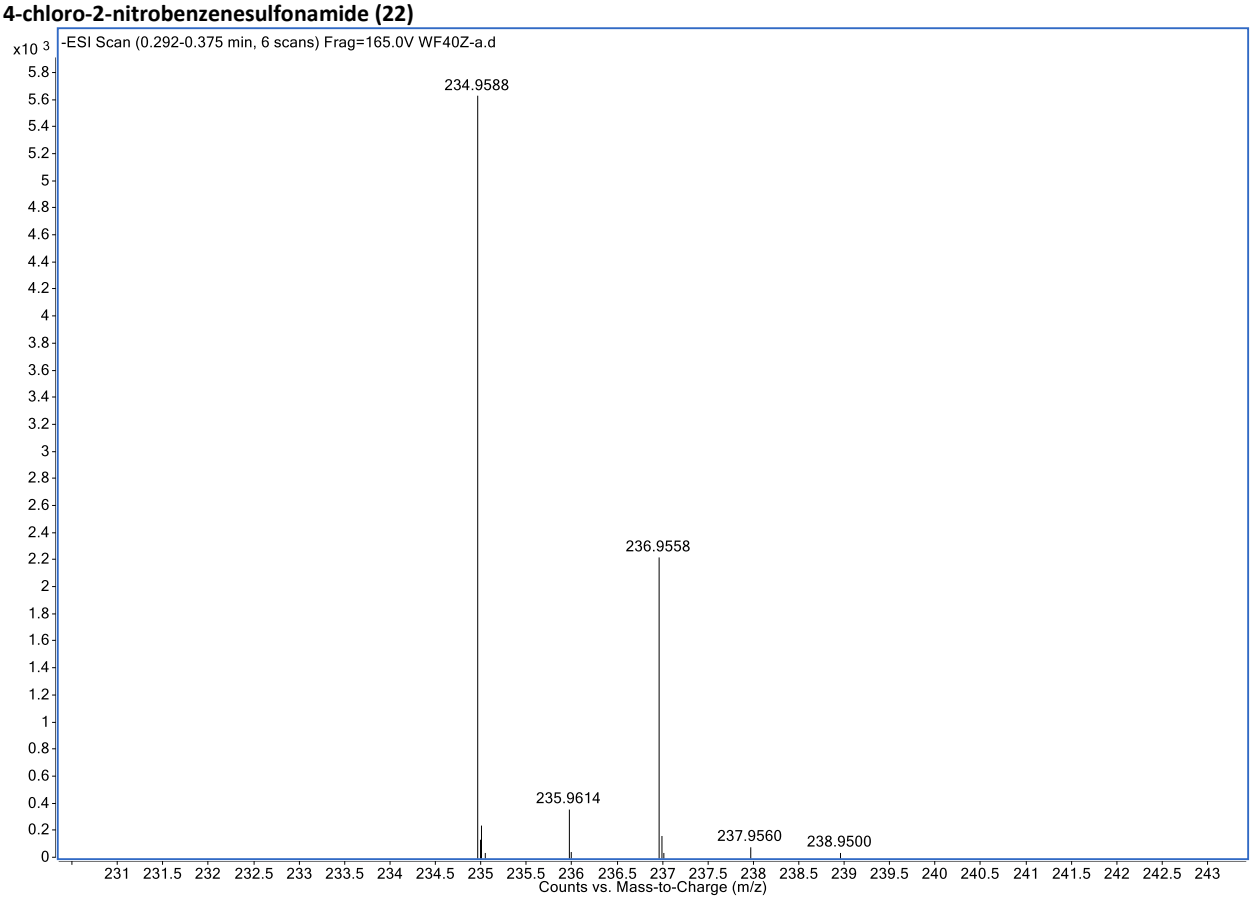

4-chloro-2-nitrobenzenesulfonamide (22)

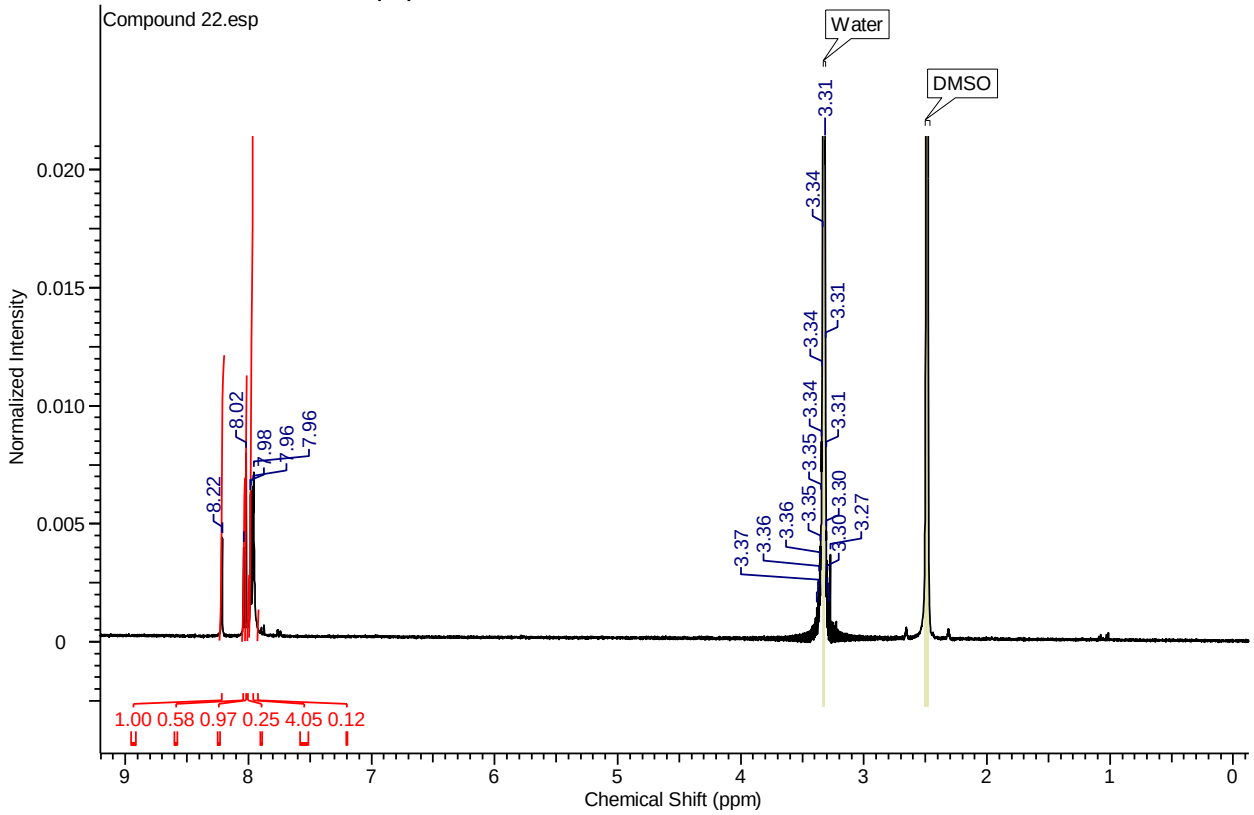

2-amino-4-chlorobenzenesulfonamide (23)

F: - c Full ms [100.00-350.00]

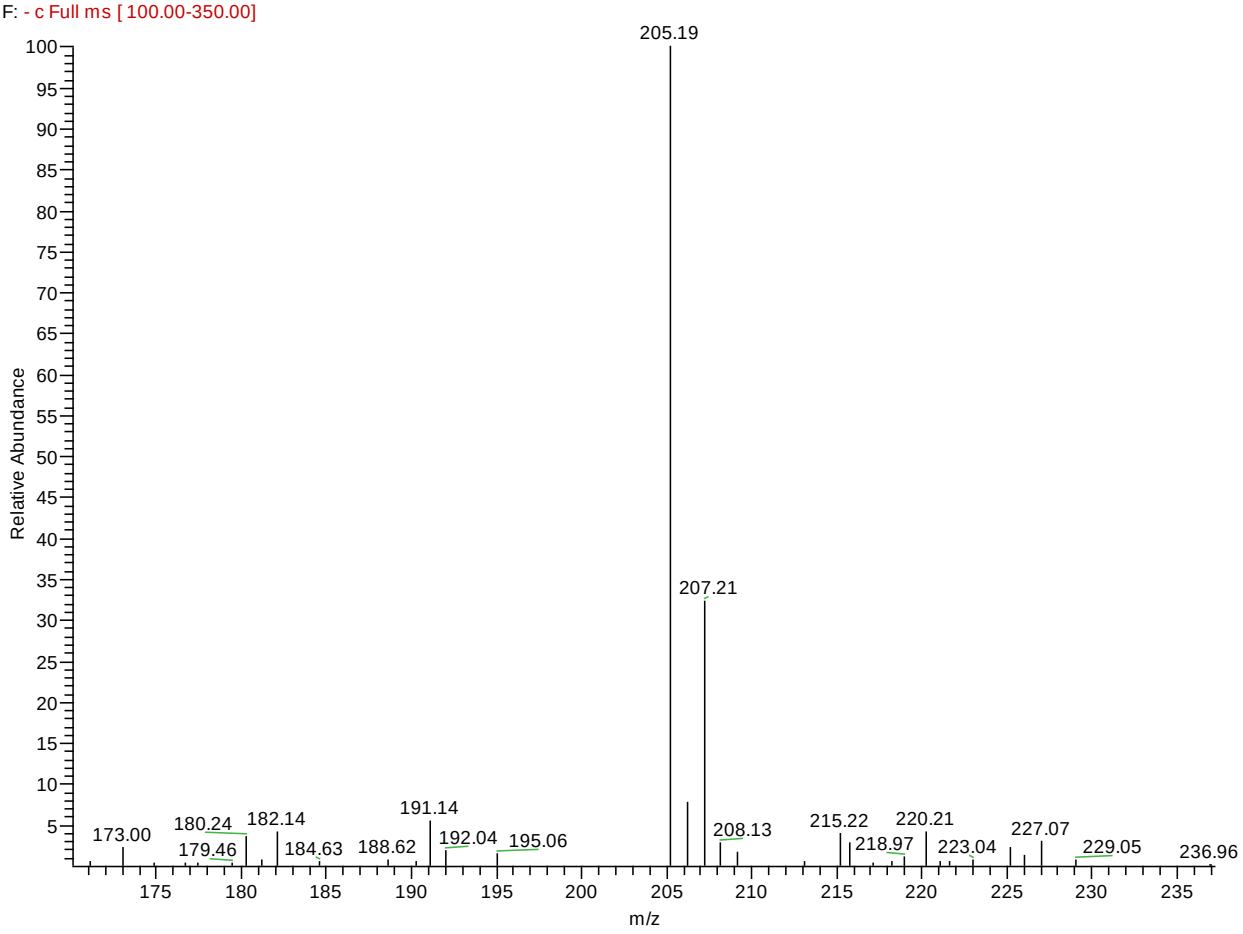

2-amino-4-chlorobenzenesulfonamide (23)

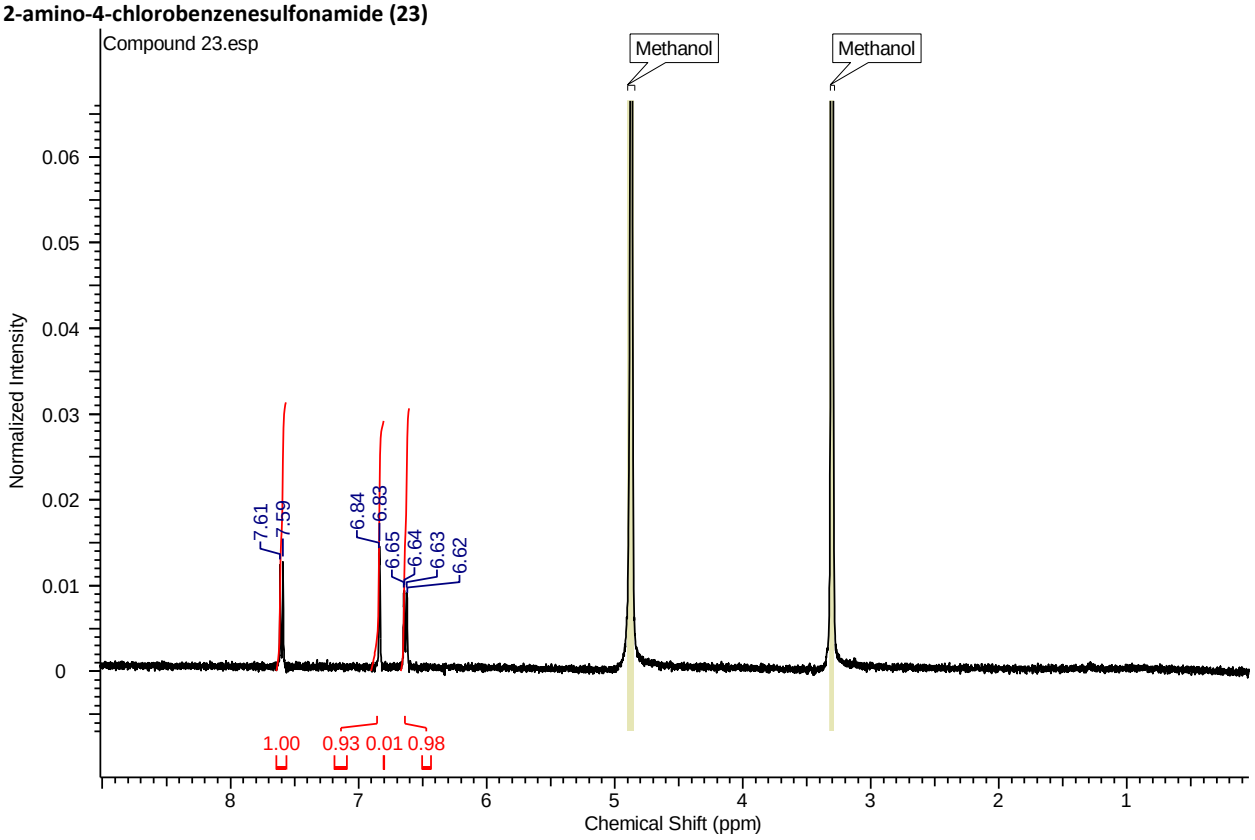

4-chloro-2-((3-(dimethylamino)propyl)amino)benzenesulfonamide (25)

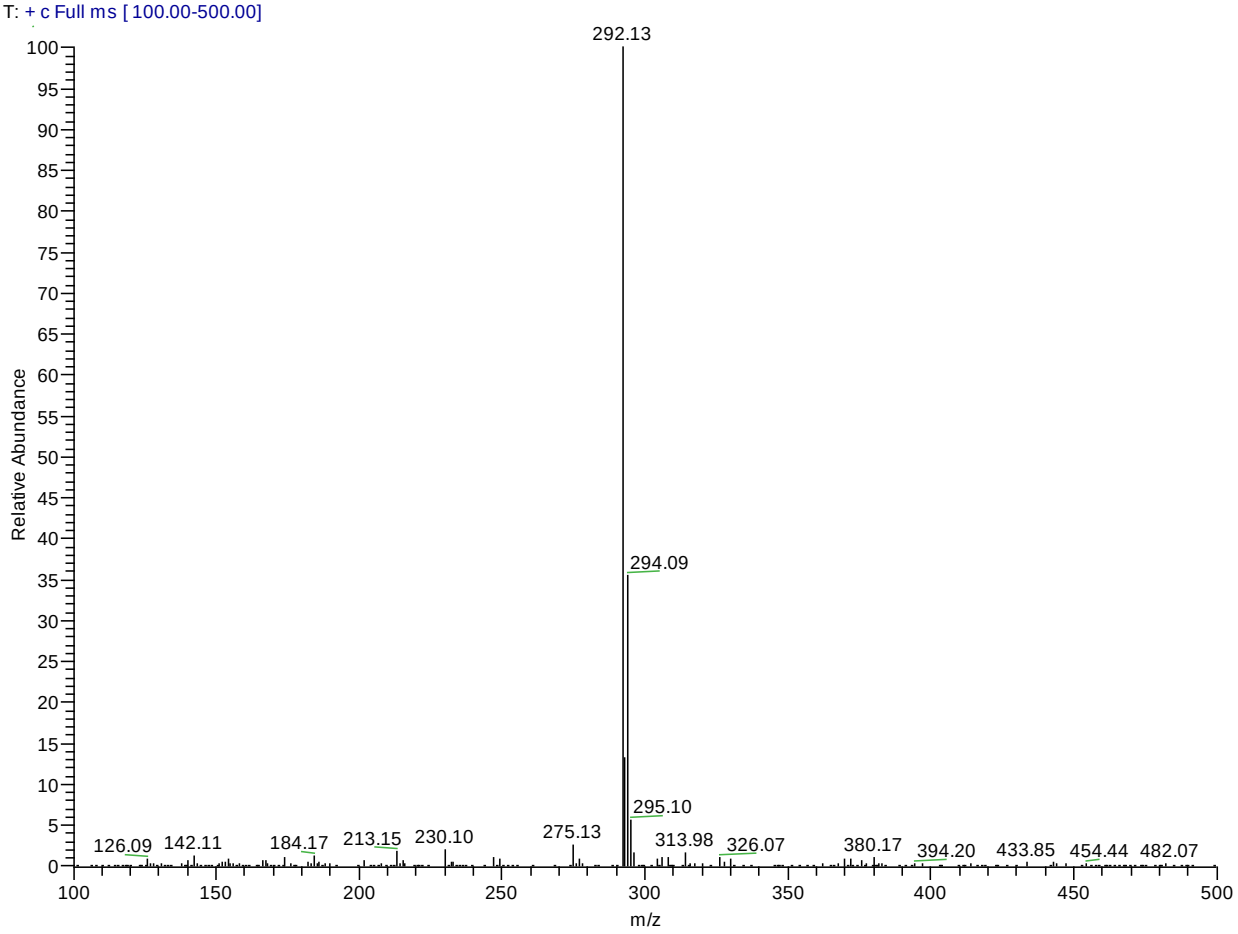

4-chloro-2-((3-(dimethylamino)propyl)amino)benzenesulfonamide (25)

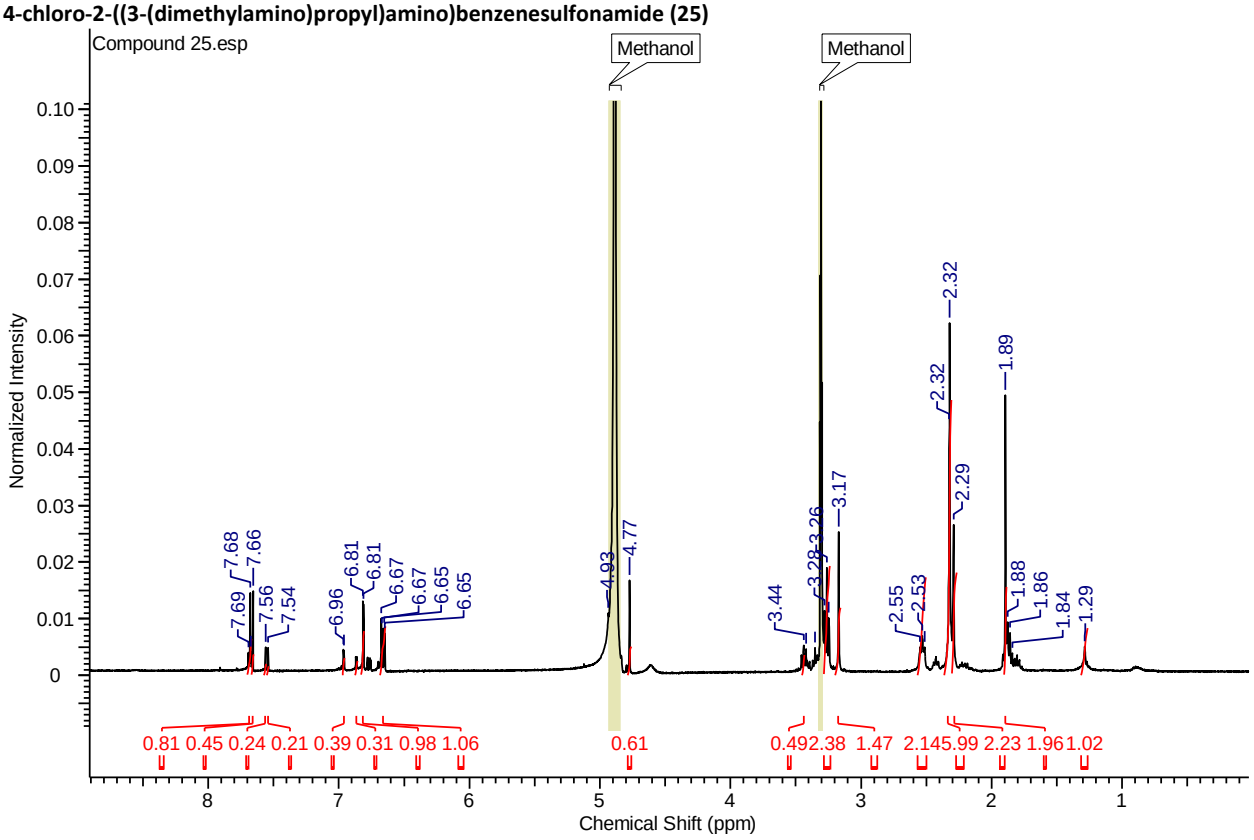

3-amino-6-chloro-4H-benzo[e][1,2,4]thiadiazine 1,1-dioxide (27)

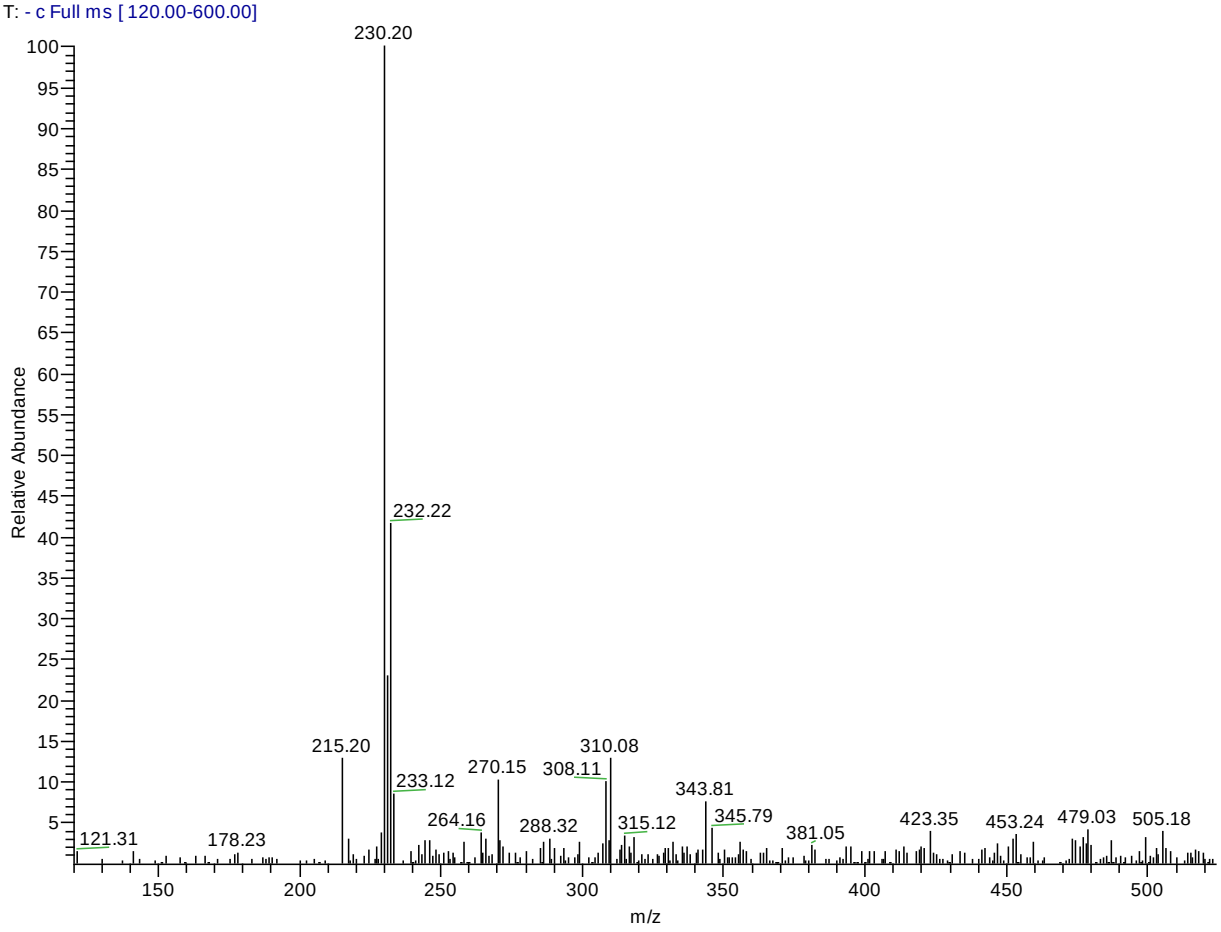

3-amino-6-chloro-4-(3-(dimethylamino)propyl)-4H-benzo[e][1,2,4]thiadiazine 1,1-dioxide (26)

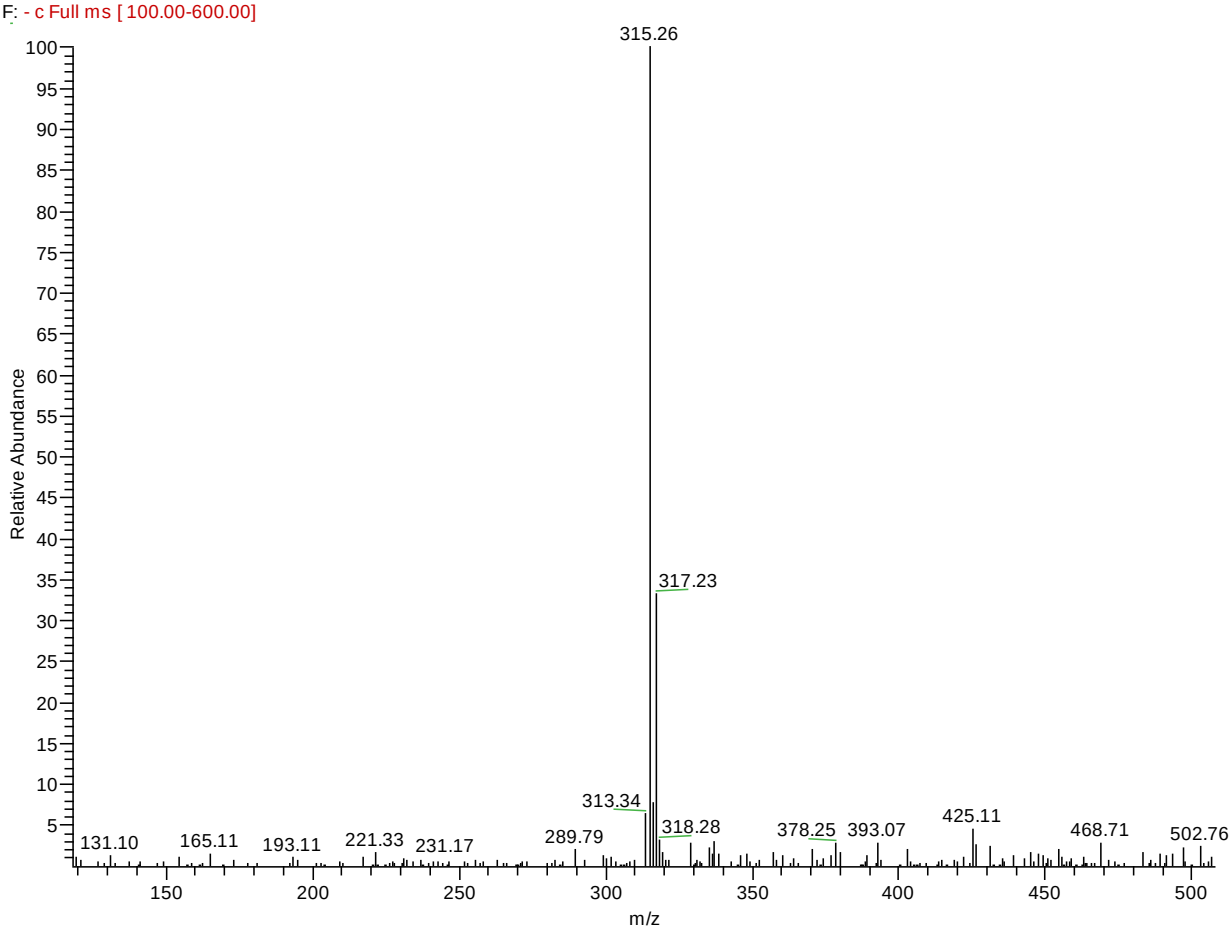

Benzene-(1,3,2)-dithiazole (33)

F: - c Full ms [100.00-400.00]

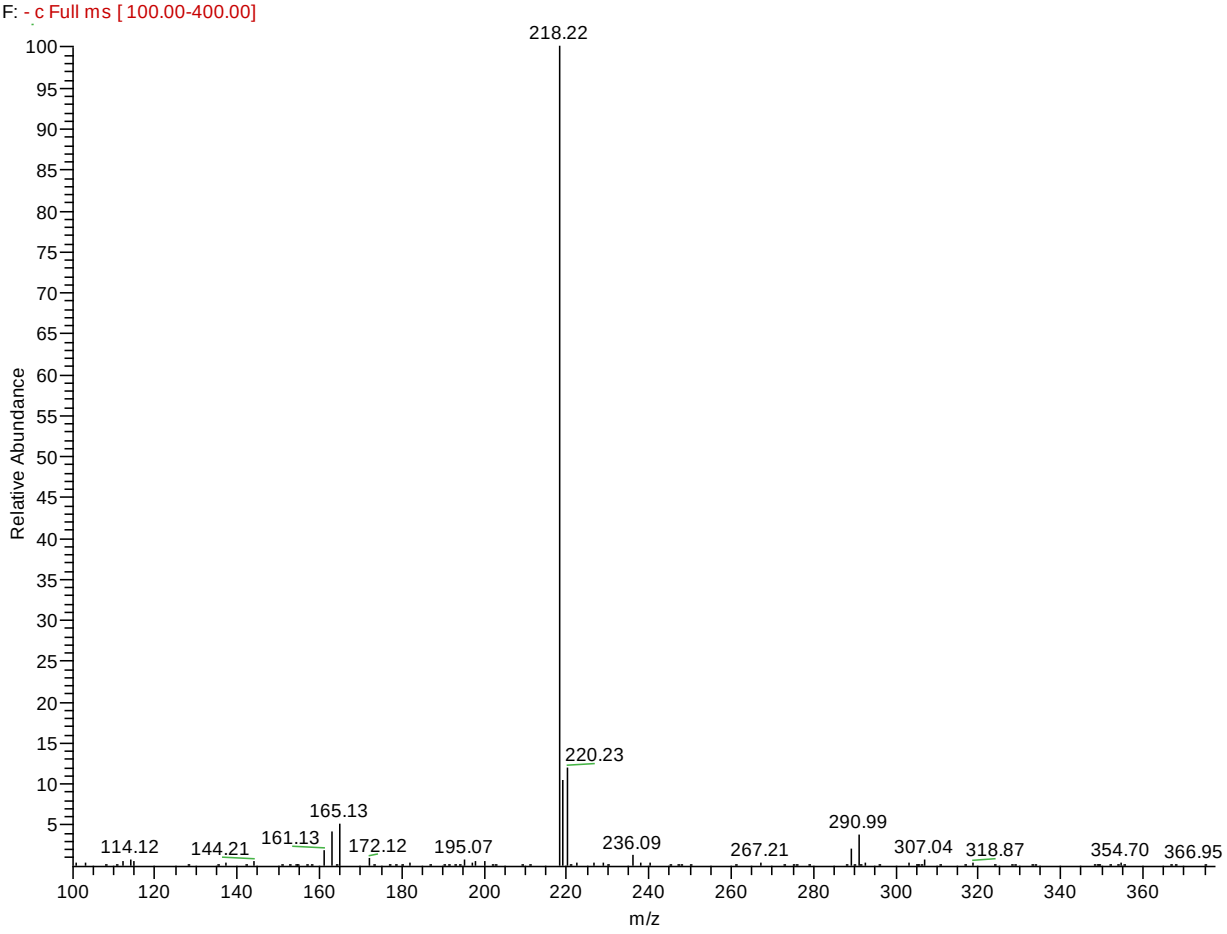

***N*,*N*-di-tert-butylbenzene-1,2-disulfonamide (34)**

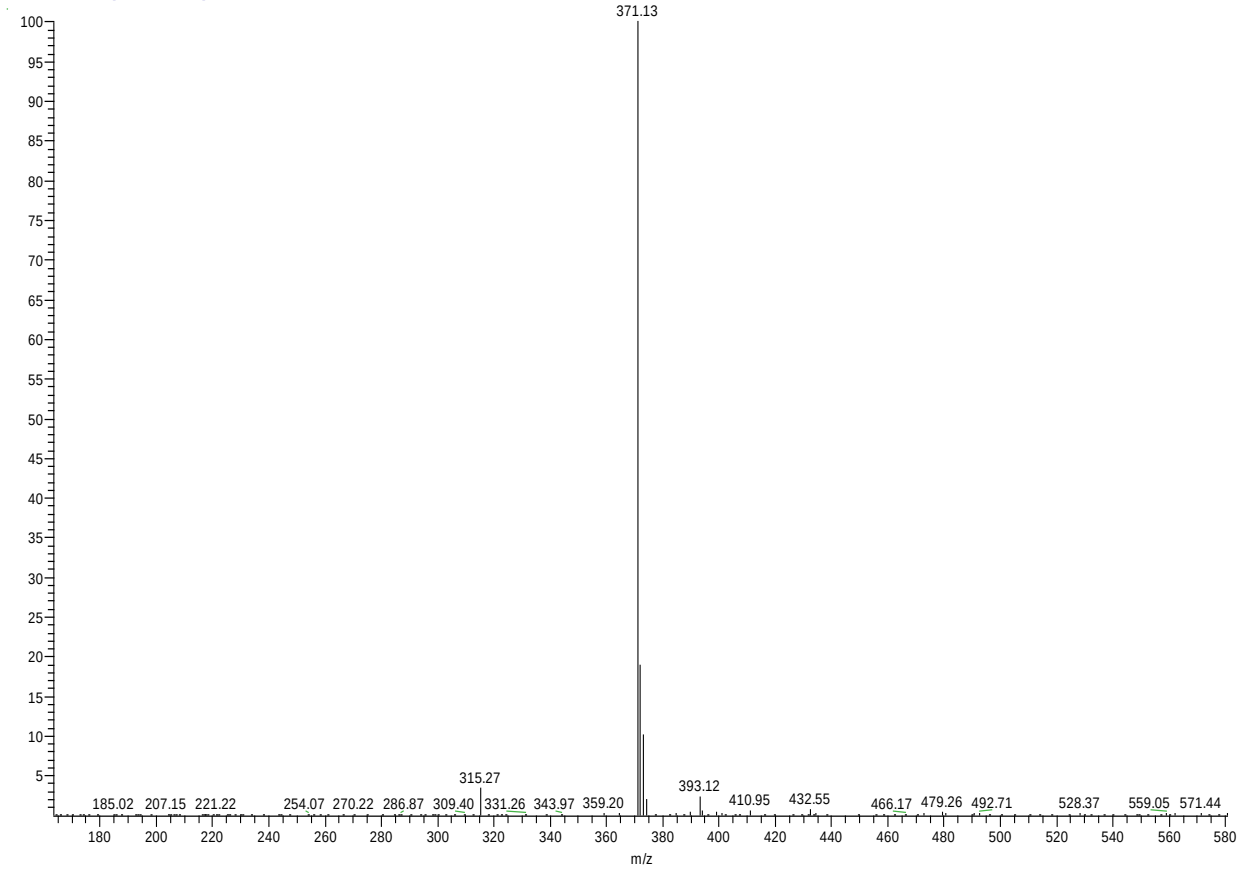

Benzene-1,2-disulfonamide (31)

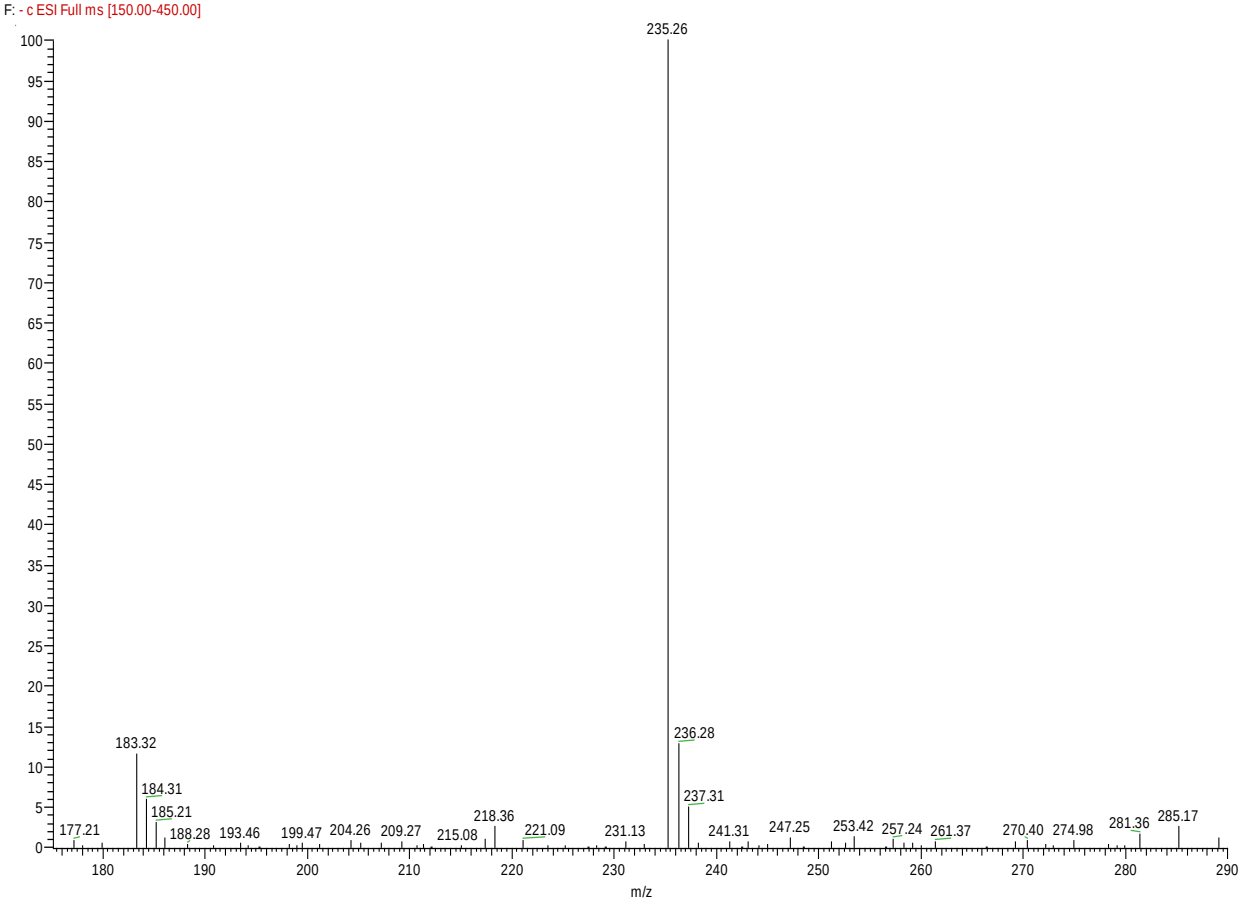

3-aminobenzoisothiazole (36)

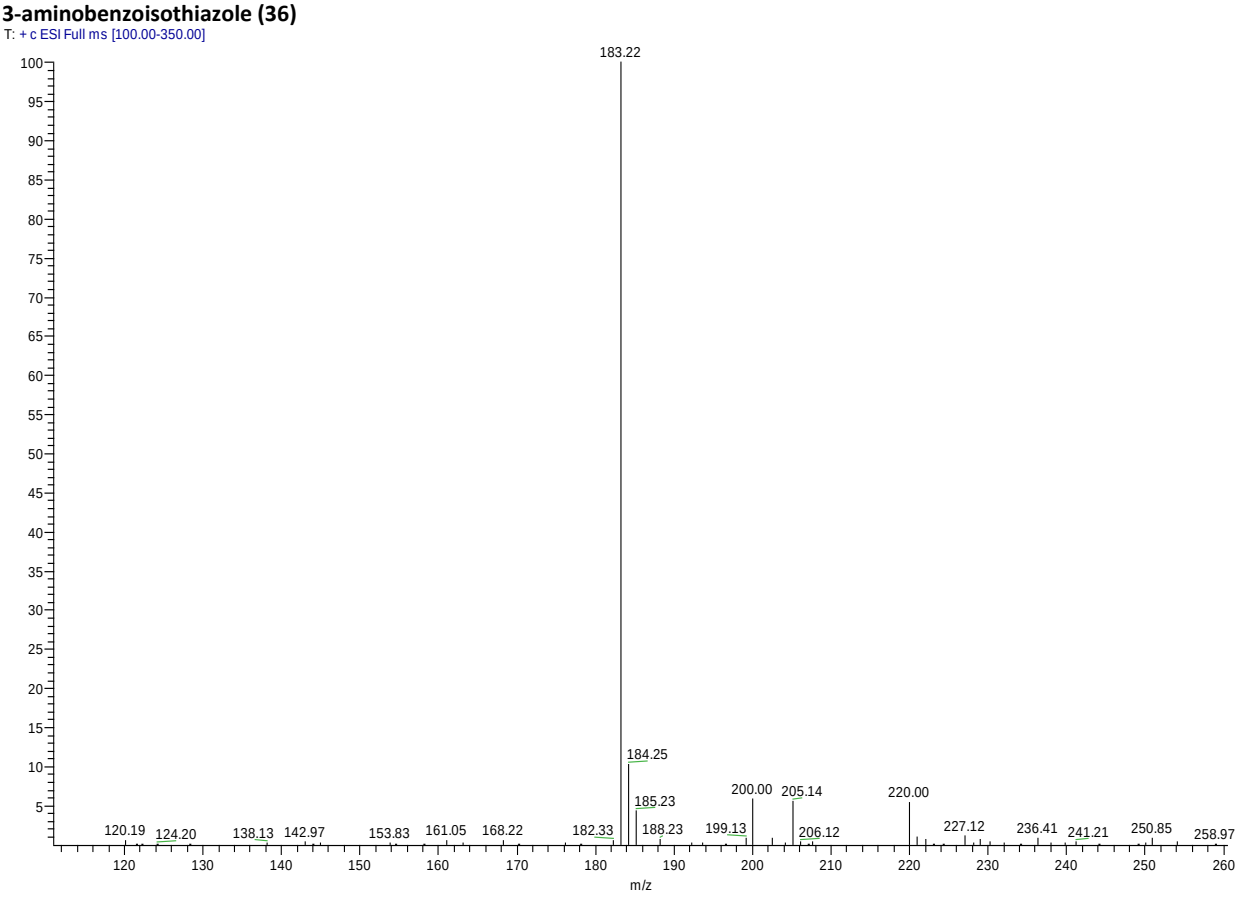

3-aminobenzoisothiazole (36)

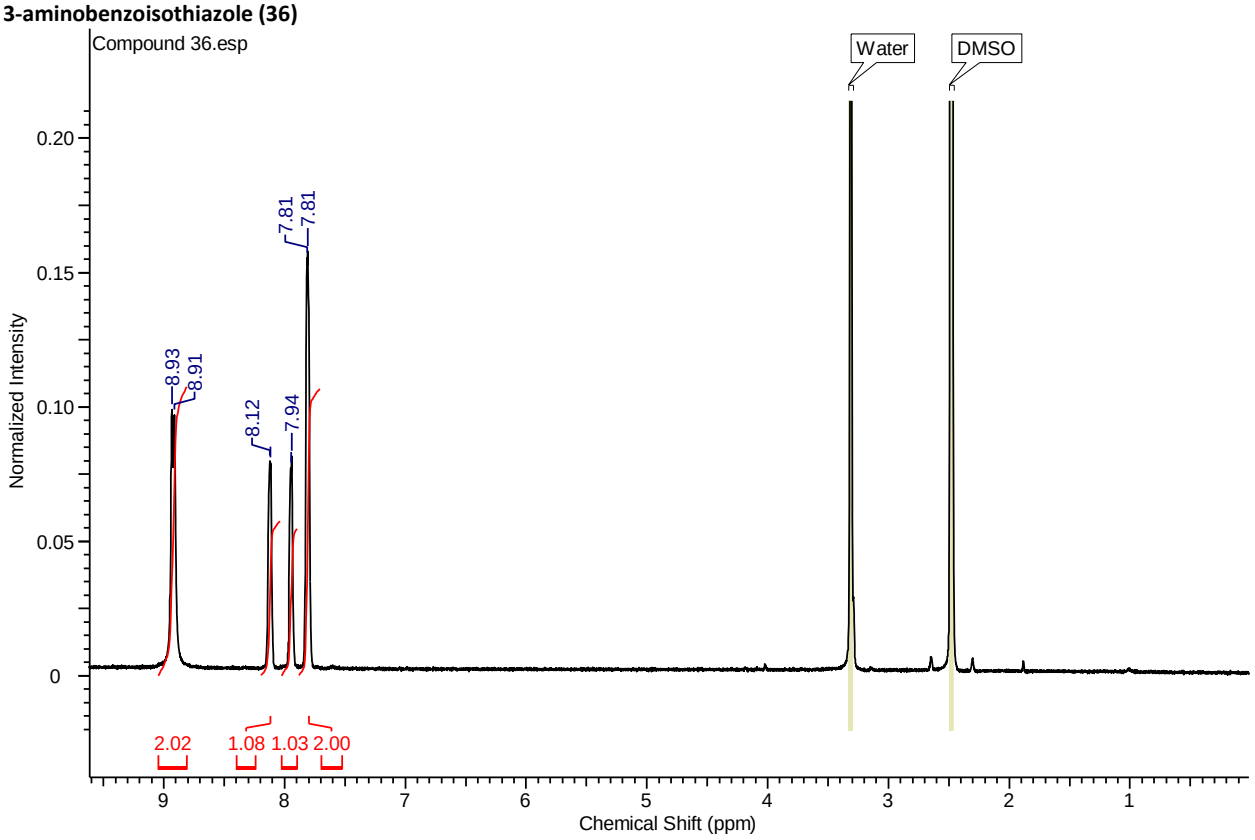

2-(aminomethyl)benzenesulfonamide (35)

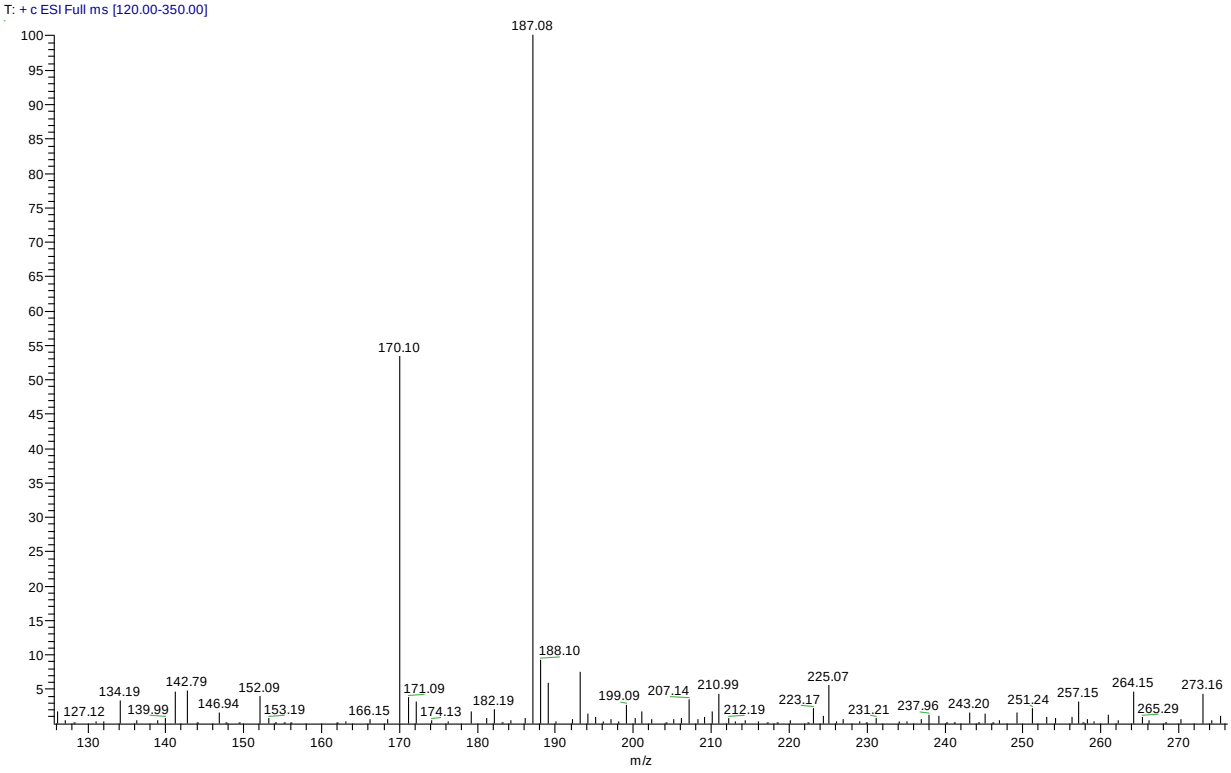

N,N’-diisopropyl-benzo[1,3]thiadiazepine (37)

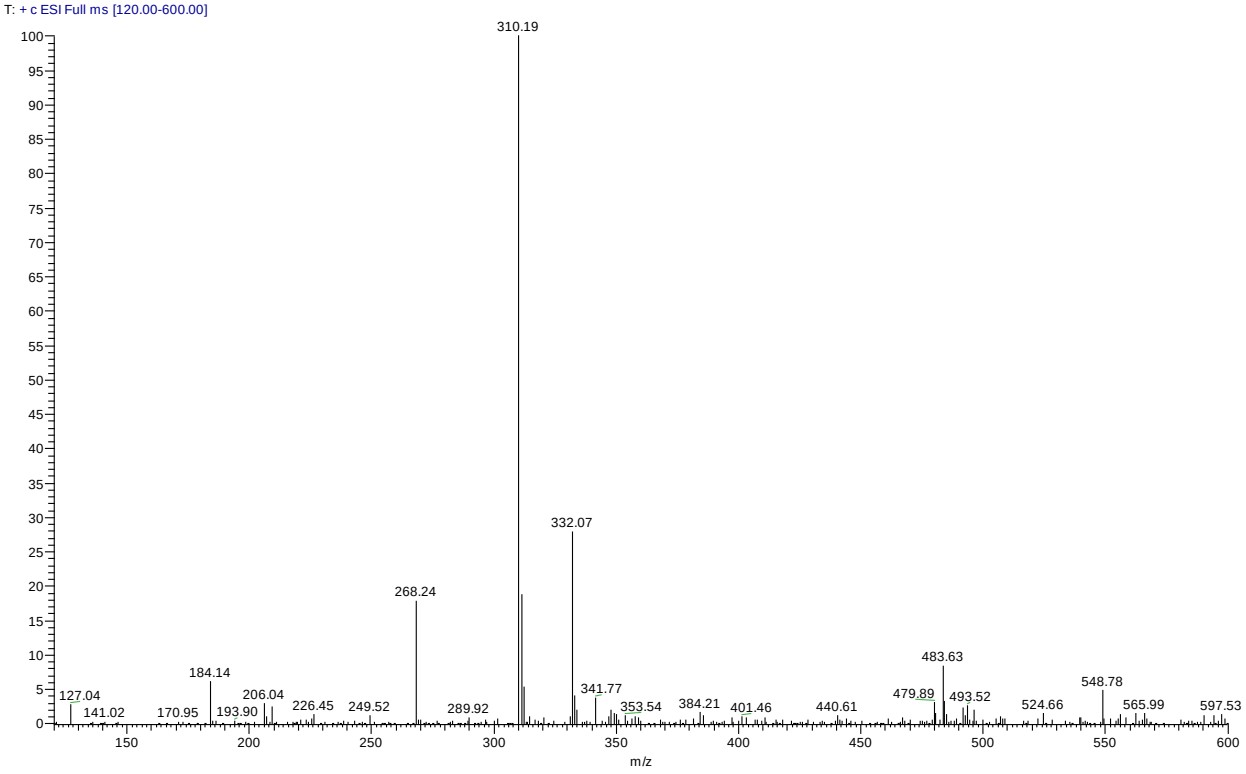

***N*-ethyl-*N'*-(3-(dimethylamino)propyl)amino)-benzo[1,3]thiadiazepine (38)**

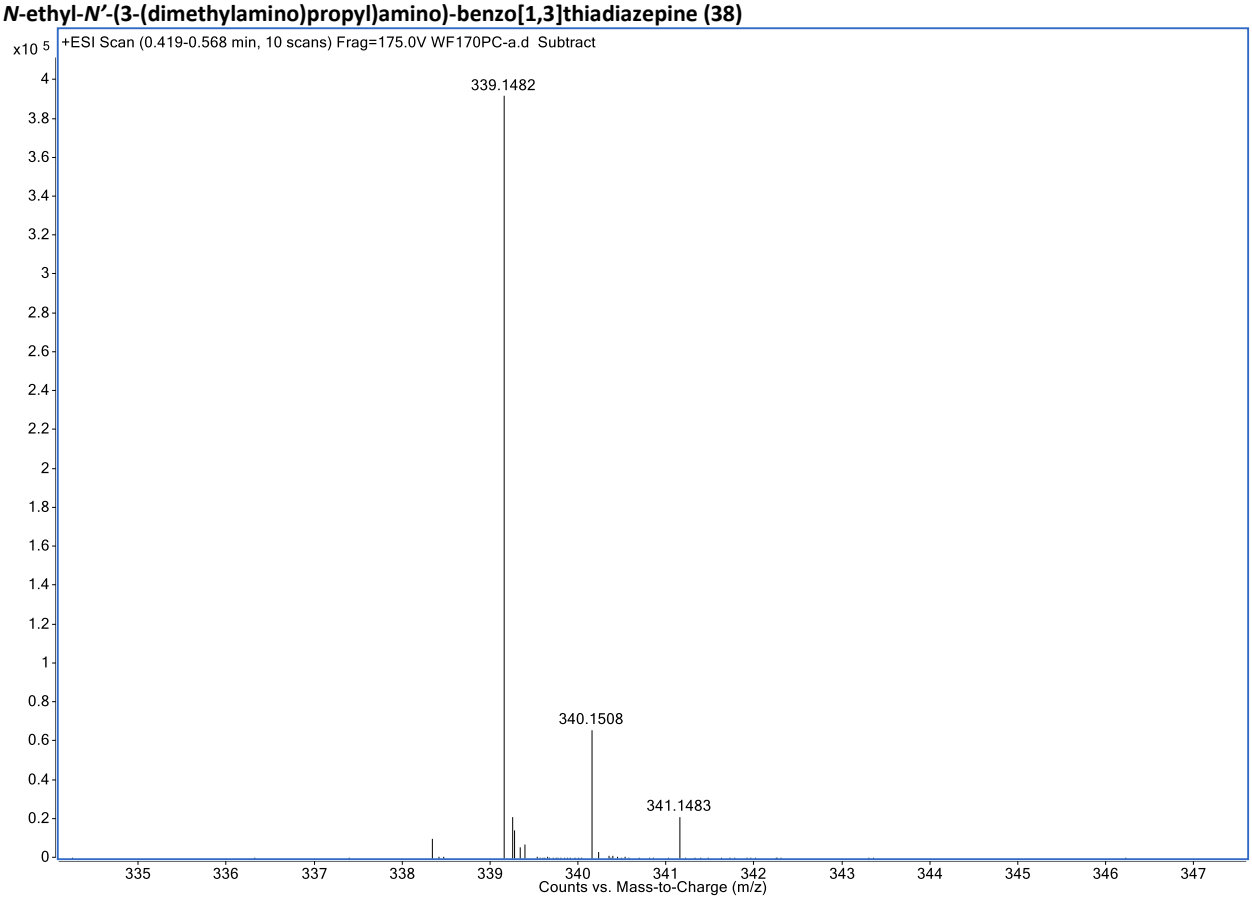

***N*-ethyl-*N'*-(3-(dimethylamino)propyl)amino)-benzo[1,3]thiadiazepine (38)**

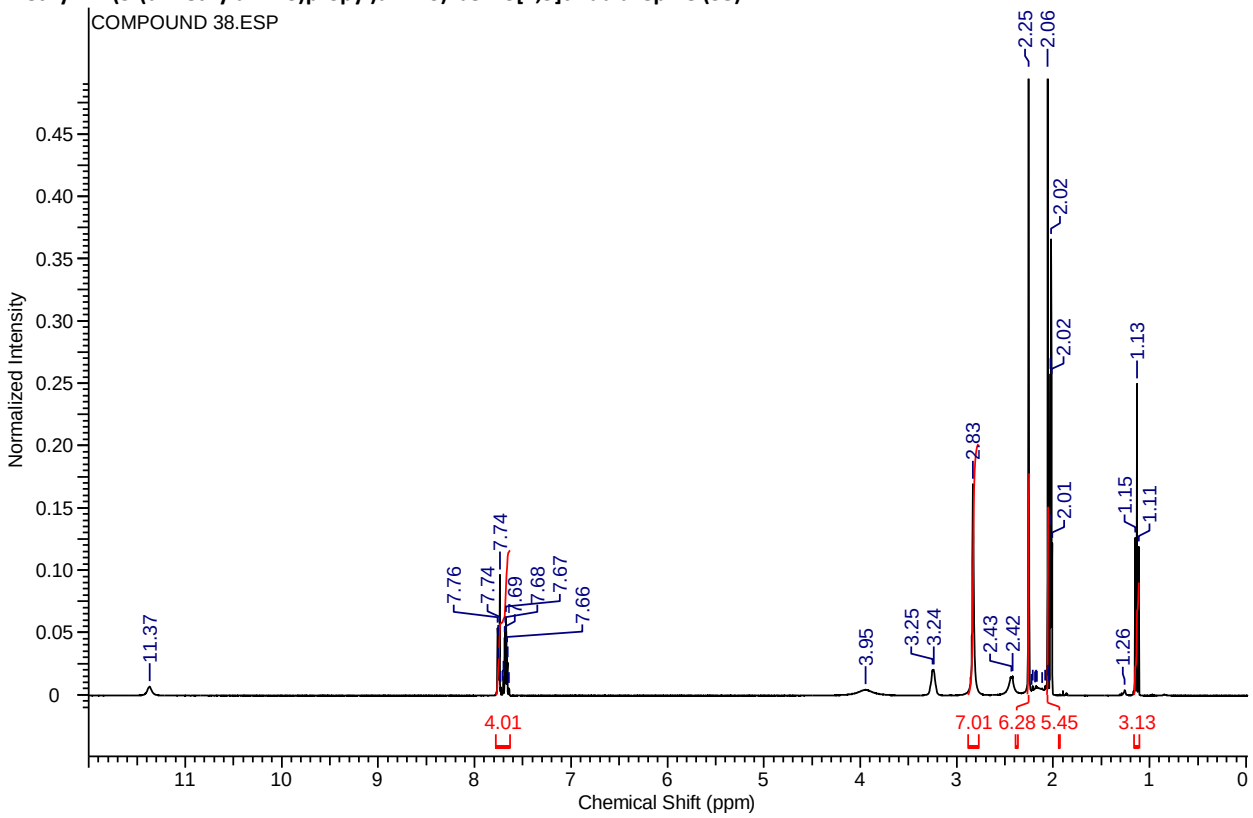

***N*-ethyl-*N'*-(3-(dimethylamino)propyl)amino)-benzo[1,3]thiadiazepine (38)**

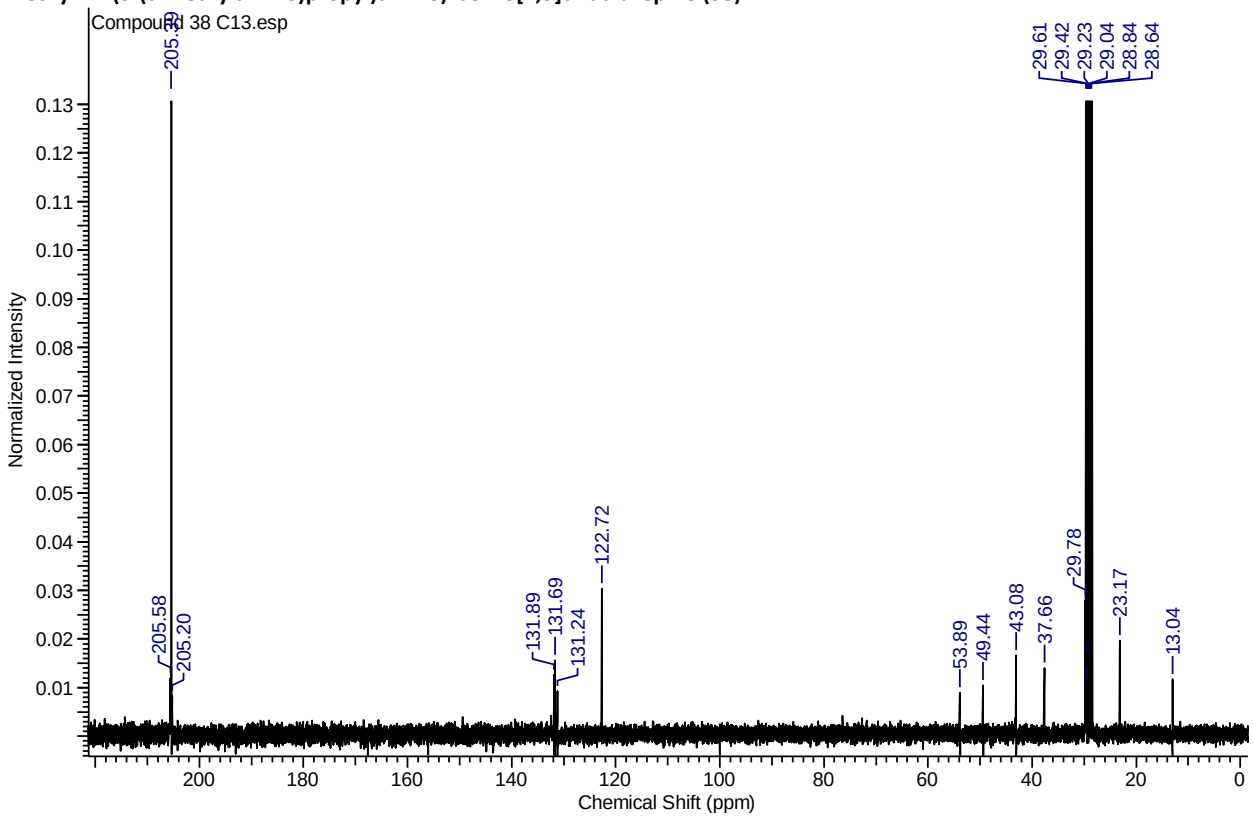

4-(2-(3-(cyclohexylamino)-1,1-dioxido-5-oxobenzo[f][1,2,4]thiadiazepin-4(5H)-yl)ethyl)-4-methylmorpholin-4-ium metho-p-toluene sulfonate (39)

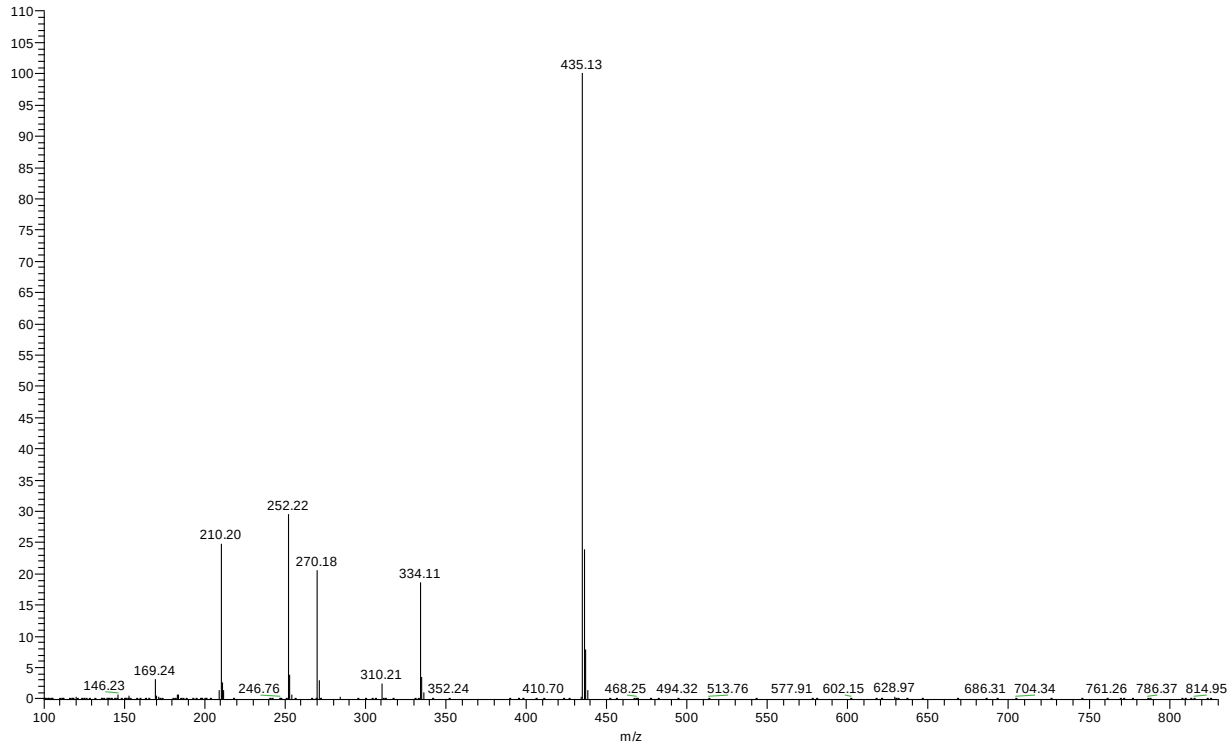

1-(4,4'-Dimethoxybenzhydryl)-3-(ethoxycarbonyl)thiourea (44)

T: + c Full ms [120.00-400.00]

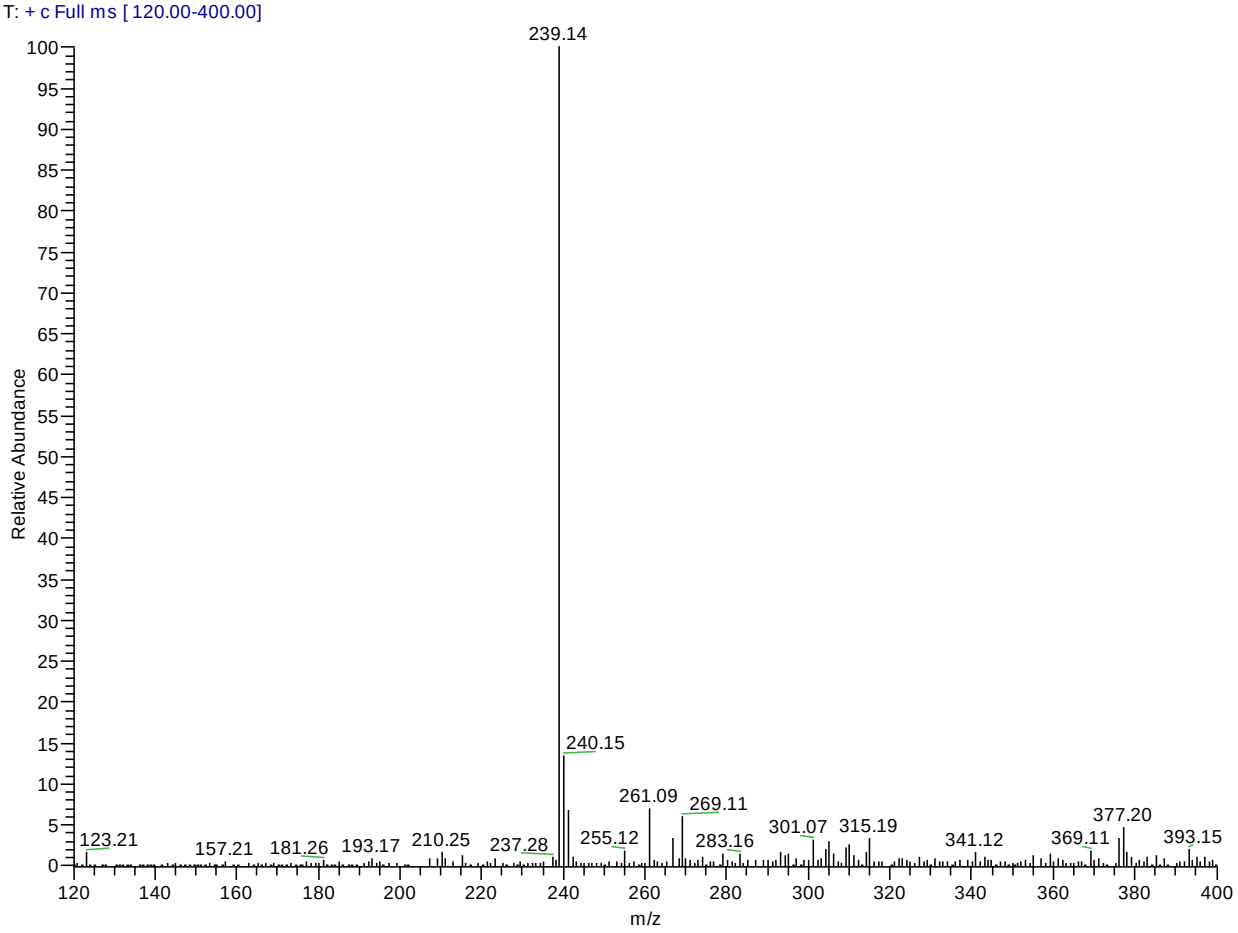

Ethyl-(2-benzyl-1-hydroxy-1,2-dihydrobenzo[c][1,5,2]diazaborinin-3-yl)carbamate (46)

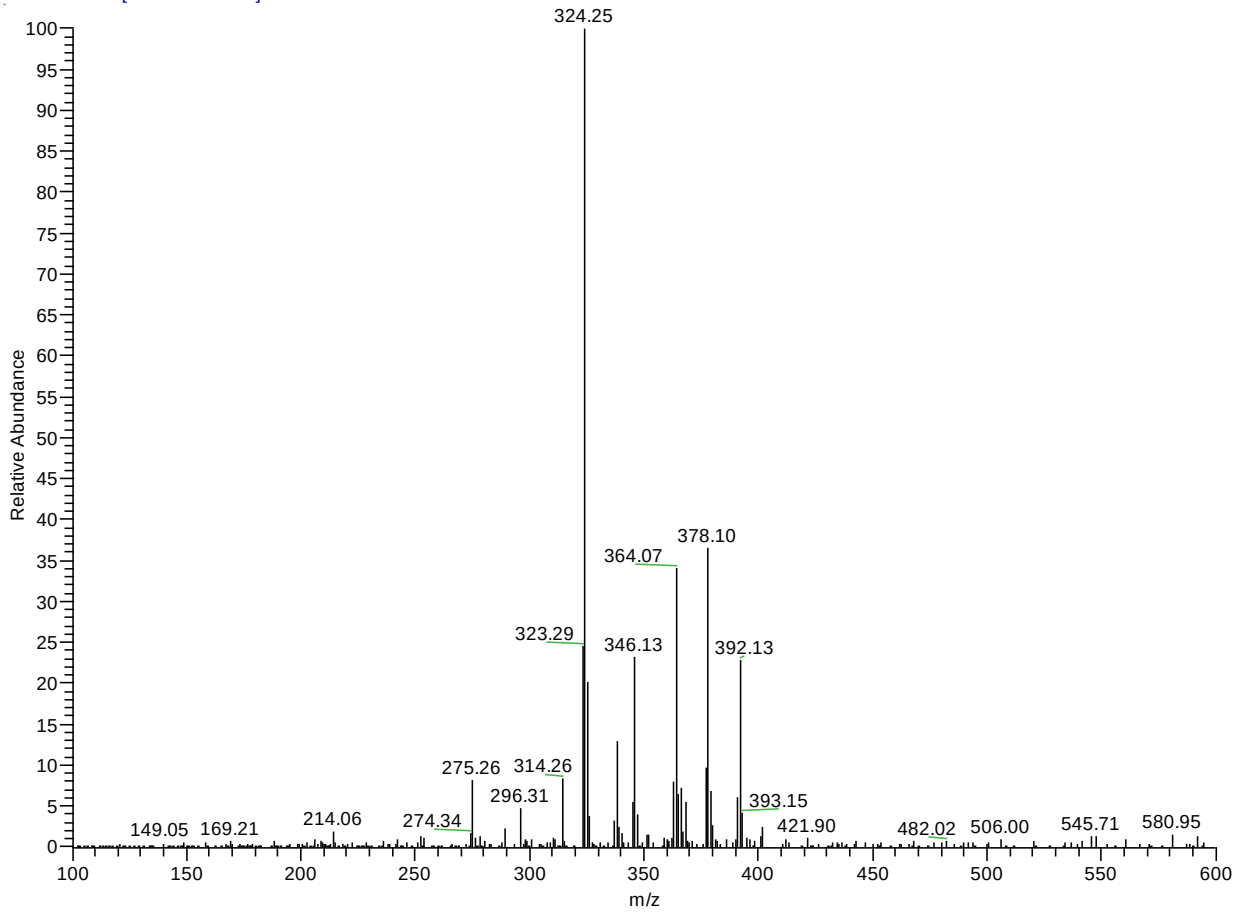

3-(benzylamino)benzo[c][1,5,2]diazaborinin-1(2H)-ol (47)

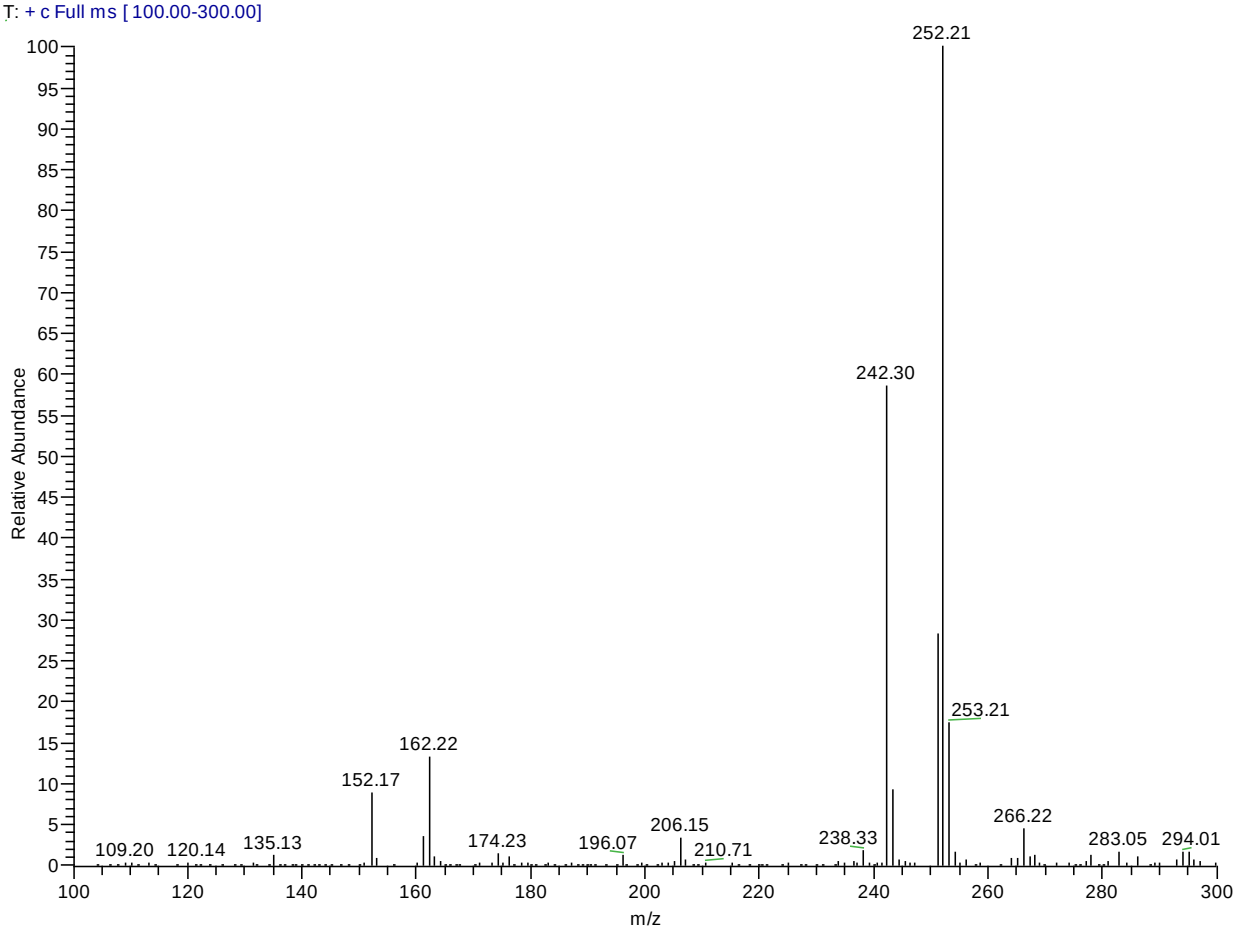

3-aminobenzo[e][1,2,4]triazine 1-oxide (49)

T: + c Full ms [100.00-300.00]

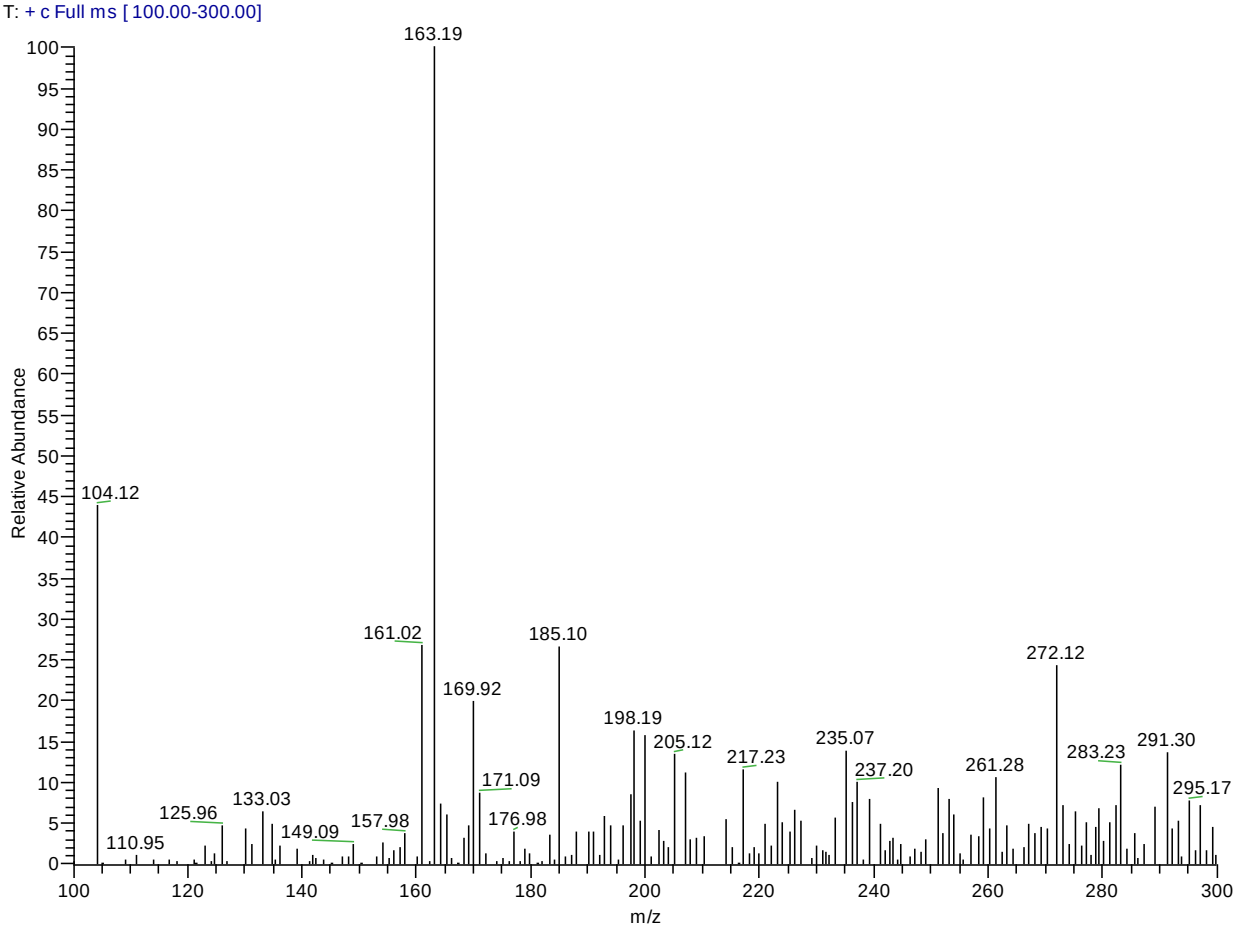

3-aminobenzo[e][1,2,4]triazine 1-oxide (49)

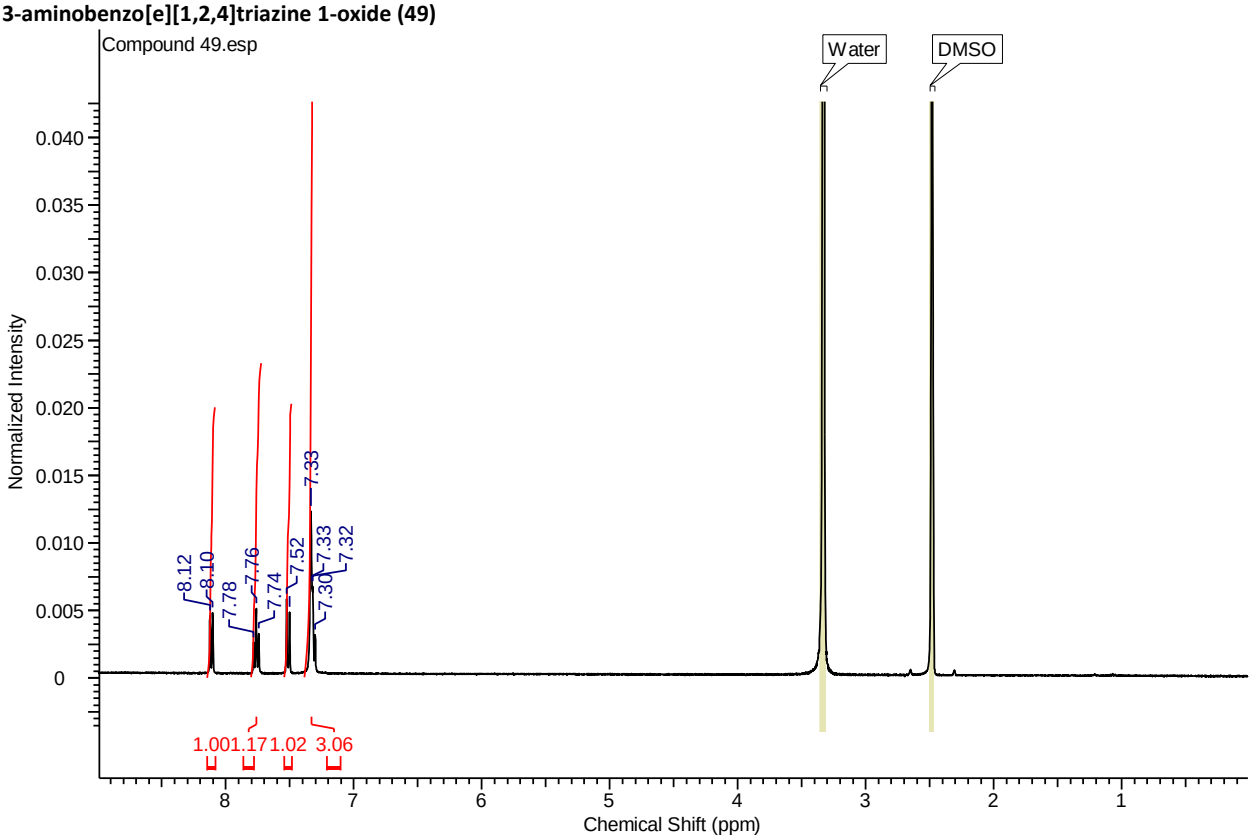

3-aminobenzoisothiazole (36)

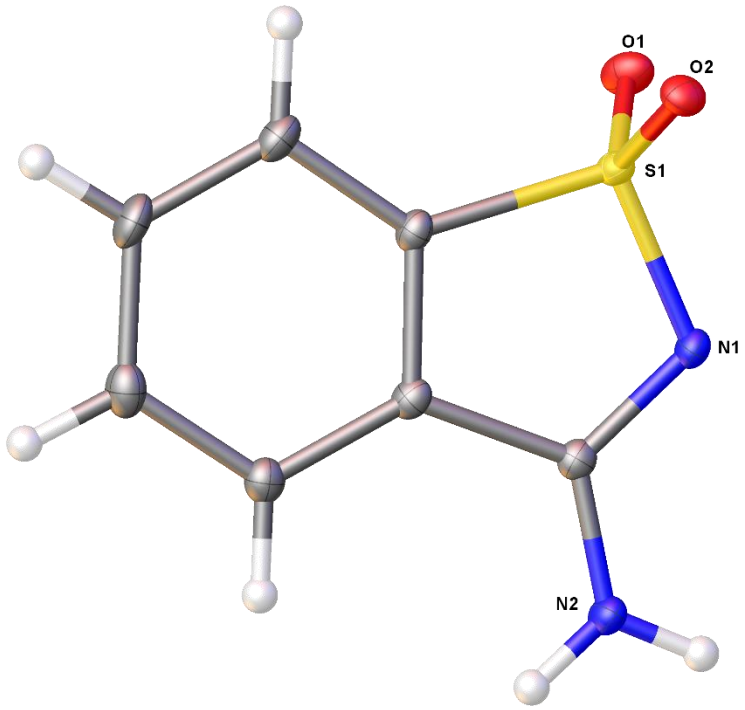

Table 1. Crystal data and structure refinement for hermann10_0m_a.

Identification code	WF140	
Empirical formula	C7 H6 N2 O2 S	
Formula weight	182.20	
Temperature	100.0 K	
Wavelength	0.71073 Å	
Crystal system	Monoclinic	
Space group	P 21/n	
Unit cell dimensions	a = 6.8864(7) Å	α= 90°.
	b = 12.7754(12) Å	β= 92.139(3)°.
	c = 8.5622(7) Å	γ = 90°.
Volume	752.75(12) $Å^3$	
Z	4	
Density (calculated)	1.608 Mg/m^3	
Absorption coefficient	0.383 mm^{-1}	
F(000)	376	
Crystal size	0.31 x 0.29 x 0.28 mm^3	
Theta range for data collection	2.865 to 28.284°.	
Index ranges	-9<=h<=9, -17<=k<=17, -11<=l<=10	
Reflections collected	5386	
Independent reflections	1852 [R(int) = 0.0352]	
Completeness to theta = 25.242°	99.7 %	
Absorption correction	Semi-empirical from equivalents	
Max. and min. transmission	0.7457 and 0.6927	
Refinement method	Full-matrix least-squares on F^2	
Data / restraints / parameters	1852 / 0 / 117	
Goodness-of-fit on F^2	1.081	
Final R indices [I>2sigma(I)]	R1 = 0.0306, wR2 = 0.0856	
R indices (all data)	R1 = 0.0325, wR2 = 0.0873	
Extinction coefficient	n/a	

Largest diff. peak and hole 0.460 and -0.385 e.Å^{-3}

Table 2. Atomic coordinates (x 10^4) and equivalent isotropic displacement parameters (Å^{2}x 10^3) for hermann10_0m_a. U(eq) is defined as one third of the trace of the orthogonalized U^{ij} tensor.

	x	y	z	U(eq)
S(1)	2773(1)	6601(1)	2791(1)	11(1)
O(2)	1590(1)	6900(1)	1435(1)	15(1)
O(1)	3435(2)	7445(1)	3790(1)	17(1)
N(2)	2061(2)	3985(1)	4538(1)	14(1)
N(1)	1656(2)	5713(1)	3788(1)	12(1)
C(2)	4474(2)	4830(1)	2908(1)	11(1)
C(1)	2643(2)	4820(1)	3786(1)	11(1)
C(3)	5861(2)	4052(1)	2721(2)	13(1)
C(4)	7480(2)	4295(1)	1858(2)	16(1)
C(7)	4733(2)	5812(1)	2251(1)	11(1)
C(6)	6317(2)	6070(1)	1387(2)	15(1)
C(5)	7700(2)	5287(1)	1200(2)	17(1)

Table 3. Bond lengths [Å] and angles [°] for hermann10_0m_a.

S(1)-O(2)	1.4450(10)
S(1)-O(1)	1.4404(10)
S(1)-N(1)	1.6302(11)
S(1)-C(7)	1.7597(13)
N(2)-C(1)	1.3168(17)
N(2)-H(2A)	0.87(2)
N(2)-H(2B)	0.87(2)
N(1)-C(1)	1.3276(16)
C(2)-C(1)	1.4915(17)
C(2)-C(3)	1.3915(17)
C(2)-C(7)	1.3895(18)
C(3)-H(3)	0.9500
C(3)-C(4)	1.3949(19)
C(4)-H(4)	0.9500
C(4)-C(5)	1.398(2)
C(7)-C(6)	1.3804(18)
C(6)-H(6)	0.9500
C(6)-C(5)	1.3940(19)
C(5)-H(5)	0.9500

O(2)-S(1)-N(1)	110.01(6)
O(2)-S(1)-C(7)	110.83(6)
O(1)-S(1)-O(2)	115.81(6)
O(1)-S(1)-N(1)	110.81(6)
O(1)-S(1)-C(7)	110.86(6)
N(1)-S(1)-C(7)	96.94(6)
C(1)-N(2)-H(2A)	121.0(14)
C(1)-N(2)-H(2B)	119.8(12)
H(2A)-N(2)-H(2B)	119.0(18)
C(1)-N(1)-S(1)	110.17(9)
C(3)-C(2)-C(1)	130.46(12)
C(7)-C(2)-C(1)	109.56(11)
C(7)-C(2)-C(3)	119.95(12)
N(2)-C(1)-N(1)	121.98(12)

N(2)-C(1)-C(2)	122.11(12)
N(1)-C(1)-C(2)	115.89(11)
C(2)-C(3)-H(3)	121.1
C(2)-C(3)-C(4)	117.87(12)
C(4)-C(3)-H(3)	121.1
C(3)-C(4)-H(4)	119.5
C(3)-C(4)-C(5)	121.08(13)
C(5)-C(4)-H(4)	119.5
C(2)-C(7)-S(1)	107.43(9)
C(6)-C(7)-S(1)	129.30(10)
C(6)-C(7)-C(2)	123.24(12)
C(7)-C(6)-H(6)	121.7
C(7)-C(6)-C(5)	116.58(12)
C(5)-C(6)-H(6)	121.7
C(4)-C(5)-H(5)	119.4
C(6)-C(5)-C(4)	121.27(13)
C(6)-C(5)-H(5)	119.4

Symmetry transformations used to generate equivalent atoms:

Table 4. Anisotropic displacement parameters ($Å^2 x\ 10^3$) for hermann10_0m_a. The anisotropic displacement factor exponent takes the form: $-2\pi^2[\ h^2\ a^{*2}U^{11} + ... + 2\ h\ k\ a^*\ b^*\ U^{12}\ ]$

	U^{11}	U^{22}	U^{33}	U^{23}	U^{13}	U^{12}
S(1)	12(1)	9(1)	11(1)	0(1)	2(1)	-1(1)
O(2)	17(1)	12(1)	15(1)	2(1)	0(1)	2(1)
O(1)	23(1)	12(1)	16(1)	-4(1)	3(1)	-3(1)
N(2)	15(1)	11(1)	15(1)	0(1)	5(1)	-1(1)
N(1)	13(1)	11(1)	13(1)	1(1)	4(1)	0(1)
C(2)	10(1)	12(1)	9(1)	-1(1)	0(1)	-2(1)
C(1)	11(1)	12(1)	9(1)	-1(1)	0(1)	-1(1)
C(3)	14(1)	13(1)	13(1)	-1(1)	0(1)	0(1)
C(4)	13(1)	19(1)	16(1)	-4(1)	1(1)	2(1)
C(7)	11(1)	12(1)	10(1)	-1(1)	1(1)	0(1)
C(6)	15(1)	17(1)	13(1)	0(1)	2(1)	-3(1)
C(5)	12(1)	23(1)	15(1)	-2(1)	4(1)	-2(1)

Table 5. Hydrogen coordinates (x 10^4) and isotropic displacement parameters ($Å^2$x 10^3) for hermann10_0m_a.

	x	y	z	U(eq)
H(3)	5711	3378	3168	16
H(4)	8448	3778	1716	19
H(6)	6457	6746	943	18
H(5)	8813	5431	613	20
H(2A)	2660(30)	3393(16)	4460(20)	26(5)
H(2B)	1000(30)	4010(14)	5050(20)	21(5)

***N*-ethyl-*N'*-(3-(dimethylamino)propyl)amino-benzo[1,3]thiadiazepine (38)**

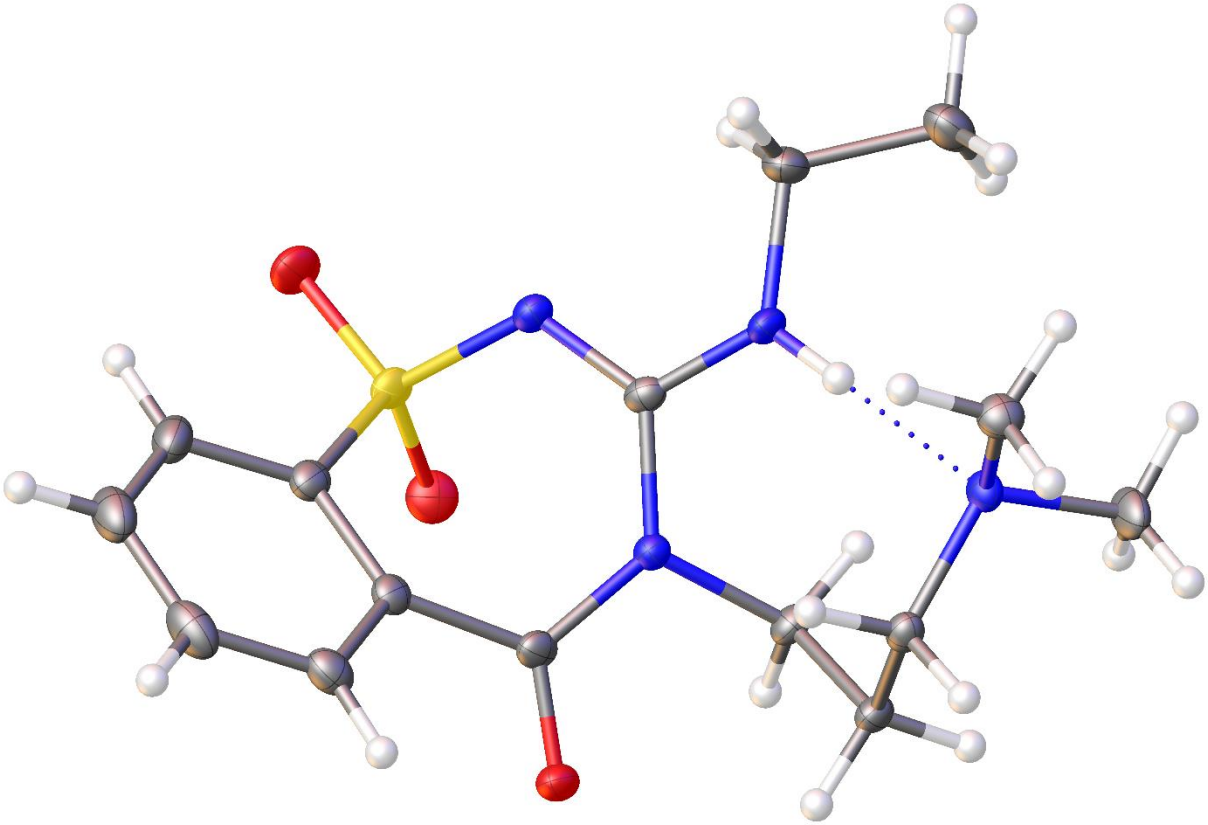

Table 1. Crystal data and structure refinement for Hermann_WF170PC.

Identification code	hermann_wf170pc_a	
Empirical formula	C18 H28 N4 O4 S	
Formula weight	396.50	
Temperature	100.0 K	
Wavelength	1.54178 Å	
Crystal system	Orthorhombic	
Space group	$Pna2_1$	
Unit cell dimensions	a = 7.45980(10) Å	α= 90°.
	b = 16.9055(3) Å	β= 90°.
	c = 15.9003(3) Å	γ = 90°.
Volume	2005.21(6) $Å^3$	
Z	4	
Density (calculated)	1.313 Mg/m^3	
Absorption coefficient	1.698 mm^{-1}	
F(000)	848	
Crystal size	0.19 x 0.15 x 0.15 mm^3	
Theta range for data collection	3.816 to 70.075°.	
Index ranges	-9<=h<=9, -20<=k<=19, -19<=l<=19	
Reflections collected	36964	
Independent reflections	3809 [R(int) = 0.0352]	
Completeness to theta = 67.679°	100.0 %	
Absorption correction	Semi-empirical from equivalents	
Max. and min. transmission	0.7533 and 0.6080	
Refinement method	Full-matrix least-squares on F^2	
Data / restraints / parameters	3809 / 1 / 249	
Goodness-of-fit on F^2	1.062	
Final R indices [I>2sigma(I)]	R1 = 0.0275, wR2 = 0.0769	
R indices (all data)	R1 = 0.0282, wR2 = 0.0775	
Absolute structure parameter	0.018(4)	
Largest diff. peak and hole	0.395 and -0.275 $e.Å^{-3}$	

Table 2. Atomic coordinates (x 10^4) and equivalent isotropic displacement parameters ($Å^2$x 10^3) for Hermann_WF170PC. U(eq) is defined as one third of the trace of the orthogonalized U^{ij} tensor.

	x	y	z	U(eq)
S(1)	991(1)	5573(1)	3320(1)	16(1)
O(1)	-685(2)	5339(1)	3702(1)	22(1)
O(2)	1406(3)	5237(1)	2513(1)	25(1)
O(3)	-942(2)	6957(1)	5213(1)	22(1)
N(1)	3958(2)	5378(1)	5217(1)	16(1)
N(2)	2680(3)	5419(1)	3924(1)	16(1)
N(3)	1265(2)	6051(1)	5135(1)	13(1)
N(4)	4235(3)	6022(1)	6833(1)	14(1)
C(1)	6076(4)	4353(2)	5658(2)	26(1)
C(2)	5332(3)	4825(2)	4921(2)	22(1)
C(3)	2635(3)	5618(1)	4726(1)	14(1)
C(4)	1030(3)	6607(1)	3235(2)	17(1)
C(5)	1380(4)	6980(2)	2476(2)	22(1)
C(6)	1419(4)	7798(2)	2446(2)	27(1)
C(7)	1114(3)	8236(2)	3169(2)	26(1)
C(8)	751(3)	7862(2)	3928(2)	20(1)
C(9)	742(3)	7036(1)	3970(2)	15(1)
C(10)	272(3)	6675(1)	4801(1)	15(1)
C(11)	643(3)	5767(1)	5975(1)	15(1)
C(12)	965(3)	6336(1)	6701(1)	15(1)
C(13)	2873(3)	6649(1)	6774(1)	15(1)
C(14)	6024(3)	6378(1)	6844(2)	19(1)
C(15)	3988(3)	5528(2)	7579(2)	23(1)
O(1S)	4318(6)	2502(2)	5129(3)	93(1)
C(1S)	5485(9)	1925(4)	3880(3)	92(2)
C(2S)	5166(5)	1991(2)	4783(2)	41(1)
C(3S)	5869(5)	1303(2)	5276(3)	50(1)

Table 3. Bond lengths [Å] and angles [°] for Hermann_WF170PC.

S(1)-O(1)	1.4447(19)	C(14)-H(14B)	0.9800
S(1)-O(2)	1.4372(18)	C(14)-H(14C)	0.9800
S(1)-N(2)	1.606(2)	C(15)-H(15A)	0.9800
S(1)-C(4)	1.754(2)	C(15)-H(15B)	0.9800
O(3)-C(10)	1.215(3)	C(15)-H(15C)	0.9800
N(1)-H(1)	0.8800	O(1S)-C(2S)	1.204(5)
N(1)-C(2)	1.464(3)	C(1S)-H(1SA)	0.9800
N(1)-C(3)	1.323(3)	C(1S)-H(1SB)	0.9800
N(2)-C(3)	1.319(3)	C(1S)-H(1SC)	0.9800
N(3)-C(3)	1.415(3)	C(1S)-C(2S)	1.459(6)
N(3)-C(10)	1.394(3)	C(2S)-C(3S)	1.498(5)
N(3)-C(11)	1.493(3)	C(3S)-H(3SA)	0.9800
N(4)-C(13)	1.471(3)	C(3S)-H(3SB)	0.9800
N(4)-C(14)	1.464(3)	C(3S)-H(3SC)	0.9800
N(4)-C(15)	1.463(3)		
C(1)-H(1A)	0.9800	O(1)-S(1)-N(2)	112.58(11)
C(1)-H(1B)	0.9800	O(1)-S(1)-C(4)	108.65(11)
C(1)-H(1C)	0.9800	O(2)-S(1)-O(1)	116.92(11)
C(1)-C(2)	1.522(4)	O(2)-S(1)-N(2)	107.47(11)
C(2)-H(2A)	0.9900	O(2)-S(1)-C(4)	108.78(12)
C(2)-H(2B)	0.9900	N(2)-S(1)-C(4)	101.26(10)
C(4)-C(5)	1.387(3)	C(2)-N(1)-H(1)	119.0
C(4)-C(9)	1.392(3)	C(3)-N(1)-H(1)	119.0
C(5)-H(5)	0.9500	C(3)-N(1)-C(2)	121.9(2)
C(5)-C(6)	1.383(4)	C(3)-N(2)-S(1)	121.07(16)
C(6)-H(6)	0.9500	C(3)-N(3)-C(11)	117.99(18)
C(6)-C(7)	1.386(4)	C(10)-N(3)-C(3)	126.9(2)
C(7)-H(7)	0.9500	C(10)-N(3)-C(11)	114.75(18)
C(7)-C(8)	1.388(4)	C(14)-N(4)-C(13)	109.53(17)
C(8)-H(8)	0.9500	C(15)-N(4)-C(13)	112.07(18)
C(8)-C(9)	1.399(3)	C(15)-N(4)-C(14)	109.88(19)
C(9)-C(10)	1.497(3)	H(1A)-C(1)-H(1B)	109.5
C(11)-H(11A)	0.9900	H(1A)-C(1)-H(1C)	109.5
C(11)-H(11B)	0.9900	H(1B)-C(1)-H(1C)	109.5
C(11)-C(12)	1.522(3)	C(2)-C(1)-H(1A)	109.5
C(12)-H(12A)	0.9900	C(2)-C(1)-H(1B)	109.5
C(12)-H(12B)	0.9900	C(2)-C(1)-H(1C)	109.5
C(12)-C(13)	1.523(3)	N(1)-C(2)-C(1)	110.0(2)
C(13)-H(13A)	0.9900	N(1)-C(2)-H(2A)	109.7
C(13)-H(13B)	0.9900	N(1)-C(2)-H(2B)	109.7
C(14)-H(14A)	0.9800	C(1)-C(2)-H(2A)	109.7

C(1)-C(2)-H(2B)	109.7
H(2A)-C(2)-H(2B)	108.2
N(1)-C(3)-N(3)	115.24(19)
N(2)-C(3)-N(1)	118.22(19)
N(2)-C(3)-N(3)	126.5(2)
C(5)-C(4)-S(1)	121.6(2)
C(5)-C(4)-C(9)	121.6(2)
C(9)-C(4)-S(1)	116.83(18)
C(4)-C(5)-H(5)	120.4
C(6)-C(5)-C(4)	119.2(2)
C(6)-C(5)-H(5)	120.4
C(5)-C(6)-H(6)	119.9
C(5)-C(6)-C(7)	120.2(2)
C(7)-C(6)-H(6)	119.9
C(6)-C(7)-H(7)	119.7
C(6)-C(7)-C(8)	120.6(2)
C(8)-C(7)-H(7)	119.7
C(7)-C(8)-H(8)	120.1
C(7)-C(8)-C(9)	119.9(2)
C(9)-C(8)-H(8)	120.1
C(4)-C(9)-C(8)	118.6(2)
C(4)-C(9)-C(10)	124.4(2)
C(8)-C(9)-C(10)	116.8(2)
O(3)-C(10)-N(3)	119.2(2)
O(3)-C(10)-C(9)	119.4(2)
N(3)-C(10)-C(9)	121.34(19)
N(3)-C(11)-H(11A)	108.5
N(3)-C(11)-H(11B)	108.5
N(3)-C(11)-C(12)	115.22(18)
H(11A)-C(11)-H(11B)	107.5
C(12)-C(11)-H(11A)	108.5
C(12)-C(11)-H(11B)	108.5
C(11)-C(12)-H(12A)	108.5
C(11)-C(12)-H(12B)	108.5
C(11)-C(12)-C(13)	115.13(18)
H(12A)-C(12)-H(12B)	107.5
C(13)-C(12)-H(12A)	108.5
C(13)-C(12)-H(12B)	108.5
N(4)-C(13)-C(12)	113.59(18)
N(4)-C(13)-H(13A)	108.8
N(4)-C(13)-H(13B)	108.8
C(12)-C(13)-H(13A)	108.8
C(12)-C(13)-H(13B)	108.8
H(13A)-C(13)-H(13B)	107.7
N(4)-C(14)-H(14A)	109.5
N(4)-C(14)-H(14B)	109.5
N(4)-C(14)-H(14C)	109.5
H(14A)-C(14)-H(14B)	109.5
H(14A)-C(14)-H(14C)	109.5
H(14B)-C(14)-H(14C)	109.5
N(4)-C(15)-H(15A)	109.5
N(4)-C(15)-H(15B)	109.5
N(4)-C(15)-H(15C)	109.5
H(15A)-C(15)-H(15B)	109.5
H(15A)-C(15)-H(15C)	109.5
H(15B)-C(15)-H(15C)	109.5
H(1SA)-C(1S)-H(1SB)	109.5
H(1SA)-C(1S)-H(1SC)	109.5
H(1SB)-C(1S)-H(1SC)	109.5
C(2S)-C(1S)-H(1SA)	109.5
C(2S)-C(1S)-H(1SB)	109.5
C(2S)-C(1S)-H(1SC)	109.5
O(1S)-C(2S)-C(1S)	126.2(5)
O(1S)-C(2S)-C(3S)	120.1(4)
C(1S)-C(2S)-C(3S)	113.5(4)
C(2S)-C(3S)-H(3SA)	109.5
C(2S)-C(3S)-H(3SB)	109.5
C(2S)-C(3S)-H(3SC)	109.5
H(3SA)-C(3S)-H(3SB)	109.5
H(3SA)-C(3S)-H(3SC)	109.5
H(3SB)-C(3S)-H(3SC)	109.5

Symmetry transformations used to generate equivalent atoms:

Table 4. Anisotropic displacement parameters ($Å^2 x\ 10^3$) for Hermann_WF170PC. The anisotropic displacement factor exponent takes the form: $-2\pi^2[\ h^2\ a^{*2}U^{11} + ...\ + 2\ h\ k\ a^*\ b^*\ U^{12}]$

	U^{11}	U^{22}	U^{33}	U^{23}	U^{13}	U^{12}
S(1)	18(1)	18(1)	12(1)	-5(1)	-2(1)	1(1)
O(1)	21(1)	22(1)	24(1)	-3(1)	-3(1)	-4(1)
O(2)	31(1)	29(1)	15(1)	-10(1)	-3(1)	6(1)
O(3)	22(1)	30(1)	14(1)	-3(1)	1(1)	12(1)
N(1)	17(1)	21(1)	10(1)	-3(1)	1(1)	5(1)
N(2)	18(1)	17(1)	12(1)	-2(1)	1(1)	3(1)
N(3)	14(1)	15(1)	12(1)	-1(1)	0(1)	2(1)
N(4)	15(1)	13(1)	14(1)	3(1)	0(1)	0(1)
C(1)	28(1)	25(1)	27(1)	-1(1)	-4(1)	11(1)
C(2)	21(1)	27(1)	20(1)	-2(1)	2(1)	10(1)
C(3)	15(1)	12(1)	14(1)	-2(1)	2(1)	0(1)
C(4)	13(1)	22(1)	15(1)	-1(1)	-2(1)	2(1)
C(5)	19(1)	33(1)	15(1)	3(1)	1(1)	3(1)
C(6)	22(1)	33(1)	26(1)	12(1)	1(1)	2(1)
C(7)	21(1)	21(1)	35(2)	9(1)	-4(1)	0(1)
C(8)	18(1)	19(1)	24(1)	-1(1)	-5(1)	3(1)
C(9)	12(1)	19(1)	15(1)	-1(1)	-3(1)	1(1)
C(10)	16(1)	18(1)	12(1)	-5(1)	-2(1)	3(1)
C(11)	16(1)	17(1)	12(1)	0(1)	3(1)	-2(1)
C(12)	15(1)	19(1)	11(1)	-2(1)	1(1)	2(1)
C(13)	19(1)	13(1)	12(1)	-1(1)	0(1)	1(1)
C(14)	16(1)	21(1)	21(1)	0(1)	0(1)	-1(1)
C(15)	23(1)	25(1)	21(1)	13(1)	4(1)	3(1)
O(1S)	103(3)	63(2)	113(3)	-36(2)	-26(3)	38(2)
C(1S)	92(4)	146(6)	40(2)	32(3)	-7(3)	-15(4)
C(2S)	40(2)	35(2)	50(2)	-11(1)	-12(2)	3(1)
C(3S)	46(2)	60(2)	44(2)	11(2)	3(2)	9(2)

Table 5. Hydrogen coordinates (x 10^4) and isotropic displacement parameters ($Å^2$x 10^3) for Hermann_WF170PC.

	x	y	z	U(eq)
H(1)	4015	5555	5736	19
H(1A)	6980	3979	5453	40
H(1B)	5101	4062	5931	40
H(1C)	6628	4715	6064	40
H(2A)	6314	5122	4646	27
H(2B)	4805	4460	4502	27
H(5)	1589	6678	1982	27
H(6)	1656	8060	1930	32
H(7)	1155	8797	3145	31
H(8)	508	8167	4416	24
H(11A)	1257	5262	6103	18
H(11B)	-658	5655	5941	18
H(12A)	652	6064	7233	18
H(12B)	142	6792	6639	18
H(13A)	3137	6982	6277	18
H(13B)	2958	6989	7279	18
H(14A)	6245	6647	6308	29
H(14B)	6926	5963	6927	29
H(14C)	6100	6761	7305	29
H(15A)	4001	5861	8083	35
H(15B)	4961	5139	7613	35
H(15C)	2836	5251	7541	35
H(1SA)	4622	1554	3635	138
H(1SB)	6706	1731	3782	138
H(1SC)	5342	2445	3617	138
H(3SA)	5662	1394	5877	75
H(3SB)	7158	1246	5173	75
H(3SC)	5248	820	5101	75

References

(1) Li, J.; Liu, C. Coding or Noncoding, the Converging Concepts of RNAs. *Front. Genet.* **2019**, *10* (MAY), 496. https://doi.org/10.3389/FGENE.2019.00496/BIBTEX.

(2) Hermann, T. Drugs Targeting the Ribosome. *Curr. Opin. Struct. Biol.* **2005**, *15* (3), 355–366. https://doi.org/10.1016/J.SBI.2005.05.001.

(3) Guan, L.; Disney, M. D. Recent Advances in Developing Small Molecules Targeting RNA. *ACS Chem. Biol.* **2012**, *7* (1), 73–86. https://doi.org/10.1021/CB200447R.

(4) Howe, J. A.; Wang, H.; Fischmann, T. O.; Balibar, C. J.; Xiao, L.; Galgoci, A. M.; Malinverni, J. C.; Mayhood, T.; Villafania, A.; Nahvi, A.; Murgolo, N.; Barbieri, C. M.; Mann, P. A.; Carr, D.; Xia, E.; Zuck, P.; Riley, D.; Painter, R. E.; Walker, S. S.; Sherborne, B.; De Jesus, R.; Pan, W.; Plotkin, M. A.; Wu, J.; Rindgen, D.; Cummings, J.; Garlisi, C. G.; Zhang, R.; Sheth, P. R.; Gill, C. J.; Tang, H.; Roemer, T. Selective Small-Molecule Inhibition of an RNA Structural Element. *Nat. 2015 5267575* **2015**, *526* (7575), 672–677. https://doi.org/10.1038/nature15542.

(5) Connelly, C. M.; Moon, M. H.; Schneekloth, J. S. The Emerging Role of RNA as a Therapeutic Target for Small Molecules. *Cell Chem. Biol.* **2016**, *23* (9), 1077–1090. https://doi.org/10.1016/J.CHEMBIOL.2016.05.021.

(6) Dibrov, S. M.; Parsons, J.; Carnevali, M.; Zhou, S.; Rynearson, K. D.; Ding, K.; Garcia Sega, E.; Brunn, N. D.; Boerneke, M. A.; Castaldi, M. P.; Hermann, T. Hepatitis C Virus Translation Inhibitors Targeting the Internal Ribosomal Entry Site. *J. Med. Chem.* **2013**, *57* (5), 1694–1707. https://doi.org/10.1021/JM401312N.

(7) Hermann, T. Small Molecules Targeting Viral RNA. *Wiley Interdiscip. Rev. RNA* **2016**, *7* (6), 726–743. https://doi.org/10.1002/wrna.1373.

(8) Qiu, P.; Stevens, R.; Wei, B.; Lahser, F.; Howe, A. Y. M.; Klappenbach, J. A.; Marton, M. J. HCV Genotyping from NGS Short Reads and Its Application in Genotype Detection from HCV Mixed Infected Plasma. *PLoS One* **2015**, *10* (4), e0122082. https://doi.org/10.1371/journal.pone.0122082.

(9) Hermann, T. Viral RNA Targets and Their Small Molecule Ligands. *Top. Med. Chem.* **2018**, *27*, 111–134. https://doi.org/10.1007/7355_2016_20.

(10) WHO Hepatitis C https://www.who.int/news-room/fact-sheets/detail/hepatitis-c (accessed Jan 18, 2022).

(11) Zhang, X. Direct Anti-HCV Agents. *Acta Pharm. Sin. B* **2016**, *6* (1), 26. https://doi.org/10.1016/J.APSB.2015.09.008.

(12) Aregay, A.; Owusu Sekyere, S.; Deterding, K.; Port, K.; Dietz, J.; Berkowski, C.; Sarrazin, C.; Manns, M. P.; Cornberg, M.; Wedemeyer, H. Elimination of Hepatitis C Virus Has Limited Impact on the Functional and Mitochondrial Impairment of HCV-

Specific CD8+ T Cell Responses. *J. Hepatol.* **2019**, *71* (5), 889–899. https://doi.org/10.1016/J.JHEP.2019.06.025.

(13) Halliday, J.; Klenerman, P.; Barnes, E. Vaccination for Hepatitis C Virus: Closing in on an Evasive Target Europe PMC Funders Group. *Expert Rev Vaccines* **2011**, *10* (5), 659–672. https://doi.org/10.1586/erv.11.55.

(14) Bukh, J.; Miller, R. H.; Purcell, R. H. Genetic Heterogeneity of Hepatitis C Virus: Quasispecies and Genotypes. *Semin. Liver Dis.* **1995**, *15* (1), 41–63. https://doi.org/10.1055/S-2007-1007262.

(15) Boerneke, M. A.; Hermann, T. Ligand-Responsive RNA Mechanical Switches. *http://dx.doi.org/10.1080/15476286.2015.1054592* **2015**, *12* (8), 780–786. https://doi.org/10.1080/15476286.2015.1054592.

(16) Niepmann, M.; Gerresheim, G. K. Hepatitis C Virus Translation Regulation. *Int. J. Mol. Sci. 2020, Vol. 21, Page 2328* **2020**, *21* (7), 2328. https://doi.org/10.3390/IJMS21072328.

(17) Berry, K. E.; Waghray, S.; Mortimer, S. A.; Bai, Y.; Doudna, J. A. Crystal Structure of the HCV IRES Central Domain Reveals Strategy for Start-Codon Positioning. *Structure* **2011**, *19* (10), 1456–1466. https://doi.org/10.1016/j.str.2011.08.002.

(18) Ji, H.; Fraser, C. S.; Yu, Y.; Leary, J.; Doudna, J. A. Coordinated Assembly of Human Translation Initiation Complexes by the Hepatitis C Virus Internal Ribosome Entry Site RNA. *Proc. Natl. Acad. Sci.* **2004**, *101* (49), 16990–16995. https://doi.org/10.1073/PNAS.0407402101.

(19) Dibrov, S. M.; Parsons, J.; Carnevali, M.; Zhou, S.; Rynearson, K. D.; Ding, K.; Garcia Sega, E.; Brunn, N. D.; Boerneke, M. A.; Castaldi, M. P.; Hermann, T. Hepatitis C Virus Translation Inhibitors Targeting the Internal Ribosomal Entry Site. *J. Med. Chem.* **2014**, *57* (5), 1694–1707. https://doi.org/10.1021/JM401312N.

(20) Dibrov, S. M.; Johnston-Cox, H.; Weng, Y.-H.; Hermann, T.; Dibrov, S. M.; Johnston-Cox, H.; Weng, Y.-H.; Hermann, T. Functional Architecture of HCV IRES Domain II Stabilized by Divalent Metal Ions in the Crystal and in Solution. *Angew. Chemie Int. Ed.* **2007**, *46* (1–2), 226–229. https://doi.org/10.1002/ANIE.200603807.

(21) Dibrov, S. M.; Ding, K.; Brunn, N. D.; Parker, M. A.; Bergdahl, B. M.; Wyles, D. L.; Hermann, T. Structure of a Hepatitis C Virus RNA Domain in Complex with a Translation Inhibitor Reveals a Binding Mode Reminiscent of Riboswitches. *Proc. Natl. Acad. Sci. U. S. A.* **2012**, *109* (14), 5223–5228. https://doi.org/10.1073/pnas.1118699109.

(22) Dibrov, S. M.; Ding, K.; Brunn, N. D.; Parker, M. A.; Bergdahl, B. M.; Wyles, D. L.; Hermann, T. Structure of a Hepatitis C Virus RNA Domain in Complex with a Translation Inhibitor Reveals a Binding Mode Reminiscent of Riboswitches. *Proc. Natl. Acad. Sci. U. S. A.* **2012**, *109* (14), 5223–5228. https://doi.org/10.1073/pnas.1118699109.

(23) Kuiken, C.; Hraber, P.; Thurmond, J.; Yusim, K. The Hepatitis C Sequence Database in

Los Alamos. *Nucleic Acids Res.* **2008**, *36* (Database issue), D512. https://doi.org/10.1093/NAR/GKM962.

(24) Seth, P. P.; Miyaji, A.; Jefferson, E. A.; Sannes-Lowery, K. A.; Osgood, S. A.; Propp, S. S.; Ranken, R.; Massire, C.; Sampath, R.; Ecker, D. J.; Swayze, E. E.; Griffey, R. H. SAR by MS: Discovery of a New Class of RNA-Binding Small Molecules for the Hepatitis C Virus: Internal Ribosome Entry Site IIA Subdomain. *J. Med. Chem.* **2005**, *48* (23), 7099–7102. https://doi.org/10.1021/JM050815O.

(25) Parsons, J.; Castaldi, M. P.; Dutta, S.; Dibrov, S. M.; Wyles, D. L.; Hermann, T. Conformational Inhibition of the Hepatitis C Virus Internal Ribosome Entry Site RNA. *Nat. Chem. Biol. 2009 511* **2009**, *5* (11), 823–825. https://doi.org/10.1038/nchembio.217.

(26) Boerneke, M. A.; Dibrov, S. M.; Gu, J.; Wyles, D. L.; Hermann, T. Functional Conservation despite Structural Divergence in Ligand-Responsive RNA Switches. *Proc. Natl. Acad. Sci. U. S. A.* **2014**, *111* (45), 15952–15957. https://doi.org/10.1073/PNAS.1414678111.

(27) Zhou, S.; Rynearson, K. D.; Ding, K.; Brunn, N. D.; Hermann, T. Screening for Inhibitors of the Hepatitis C Virus Internal Ribosome Entry Site RNA. **2013**, *21* (20), 6139–6144. https://doi.org/10.1016/J.BMC.2013.03.054.

(28) Charrette, B. P.; Boerneke, M. A.; Hermann, T. Ligand Optimization by Improving Shape Complementarity at a Hepatitis C Virus RNA Target. *ACS Chem. Biol.* **2016**, *11* (12), 3263–3267. https://doi.org/10.1021/ACSCHEMBIO.6B00687/SUPPL_FILE/CB6B00687_SI_001.PDF.

(29) Novello, F. C.; Bell, S. C.; Abrams, E. L. A.; Ziegler, C.; Sprague, J. M. Diureticss 1, 2, 4-Benzothiadiazine-1, 1-Dioxides. *J. Org. Chem.* **1960**, *25* (6), 970–981. https://doi.org/10.1021/jo01076a028.

(30) Das, D.; Hong, J.; Chen, S. H.; Wang, G.; Beigelman, L.; Seiwert, S. D.; Buckman, B. O. Recent Advances in Drug Discovery of Benzothiadiazine and Related Analogs as HCV NS5B Polymerase Inhibitors. *Bioorg. Med. Chem.* **2011**, *19* (16), 4690–4703. https://doi.org/10.1016/J.BMC.2011.06.079.

(31) Topliss, J. G.; Konzelman, L. M. 3,4-Dihydro-3-imino-2H-1,2,4-benzothiadiazine 1,1-Dioxides http://pubs.acs.org/doi/pdf/10.1021/jo01044a038?source=chemport (accessed Apr 24, 2015).

(32) Liu, B.; Chang, J.; Gordon, W. P.; Isbell, J.; Zhou, Y.; Tuntland, T. Snapshot PK: A Rapid Rodent in Vivo Preclinical Screening Approach. *Drug Discov. Today* **2008**, *13* (7–8), 360–367. https://doi.org/10.1016/J.DRUDIS.2007.10.014.

(33) Tedesco, R.; Shaw, A. N.; Bambal, R.; Chai, D.; Concha, N. O.; Darcy, M. G.; Dhanak, D.; Fitch, D. M.; Gates, A.; Gerhardt, W. G.; Halegoua, D. L.; Han, C.; Hofmann, G. A.; Johnston, V. K.; Kaura, A. C.; Liu, N.; Keenan, R. M.; Lin-Goerke, J.; Sarisky, R. T.;

Wiggall, K. J.; Zimmerman, M. N.; Duffy, K. J. 3-(1,1-Dioxo-2H-(1,2,4)-Benzothiadiazin-3-Yl)-4-Hydroxy-2(1H)-Quinolinones, Potent Inhibitors of Hepatitis C Virus RNA-Dependent RNA Polymerase. *J. Med. Chem.* **2006**, *49* (3), 971–983. https://doi.org/10.1021/JM050855S/SUPPL_FILE/JM050855SSI20051115_103718.PDF.

(34) Rajesh, K.; Somasundaram, M.; Saiganesh, R.; Balasubramanian, K. K. Bromination of Deactivated Aromatics: A Simple and Efficient Method. *J. Org. Chem.* **2007**, *72* (15), 5867–5869. https://doi.org/10.1021/JO070477U/SUPPL_FILE/JO070477USI20070524_082924.PDF.

(35) Fukuyama, T.; Cheung, M.; Jow, C.-K.; Hidai, Y.; Kan, T. 2,4-Dinitrobenzenesulfonamides: A Simple and Practical Method for the Preparation of a Variety of Secondary Amines and Diamines. *Tetrahedron Lett.* **1997**, *38* (33), 5831–5834. https://doi.org/10.1016/S0040-4039(97)01334-8.

(36) Paul, S.; Smith, W. T. Removal of Chlorine from Aromatic Nitrochloro Compounds. Preparation of 1,3-Dinitronaphthalene. *J. Am. Chem. Soc.* **2002**, *71* (8), 2855–2856. https://doi.org/10.1021/JA01176A078.

(37) Marques, C. A.; Selva, M.; Tundo, P. Facile Hydrodehalogenation with H2 and Pd/C Catalyst under Multiphase Conditions. 3. Selective Removal of Halogen from Functionalized Aryl Ketones. 4. Aryl Halide-Promoted Reduction of Benzyl Alcohols to Alkanes. *J. Org. Chem.* **2002**, *60* (8), 2430–2435. https://doi.org/10.1021/JO00113A024.

(38) Gamble, A. B.; Garner, J. A.; Gordon, C.; O'Conner, S. M. J.; Keller, P. A. Aryl Nitro Reduction with Iron Powder or Stannous Chloride under Ultrasonic Irradiation. *Synth. Commun.* **2007**, *37* (16), 2777–2786. https://doi.org/10.1080/00397910701481195.

(39) Olender, D.; Zwawiak, J.; Zaprutko, L. Selective Reduction of 2,4-Dinitro- and 4,5-Dinitroimidazole Derivatives Using Iron Dust. *J. Heterocycl. Chem.* **2010**, *47* (5), 1049–1055. https://doi.org/10.1002/JHET.418.

(40) Kumar, J. S. D.; Ho, M. M.; Toyokuni, T. Simple and Chemoselective Reduction of Aromatic Nitro Compounds to Aromatic Amines: Reduction with Hydriodic Acid Revisited. *Tetrahedron Lett.* **2001**, *42* (33), 5601–5603. https://doi.org/10.1016/S0040-4039(01)01083-8.

(41) Saha, D.; Jain, G.; Sharma, A. Benzothiazepines: Chemistry of a Privileged Scaffold. *RSC Adv.* **2015**, *5* (86), 70619–70639. https://doi.org/10.1039/C5RA12422K.

(42) Zheng, X.; Gao, L.; Wang, L.; Liang, C.; Wang, B.; Liu, Y.; Feng, S.; Zhang, B.; Zhou, M.; Yu, X.; Xiang, K.; Chen, L.; Guo, T.; Shen, H. C.; Zou, G.; Wu, J. Z.; Yun, H. Discovery of Ziresovir as a Potent, Selective, and Orally Bioavailable Respiratory Syncytial Virus Fusion Protein Inhibitor. *J. Med. Chem.* **2019**, *62* (13), 6315–6329. https://doi.org/10.1021/ACS.JMEDCHEM.9B00654/SUPPL_FILE/JM9B00654_SI_001.CSV.

(43) Artico, M.; Silvestri, R.; Pagnozzi, E.; Stefancich, G.; Massa, S.; Loi, A. G.; Putzolu, M.;

Corrias, S.; Spiga, M. G.; La Colla, P. 5H-Pyrrolo[1,2-b][1,2,5]Benzothiadiazepines (PBTDs): A Novel Class of Non-Nucleoside Reverse Transcriptase Inhibitors. *Bioorg. Med. Chem.* **1996**, *4* (6), 837–850. https://doi.org/10.1016/0968-0896(96)00075-2.

(44) Di Santo, R.; Costi, R. 2H-Pyrrolo[3,4-b] [1,5]Benzothiazepine Derivatives as Potential Inhibitors of HIV-1 Reverse Transcriptase. *Farm.* **2005**, *60* (5), 385–392. https://doi.org/10.1016/J.FARMAC.2005.03.006.

(45) Moro, W. B.; Yang, Z.; Kane, T. A.; Zhou, Q.; Harville, S.; Brouillette, C. G.; Brouillette, W. J. SAR Studies for a New Class of Antibacterial NAD Biosynthesis Inhibitors. *J. Comb. Chem.* **2009**, *11* (4), 617–625. https://doi.org/10.1021/cc9000357.

(46) Bylund, J.; Ek, M. E.; Holenz, J.; Kers, A.; Ohberg, L. Bis-(Sulfonylamino) Derivatives for Treatment of Pain and Inflammation, May 12, 2010.

(47) Xiaojun Zhang; Eldon Scott Priestley; Alexandra A. Nirschl; Yan Zou. Phenylglycinamide Derivatives Useful as Anticoagulants, January 9, 2006.

(48) Zhang, H.; Huang, R.; Pillarsetty, N. V. K.; Thorek, D. L. J.; Vaidyanathan, G.; Serganova, I.; Blasberg, R. G.; Lewis, J. S. Synthesis and Evaluation of 18F-Labeled Benzylguanidine Analogs for Targeting the Human Norepinephrine Transporter. *Eur. J. Nucl. Med. Mol. Imaging* **2014**, *41* (2), 322–332. https://doi.org/10.1007/s00259-013-2558-9.

(49) Hironao Sajiki, *; Takashi Ikawa, and; Hirota*, K. Reductive and Catalytic Monoalkylation of Primary Amines Using Nitriles as an Alkylating Reagent. *Org. Lett.* **2004**, *6* (26), 4977–4980. https://doi.org/10.1021/OL047871O.

(50) Tan, D.; Friščić, T. Carbodiimide Insertion into Sulfonimides: One-Step Route to Azepine Derivatives via a Two-Atom Saccharin Ring Expansion. *Chem. Commun.* **2017**, *53* (5), 901–904. https://doi.org/10.1039/c6cc07331j.

(51) Weiss, S.; Michaud, H.; Prietzel, H.; Krommer, H. A New, Simple Synthesis of 2-Aminobenzimidazole. *Angew. Chemie Int. Ed. English* **1973**, *12* (10), 841–841. https://doi.org/10.1002/ANIE.197308411.

(52) Yamamoto, T.; Sugiyama, S.; Akimoto, K.; Hayashi, K. Organic Preparations and Procedures International ONE-POT SYNTHESIS OF ISOTHIOCYANATES FROM PRIMARY AMINES SYNTHESIS USING CYANAMIDE? **2009**. https://doi.org/10.1080/00304949209355899.

(53) Groziak, M. P.; Townsend, L. B. A New and Efficient Synthesis of Guanosine+. *J. Org. Chem* **1986**, *51*, 1277–1282.

(54) Groziak, M. P.; Canguly, A. D.; Robinsons, P. D. Boron Heterocycles Bearing a Peripheral Resemblance to Naturally-Occurring Purines: Design, Syntheses, Structures, and Properties? *J. Am. Chem. SOC* **1994**, *116*, 1591–1605.

(55) Tarra Fuchs; Goutam Chowdhury; Charles L. Barnes, A.; Gates*, K. S. 3-Amino-1,2,4-Benzotriazine 4-Oxide: Characterization of a New Metabolite Arising from Bioreductive Processing of the Antitumor Agent 3-Amino-1,2,4-Benzotriazine 1,4-Dioxide (Tirapazamine). **2000**. https://doi.org/10.1021/JO001232J.

(56) Bliss, E. A.; Griffin, R. J.; Stevens, M. F. G. Structural Studies on Bio-Active Compounds. Part 5. Synthesis and Properties of 2,4-Diaminopyrimidine Dihydrofolate Reductase Inhibitors Bearing Lipophilic Azido Groups. *J. Chem. Soc. Perkin Trans. 1* **1987**, 2217. https://doi.org/10.1039/p19870002217.

(57) Kimura, J.; Yamada, H.; Ogura, H.; Yajima, T.; Fukushima, T. Development of a Fluorescent Chelating Ligand for Gallium Ion Having a Quinazoline Structure with Two Schiff Base Moieties. *Anal. Chim. Acta* **2009**, *635* (2), 207–213. https://doi.org/10.1016/j.aca.2009.01.008.

(58) Groziak, M. P.; Chern, J.-W.; Townsend, L. B. Heterocyclic Synthesis via a 1,3-Dicyclohexylcarbodiimide-Mediated Cyclodesulfurative Annulation Reaction. New Methodology for the Preparation of Guanosine and Guanosine-Type Nucleoside Analogues'. *J. Org. Chem* **1986**, *51*, 1065–1069.